A smarter design calculation for quay walls

based on volume elements and nonlinear approaches in terms of lowering the CO_2 footprint

By

Ashish Sewcharan

In partial fulfillment of the requirements for the degree of

Master of Science
in Structural Engineering

at the Delft University of Technology

Date: 19-2-23

Student

Ashish Sewcharan
4994671

University

Delft University of Technology
Faculty: Civil Engineering and Geosciences

Structural Engineering

Stevinweg 1

2628 CN, Delft

Internship

Arcadis Nederland

Gebouw: Delftse Poort, Weena 505

3013 AL, Rotterdam

Graduation committee

Dr.ir. C.B.M. Blom	TU Delft
Prof.dr.ir. M.A.N. Hendriks	TU Delft
Dr.ir. A.A. Roubos	TU Delft
Ir. Paul van der Vorm	Arcadis
Ir. Coen van der Vliet	Arcadis
Ir. Willem Gall	Port of Rotterdam
Ir. Diego Allaix	TNO

Preface

For the Master of Science degree in Structural Engineering at Technical University of Delft, the following report, titled "A smarter design for quay walls based on volume elements and nonlinear approaches in terms of lowering the CO_2 footprint" is provided. The Port of Rotterdam has the ambition to reduce the CO_2 footprint for building new quay walls by using fewer materials and/or use different design solutions. As a result, Arcadis suggested the research topic to lessen the CO_2 impact.

I would like to thank the following individuals for their assistance in producing this report. First, let me express my gratitude to Kees Blom for helping me during the graduation period and pointing me in the right direction whenever I became disoriented. I would also like to thank Paul van der Vorm for welcoming me as an intern at Arcadis and providing me with the essential details regarding the conventional approach. My appreciation also goes to Coen van der Vliet, who assisted me with the advanced approach, and Diana FEA. Coen always took the time to thoroughly explain the background of specific issues and always gave me the appropriate guidelines to complete the tasks. In addition, I would like to thank the other committee members, Max Hendriks, Alfred Roubos, Willem Gal, and Diego Allaix for giving me feedback during the online sessions and providing me with information when necessary.

I would also like to thank Marco Bolognin from Diana Support for taking the time to answer all my questions regarding Diana FEA. Lastly, I would like to thank my family and friends for their support and motivation during the graduation process.

<div align="right">

Ashish Sewcharan

Den Haag, February 19, 2023

</div>

Summary

Port of Rotterdam has the ambition to reduce the footprint for building new quay walls, this is in line with their ambition to reduce the footprint and with national goals to limit global warming. The aim is to use less materials and/or use different design solutions.

These reinforced structures are designed in a conventional way and the internal forces are determined by performing a Linear Elastic Analysis. The reinforcement is calculated using the internal forces and is based on the Eurocode 1992 -1-1. The conventional approach includes various assumptions that affect the amount of concrete and steel used, which influences the CO_2 footprint, structure reliability, and costs. In order to know the effects of these assumptions, advanced nonlinear calculations are carried out using volume elements.

Making use of the reference project "Biomassakade Engie", some general modeling assumptions are made to simplify the analysis. For the conventional approach, a 2D and 3D model is designed using Scia-Engineering in which the relief floor is examined. Modeling in two-dimensional space is done with beam elements, and in three-dimensional space shell elements are used. The use of shell elements in three-dimensional space is also called 2.5D. The critical locations are identified, which are at about the middle of the relief floor between walls B and C (location 1) where the sagging bending moment is governing, and at the combi-wall (location 2) where the hogging bending moment is governing. At both locations, an actual and artificial reinforcement set is designed in Idea-Statica using the governing internal forces of the 2D model based on the Ultimate Limit State (ULS) and Service Ability Limit State (SLS) separately.

The advanced approach is done using the guidelines provided in RTD 1016-1:2020. The optimization is carried out at the critical locations based on the verification of the strength (ULS) and verification of the crack width (SLS). The advanced approach for verifying the strength is done according to the GRF method, in which the design value of the load P_d is computed by dividing the ultimate load P_u with the global resistance factor γ_0. For the crack width verification, an indirect method provided in the RTD 1016-1:2020 guidelines, and a direct method using the slip curve is used. The indirect method is a multiplication of the average strain of the reinforcement $\bar{\varepsilon}_s$ with the maximum crack spacing $S_{r,max}$, and the direct method a summation of the relative displacement (slip) by adopting a bond-slip model.

A 3D model with a length of one meter is built in Diana FEA using volume elements and a physical nonlinear analysis is performed at the critical locations with the conventionally designed reinforcement to meet the ULS and SLS. Performing the advanced approach for verifying the strength, the ULS unit check is less than the ULS unity check of conventional approach at locations 1 and 2, which mean that the structure is safe and there is room for optimization.

Performing the advanced approach using the indirect method for verifying the crack width, the SLS unity check is less than the conventional SLS unity check at location 2 but not at location 1. By adopting a bond slip-model, measuring the crack spacing from the analysis, and using the indirect method, the SLS unity check is less than the conventional SLS unity check at both locations. When the direct method is used for verifying the crack width, the SLS unity check is less than the SLS unity check using the indirect method. Based on the results of the crack width verification means that there is room for optimization.

Using the favorable optimization results, two design methods are applied: one that reduces the quantity of steel by optimizing the reinforcement and another that reduces the amount of concrete by optimizing the geometry. When optimizing the reinforcement based on the ULS, 7% less steel is being used, and optimizing the geometry 8% less concrete. When optimizing the reinforcement based on the SLS, 23% less steel is being used, and optimizing the geometry 22% less concrete.

Taking a look at the CO_2 footprint, optimizing the reinforcement based on the ULS results in 2% less CO_2 emission and optimizing the geometry in 7% less emission. Optimizing the reinforcement based on the SLS results in 8% less CO_2 emission and optimizing the geometry in 15% less emission. These results are based on a relieving platform with a length of 220 meters.

Table of Contents

List of tables

List of figures

List of symbols

L	:	Length
b	:	Width
h	:	Height
Ø	:	Diameter
I	:	The moment of inertia
u	:	Displacement
ε	:	Strain
σ	:	Stress
υ	:	Poisson's ratio
γ	:	Volumetric weight
γ_{dry}	:	Volumetric weight earth dry
γ_{wet}	:	Volumetric weight earth wet
γ_{water}	:	Volumetric weight earth water
λ_0	:	Neutral earth pressure
λ_a	:	Active earth pressure
δ	:	Angle of friction
β	:	Reliability index
G_k	:	Characteristic value of the permanent loading
Q_k	:	Characteristic value of the variable loading
A_d	:	Accidental loading
γ_G	:	Partial factor for permanent loads
γ_Q	:	Partial factor for variable loads
ψ	:	Reduction factor
al	:	Spreading distance from the peak
d	:	Effective depth
c	:	Reinforcement cover
l_{bd}	:	Anchorage length
$l_{b,rqd}$	:	The required anchorage length
τ_{bf}	:	The design value of the ultimate bond stress
E_{cm}	:	Young's modulus of concrete
f_{ck}	:	Characteristic compressive strength
f_{cm}	:	Mean compressive strength
$f_{ctk;0.05}$	:	Lower-bound characteristic tensile strength
f_{ctm}	:	Mean tensile strength
E_s	:	Young's modulus of steel
f_{yk}	:	Characteristic yielding strength
f_{tk}	:	Characteristic ultimate strength
G_F	:	Fracture energy
G_c	:	Compressive fracture energy
h_{eq}	:	Equivalent length
w_k	:	The design crack width
ε_{sm}	:	The mean reinforcement strain
ε_{cm}	:	The mean concrete strain between the cracks

$S_{r,max}$	:	The maximal crack spacing
$\rho_{s,eff}$	:	Effective reinforcement ratio
$A_{c,eff}$	:	Effective concrete area
$h_{c,eff}$	:	Effective height
α_e	:	Ratio modulus of elasticity
$\phi_{s,eq}$	:	The equivalent diameter of the reinforcing bars
n	:	Amount of rebars
M_z	:	Bending moment around the local z-direction
V_y	:	Shear force in the local y-direction
N_x	:	Normal force in the local x-direction
M_{yD+}	:	Design moment in y-direction on positive surface
M_{yD-}	:	Design moment in y-direction on negative surface
N_{yD}	:	Design force in y-direction
Q_{maxb}	:	Maximum shear force perpendicular to the plane

Abbreviations

ULS	: Ultimate Limit State
SLS	: Serviceability Limit State
NAP	: Normaal Amsterdams Peil
GRF	: Global Resistance Factor
FEA	: Finite Element Analysis
OWL	: Outer Water Level
GWL	: Ground Water Level

1
Introduction

The Port of Rotterdam has the ambition to reduce the footprint for building new quay walls, this is in line with their ambition to reduce the footprint and with national goals to limit global warming. The aim is to use less materials and/or use different design solutions.

Quay walls are earth-retaining structures at which ships can berth and transfer goods. Larger quay walls consist of a combined retaining wall from steel tubes and intermediate sheet piles. On top of this steel structure, a robust concrete relieving platform is placed that is supported by the combined wall at the waterside and piles at the land side. Horizontal stability is provided by anchors. The anchors are, dependent on the design, connected to the front or the back of the relief structure. The relief floor bears a part of the topsoil layers and terrain loads, which results in lesser vertical and horizontal soil stresses at the back of the combined retaining wall [1]. In Figure 1 the quay wall of Engie that is used as reference in this thesis is shown.
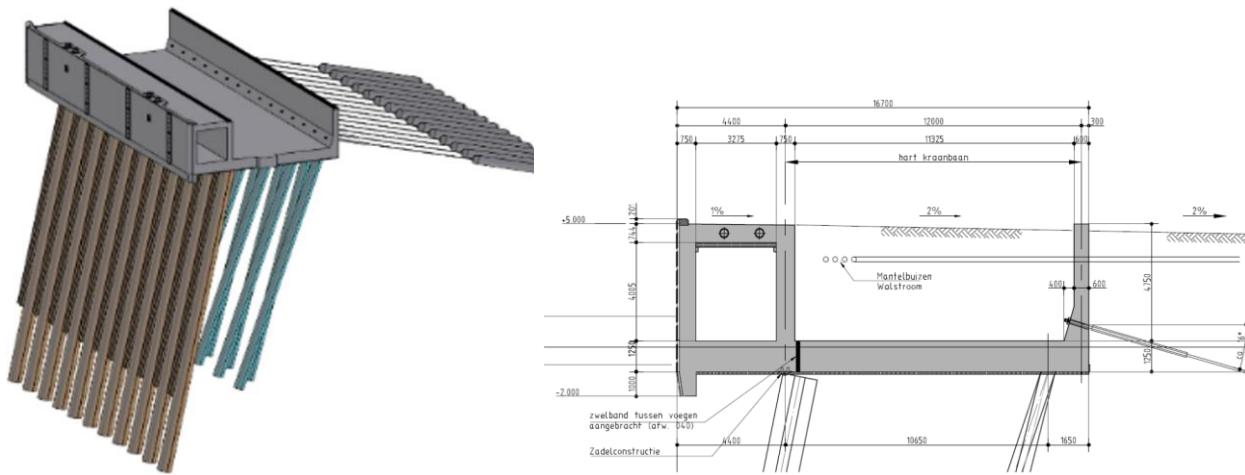
Figure 1. Cross-section quay wall with relieving platform [2]

Building activities lead to the depletion of natural resources such as fossil fuels, minerals, metals, and other raw materials. These activities also have an impact on global warming due to the emission of CO_2 and other greenhouse gases such as CH_4, N_2O, and CFCs. Although CO_2 is commonly mentioned in discussions and publications, this should imply that the effect of other greenhouse gases is also considered and that all are related to and expressed as CO_2- equivalents. Aside from global warming, a variety of other environmental effects, known as environmental impact categories, have an impact on the environment [3].

1.1. Problem description

The concrete relief floor of the quay with the front wall is constructed in massive, reinforced concrete with large dimensions resulting in sections approximately 35 meters in length containing 1000 m^3 concrete. These reinforced structures are designed in a conventional way and the internal forces are determined by performing a Linear Elastic Analysis using conventional software such as SCIA-Engineering. The reinforcement is calculated using the internal forces and is based on the Eurocode 1992 -1-1.

The linear analysis is presumed to be a lower-bound approach, meaning that the equilibrium of the stress distribution is satisfied without exceeding the yield conditions. The Eurocode's unity checks are also conservative, and as a result, it can be assumed that this method is at the safe side.

Some of these assumptions are the following:

- Plane cross-sections remain planar and normal to the neutral axis of the member before and after deformation (Euler Bernoulli hypothesis).
- Deformed beam angles (slopes) and displacement of the structure are small with respect to the dimensions.
- The stress-strain relationship is linear, meaning that the stiffness remains constant and does not change when the material starts to crack.
- The material does not experience any plastic deformation or creep during loading.

These assumptions do affect the amount of concrete and steel being used, which influences the CO_2 footprint, the reliability of the structure, and also the costs.

The problem statement for this master thesis is the following:

"It is unknown how large the effects of the conventional method's assumptions are on the amount of concrete and steel being used and can only be investigated using nonlinear advanced calculations."
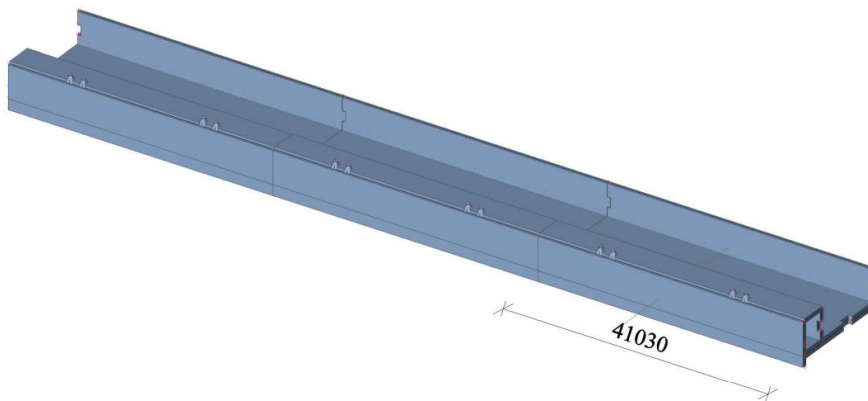
Figure 2. Overview example conventional model [4]

Research questions

The primary research question related to the problem is as follows:

"To what extent can the amount of steel and concrete of the quay wall be reduced by optimizing the reinforcement or the dimensions using nonlinear advanced calculations based on volume elements?"

The following sub- research questions are formulated in order to address the primary research question:

   I.   Which parts of the quay wall are important to model in a more advanced way?
  II.   Which limit state, SLS or ULS, is governing when determining the reinforcement using the conventional approach?
 III.   How to optimize the reinforcement or dimensions based on the SLS and ULS using the advanced approach?

IV.   How much does the conventional and advanced design differ in terms of the amount of steel and concrete?

V.   Which design strategy offers a more effective design in terms of the CO_2 footprint? Optimizing the reinforcement or the geometry?

<u>Research Objective</u>

The following research objective is defined:

"To determine to what extent the use of concrete and steel is reduced by further optimizing the reinforcement or the dimensions of the quay wall based on the limit states using nonlinear advanced calculations based on volume elements".

1.2. Scope of the study

In the context of the project "Biomassakade ENGIE", additional Cargo shipments of wood pellets are expected for the purpose of co-firing the biomass of the powerplant of ENGIE which is located in Maasvlakte Rotterdam, where the beerkanaal merges into the Missisippihaven, next to the EMO.

As a result of this development, the Port of Rotterdam asked Arcadis to design a new retaining structure M7 (approx. 220m) at the EMO terminal, that should be built in line with the existing M6 Quay.

The newly designed quay wall is used as a reference where the main focus of this study lies in the relieving platform (superstructure) of the quay. The quay wall was never built because the project was cancelled.

In Figure 3 an overview of the location of the quay wall of ENGIE is shown.
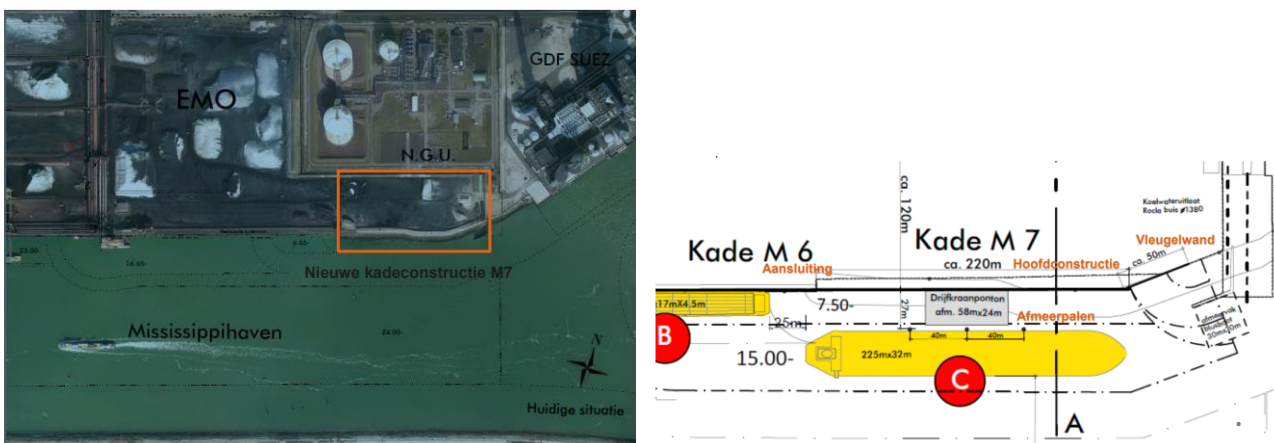
Figure 3. Overview location quay wall at EMO-site

1.3. Research approach

First, a literature study is performed on the design and loads acting on the quay wall, conventional and advanced modeling strategies, linear/nonlinear analysis, and safety formats.

Subsequently, the research phase begins, which is divided into two stages, namely the modeling and optimization stage. The modeling phase is separated into two models: conventional approach and advanced approach.

For the conventional approach a 2D-model is built using Scia-Engineer, followed by a 3D model, also called 2.5D model. Using these models, the critical locations are identified, and the reinforcement is calculated conventionally with the use of Idea Statica at these locations.

For the advance approach, a 3D model of the quay wall with a length of one meter is built in Diana FEA. A linear elastic analysis is performed to compare result of the results of the advanced model with the conventional model. Next, the conventional designed reinforcement and the governing load combinations at the critical locations are modeled in Diana FEA, and a physical nonlinear analysis is performed based on the ULS and SLS-conditions. For the SLS, the crack width is determined with and without using a bond-slip model. These findings enable us to determine whether further optimization of the structure is possible or not.

After the optimization rate is gained from the physical nonlinear analysis, the optimization stage begins. This is carried out to determine if the optimization rate is correct by optimizing the reinforcement or the geometry. The geometry is also optimized to get a better design insight in terms of reducing the CO_2 footprint.

Lastly, the comparison stage begins where amount of reinforcement, concrete and the CO_2 footprint are compared between the conventional and advanced model.

In Figure 4 a summary of the research procedure is given.
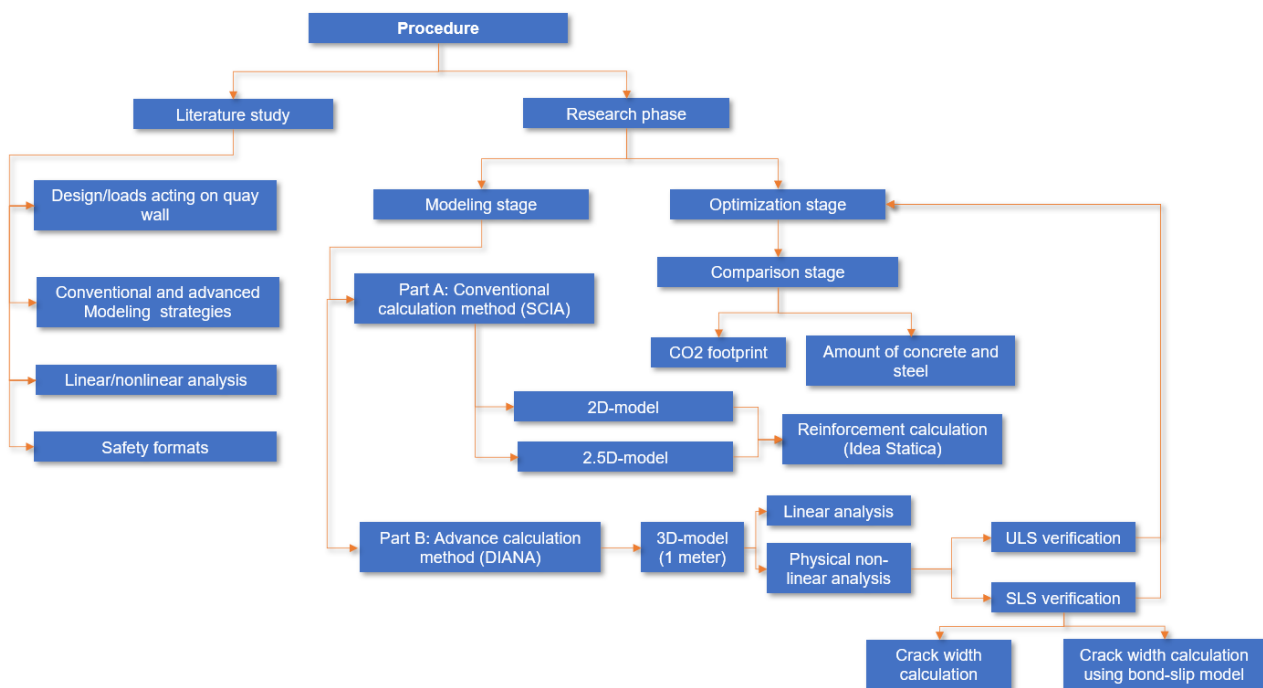
Figure 4. Research approach

TUDelft

1.4. Structure of the report

This thesis consists of eight chapters.

In the first chapter, the introduction is given. The problem statement, research objective, research questions, and the scope of the study are also explained in this chapter.

The second chapter contains a part of the theoretical background, which consist of information about the design and loads acting on the quay wall, modelling strategies, linear/nonlinear analysis, safety formats, and the crack width development. Theoretical background about the strength and crack width verifications using the advanced approach is given in chapter four.

The third chapter contains information about the conventional approach. The modeling assumptions are explained and a 2D and 2.5D model is built using Scia – Engineering. A linear analysis is then performed to determine the internal forces, which are then used to calculate reinforcement conventionally using the software package Idea Statica. In Idea Statica the reinforcement calculations are based on NEN-1992-1-1.

The fourth chapter contains information about the advanced approach. A 3D model is built using Diana FEA, and the modeling assumptions for performing a linear and nonlinear analysis are explained. A linear analysis is carried out, followed by a physical nonlinear analysis to determine if optimization is possible using the advanced approach.

In the fifth chapter, the reinforcement and geometry are optimized based on the optimization rate of the ULS and the SLS gained from the advanced approach. This is carried out to determine if the optimization rate is correct.

In the sixth chapter, the amount of steel, concrete, and CO_2 are compared between the conventional and advanced approach.

The general conclusion and recommendations are given in chapter seven and eight separately. The references and appendices can be found at the end of the thesis.

TUDelft

2
Theoretical background

2.1. General quay walls

Quay walls are earth-retaining structures where a ship can berth and transfer goods. This saves space and increases port efficiency compared to situations where there is a slope. Cranes, trucks, and trains can get close to the ship, and the freight can be managed easily.

There are different types of quay walls, such as:

- Gravity walls
- Sheet pile walls
- Structures with relieving platforms
- Open Berth quays

For this thesis, a structure with relieving platform will be examined.

2.1.1. Structures with relieving platforms

The presence of a relieving platform in this type of quay significantly reduces the horizontal load on the front wall. The relieving platform ensures that forces are distributed both horizontally and vertically concerning the superstructure. The foundation system used for these structures provides both horizontal and vertical stability to the quay wall and consists of a load-bearing sheet pile wall (combi-wall) on the waterside and usually a system with tension piles and compression piles on the landside. The connection
between combined wall and superstructure consists of an eccentric hinge with a steel saddle, thus reducing the bending moments in the wall [1]. Also, using a hinge connection result in a system that is more statically determined. In some cases, horizontal anchoring is used instead of a tension pile system. The concept of the saddle connection between the combi-wall and superstructure is shown in Figure 5.
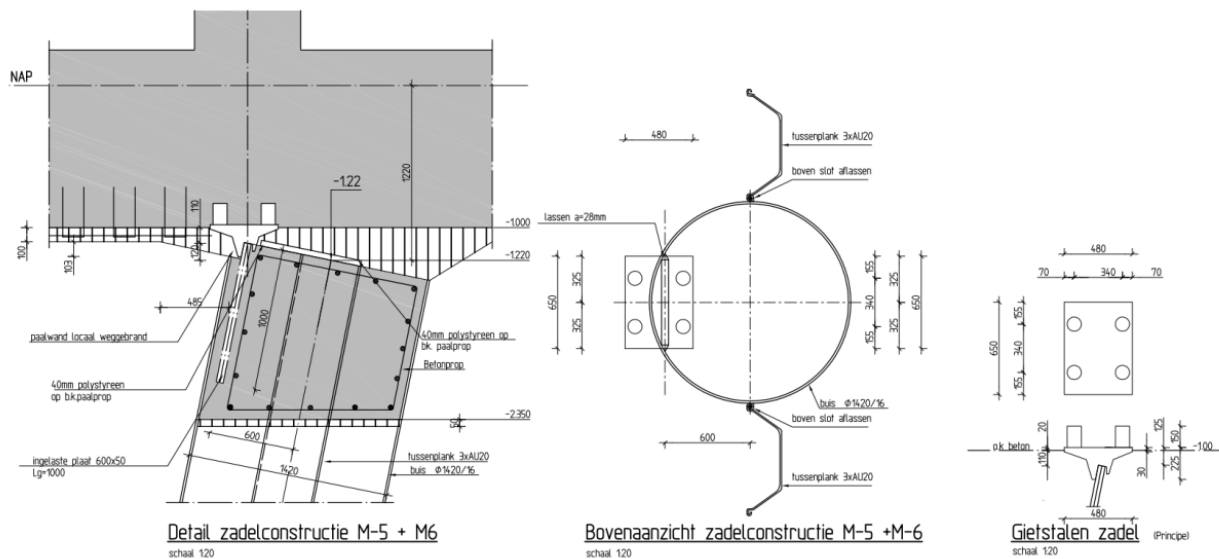
Figure 5. Principle saddle connection between combi wall and superstructure [2]
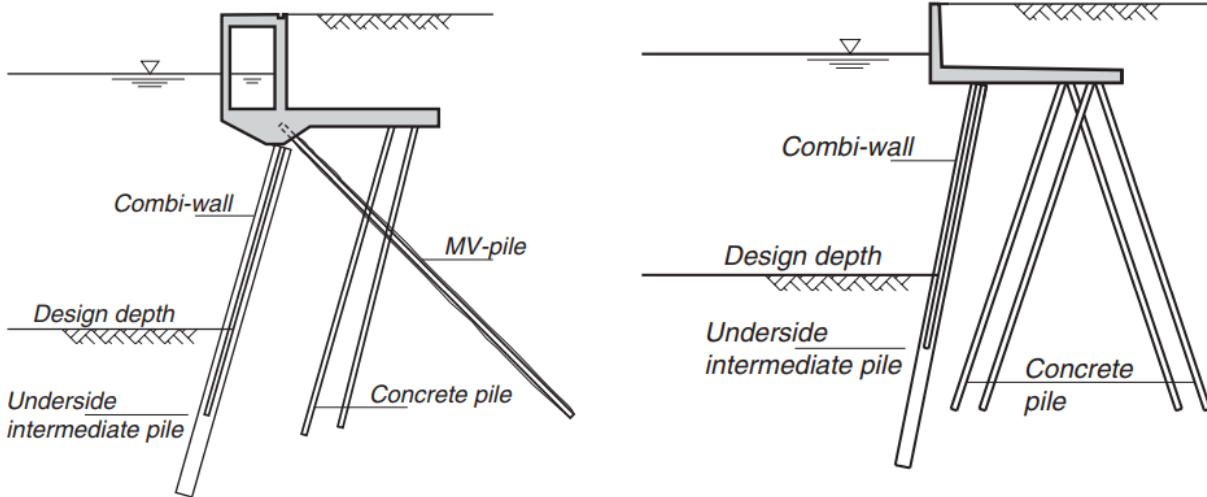
Figure 6. Quay wall with hollow box relieving platform (left) and L-shaped relieving platform (right) [1]

Figure 6 illustrated two different kinds of quay walls with a relieving platform. The use of a relieving platform primarily reduces active earth pressure on the uppermost part of the sheet pile wall. The most significant effects are cost savings on sheet piles due to a reduction in bending moment and pile depth. When the relieving platform is located on or just below the level of the quay deck, the reduction is mostly limited to the surcharge of crane, storage, and traffic loads. The earth pressure-reducing effects are much greater when deeper relieving structures are made [1]. Using deeper relieving structures, the ground water is a limited factor. Below the groundwater level, the active earth pressure increases less, while it becomes more complex to install the floor there. Consequently, a deeper relief floor requires a larger front wall.

2.1.2. Loads on the relieving platform

When modeling the relieving platform, the following general loads are considered:

- Permanent loads (remain constant over time):
    - The self-weight of the superstructure
    - The earth pressure and water pressure that result from the weight of the soil at various water levels
    - Loads resulting from the substructures (anchor/ pile forces)
- Variable loads (varies over time):
    - Loads caused by earth pressures as a result of terrain loads
    - Mooring loads such as bollard – and fender loads
    - Crane loads
    - Temperature loads
    - berthing, traffic, and surcharges behind the superstructure
    - Pile and anchor forces
- Accidental loads (low chance of occurrence):
    - Loads as a result of extreme water levels
    - Collision loads (ships)
    - Ice loads
    - Seismic loads
    - Pile and anchor forces

2.2. Modeling strategies

In this paragraph the modeling strategies for the conventional and advanced approach are explained.

2.2.1. Conventional modeling strategies

For the conventional approach a 2D model is built using beam elements, and a 3D model using Shell elements. The use of shell elements in three-dimensional space is also called 2.5D. This is carried out in chapter 3.

Beam elements

Beam elements are structural elements that meet the requirement that the dimensions perpendicular to the element axis are small in comparison to the length of the element. Axial deformations, shear deformations, curvature, and torsion are all possible in beam elements, which allows them to characterize axial force, shear force, bending moments, and torsional moments [5].

Most classical beams are two-node straight elements. The behavior of beams under axial stresses and bending is modeled by the Euler-Bernoulli beam theory. This theory is a simplified version of the linear elastic theory that enables the calculation of the load-carrying and deflection properties of beams. The two primary assumptions of the Euler-Bernoulli theory are [5]:

- The plane sections remain plane
  This assumption implies that any section of the beam that was planar prior to its deformation will remain plain when the beam deforms. Also, any section of a beam that was perpendicular to the neutral axis before deformation will stay perpendicular to the neutral axis after deformation. Figure 7 illustrates the plane sections remain plane assumption.
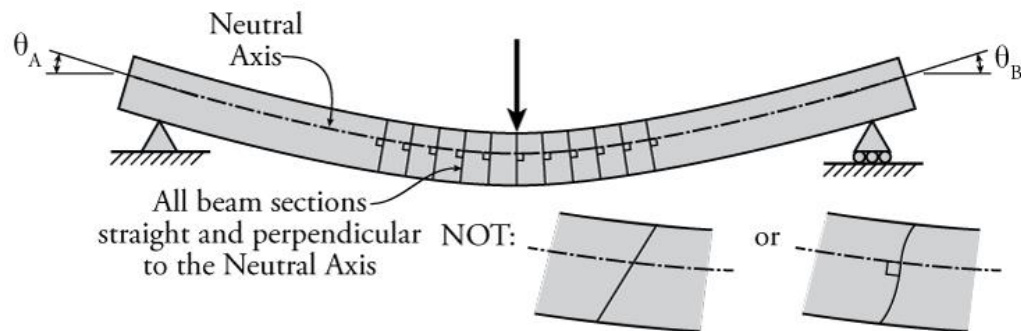
Figure 7. Plane section remain plane assumption [5]

- Deformations of the beams are small
  This assumption has the following benefits:
    - If x is the point along the length of the beam and $\Delta(x)$ is the deflection of the beam at x, then the slope θ of the beam is:

$$\theta = \frac{\partial \Delta(x)}{\partial x} \qquad (2.1)$$

If the slope is small, the square of the slope is twice as small and can be considered to be zero.

$$\theta^2 = \left(\frac{\partial \Delta(x)}{\partial x}\right)^2 \approx 0 \qquad (2.2)$$

Additionally, for small angles, the following approximations are acceptable.
$$\sin \theta \approx 0 \qquad (2.3)$$
$$\cos \theta \approx 1 \qquad (2.4)$$

The Euler-Bernoulli beam theory results in the following equation based on the assumptions given above:

$$\frac{\partial^2 \Delta}{\partial x^2} = \frac{M}{EI} \qquad (2.5)$$

Where,

$\frac{\partial^2 \Delta}{\partial x^2}$ = Second derivative of the deflection of the beam concerning location x along the beam
M = internal bending moment in the beam at location x
E = Young's modulus
I = the moment of inertia
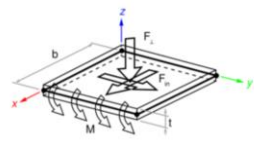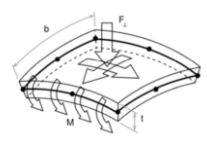
Shell elements

Shell elements are mathematical simplifications of volume elements, explained in chapter 2.2.3. Shell elements can save a lot of time because they allow you to model thin features with fewer elements than volume elements. They are also easier to mesh, and they are less likely to cause negative Jacobian errors, which can happen when employing extremely thin solid features [6]. In Table 1 the properties of shell elements are shown.

Table 1. Properties shell elements

Shell elements	
Shape dimensions	2D (flat shell elements) 3D (curved shell elements)
Topological dimension	2D
Assumed stress field	3D
Displacement field	3D
Degree of freedom per node	3 translations and two rotations ($u_x,u_y,u_z, \varphi_x,\varphi_y$)
Interpolation scheme	Linear, quadratic, and cubic
Integration scheme	Numerically integrated

Flat shell elements are a combination of plane stress elements and bending elements. Unlike the plane stress elements, the basic variables are forces rather than Cauchy stresses.

Curved Shell elements are based on degenerated solid elements by introducing two shell hypotheses:

- Thick shell elements (straight normal)
    - Can consider stresses throughout the thickness of the shell in the direction normal to the middle surface.
    - Transverse shear deformation is included.
- Thin shell elements (zero-normal-stress)
    - Do not consider the stress in the direction perpendicular to the shell surface ($\sigma_{zz} = 0$).
    - Thickness (t) must be small in relation to the largest dimensions (h) in the plane of the element (t/h ratio) [7].

2.2.2. Advanced modeling strategies

For the advanced approach a 3D model is built using volume elements. This is carried out in chapter 4.

Volume elements
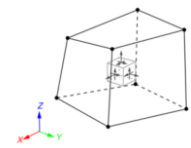
Volume (solid) elements are elements that can be used for a variety of purposes. However, because of their tendency to produce large systems of equations (large computational time), these elements are usually applied only when other elements are unsuitable or would produce inaccurate analysis results [7]. Additionally, using solid elements gives a closer representation to reality compared to beam and shell elements.

Solid elements are characterized by the following properties:

- The stress situation is three-dimensional.
- Loading can be done in any way you choose.
- The dimension in three axial directions X, Y and Z are of the same order of magnitude.

In Table 2 the properties of volume elements are shown.

Table 2. Properties volume/solid elements

Volume/solid element	
Shape dimensions	3D
Topological dimension	3D
Assumed stress field	-

Displacement field	3D
Degree of freedom per node	Displacement (u_x, u_y, u_z)
Interpolation scheme	Isoparametric mapping from global (xyz) coordinate system to a $(\xi \eta \zeta)$ local coordinate system.
Integration scheme	Numerical integration

2.3. Linear and-nonlinear analysis

Linear elastic analysis

A linear elastic analysis is an analysis where a linear relation holds between applied forces and displacements. In practice, this applies to structural problems where stresses remain in the linear elastic range and where the deformations have a small impact on the force direction of the used material. In a linear elastic analysis, the model's stiffness matrix is constant, and the solving process is relatively short compared to a nonlinear analysis of the same model. Therefore, for a first estimate, linear static analysis is often used before performing a fully nonlinear analysis [8].

Nonlinear analysis

A nonlinear analysis is an analysis where a nonlinear relation holds between applied forces and displacements. Nonlinear effects can originate from geometrical nonlinearity (i.e., large deformations), material nonlinearity (i.e., elastoplastic material), and contact nonlinearity. These effects result in a stiffness matrix that is not constant during the load application. This is opposed to the linear static analysis, where the stiffness matrix remained constant. As a result, a different solving strategy is required for the nonlinear analysis and therefore a different solver [8].

- Material nonlinearity
  Material nonlinearity involves the nonlinear behavior of a material in which material properties are functions of the state of stress or strain (e.g., nonlinear elasticity, plasticity, cracking, creep) [9].

- Geometric nonlinearity
  When performing an analysis involving geometric nonlinearity, the constitutive and equilibrium equations consider how the structure's geometry changes as it deforms. The deformation is large enough that the equilibrium equations must be written concerning the deformed structure (e.g., buckling slender column, deformation of a cable). Also, the loads may change direction as they increase [9].

- Contact nonlinearity
  Contact nonlinearity in a system can occur if kinematic constraints are presented in the model. By constraining a model's movement, one can limit the kinematic degree-of-freedom [8].
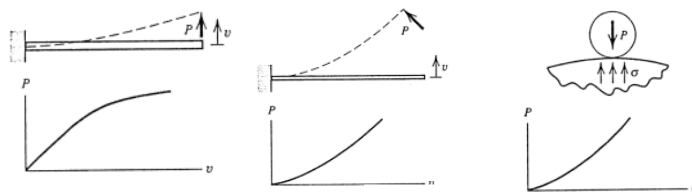
Figure 8. Material-vs geometric-vs contact nonlinearity [9]

The relationship between the load and the displacements is defined by the stiffness matrix for the structural system. In short, the stiffness matrix remains constant when completing a linear analysis, whereas this is not the case for a nonlinear analysis, which is a significant distinction between linear and nonlinear analysis. Also, calculating a linear system uses significantly less computational effort and cost than solving a non-linear system. Nonlinear analysis, on the other hand, can provide information about the structure's real behavior. While residual hidden capacity in structures is frequently present when a linear analysis is performed, these capacities become visible in a nonlinear analysis [10].

TUDelft

2.4. Safety formats according to the fib Model Code 2010

Verification of a structure with respect to a particular limit state is carried out via a model describing the limit state in terms of a function (called the limit state function) whose value depends on all relevant design parameters [11].

This fib Model Code 2010 recommends for verification of the limit states to use one of the following safety formats:

- Probabilistic safety format[1]
  The probabilistic safety format (sometimes referred to as fully probabilistic design method) allows us to explicitly include the reliability requirements in terms of the reliability index (β) and the reference period (T). This may be used for structures to be designed and for existing structures in cases where such an increased effort is economically justified. However, it will seldom be used for the design of new structures due to lack of statistical data [11].

- Partial safety factor format[2]
  The partial safety factor format is the usual way of verifying structural design. It is a simplified verification concept, which is based on past experience and calibrated in such a way that the general reliability requirements are satisfied with a sufficient margin during a defined period of time [11].

- Global resistance format[3]
  In the global resistance format the resistance is considered on a global structural level, as compared to local verification of sections with partial safety factors. It is especially suitable for design based on nonlinear analysis, where verification of limit states is performed by numerical simulations [11].

The objective of the non-linear analysis is to simulate the real structural behavior and to evaluate the representative value of the resistance. Because of this the global resistance format (referred to as the global resistance factor method) is used to verify the safety of the structure. More information about this method is given in chapter 4.

2.5. Crack width development according to the fib Model Code 2010

The following information about the crack width development is obtained from the fib Model Code 2010. The estimation of the crack width is based on the standard example of a prismatic reinforced concrete bar under axial tension illustrated in Figure 9.
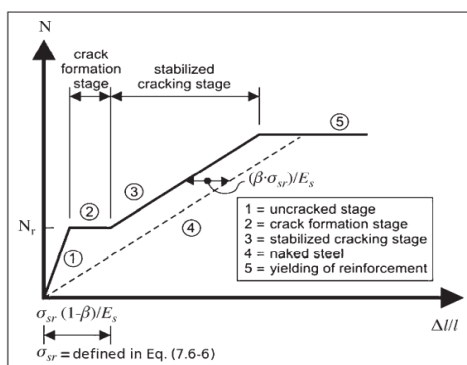
Figure 9. Simplified load - strain relation for a centrically reinforced member subjected to tension[4]

---

[1] Section 4.4 of the fib Model Code 2010
[2] Section 4.5 of the fib Model Code 2010
[3] Section 4.6 of the fib Model Code 2010
[4] fib Model Code 2010: Figure 7.6-2: Simplified load- strain relation for a centrically reinforced member subjected to tension.

Four stages are identified concerning the behavior under increasing tensile strength:

- **The uncracked stage (1)**: in the first linear branch the concrete is uncracked. In this stage, the tensile strength of concrete has not yet been reached. The stiffness is constant, and the behavior of the tensile member is linear.
- **The crack formation stage (2)**: when the cracking load N_r is reached, the crack formation starts. In this stage, the tensile strength of concrete has been reached, which causes cracks to develop. Once the concrete cracks, the perfect bond between the concrete and steel dissolves. The steel stress increases due to the redistribution of stresses until all of the tension is transferred to the steel. The bond stresses will be reintroduced further from the crack at the steel-concrete interface. As a result, the steel force is transferred to the concrete through bond stresses caused by slip between the concrete and the steel due to a difference in deformations after cracking [10]. When there are no longer any undisturbed areas due to the formation of cracks, the tensile strength of concrete can no longer be reached between the cracks, preventing no new cracks to appear.
- **The stabilized cracking stage (3)**: after the completion of the crack formation stage the force N increases. In this stage, no new cracks are formed, but the existing cracks are widened due to the elongation of the steel reinforcement. This is because the bond stress and concrete deformations stay constant. The load in this range may increase due to an increase in steel stress.
- **The steel yielding stage (5)**: in this stage, the yield strength of steel has been reached. Also, the reinforcement concrete beam behaves fully plastic in this stage.

The N - ε relation of the steel reinforcement is shown by the dotted line (4) [11].

The first crack will form at the weakest spot in the structure, and each subsequent crack will occur at a location where the tensile strength of the concrete is slightly higher. Therefore, the most accurate description might be to use the lower bound 5% characteristic concrete tensile strength for the first crack and to end with the mean tensile strength for the last crack [11].

2.6. Bond-slip model according to the fib Model Code 2010

When concrete cracks the tensile force is carried by the reinforcement. The stress on the reinforcing bars causes them to activate bond stresses, which transfer the force to the surrounding concrete. The steel force is gradually transferred to the concrete through the bond between concrete and steel.

Bond is the term used to denote the interaction and transfer of force between reinforcement and concrete. Bond influences the performance of concrete structures in several ways. At the serviceability limit state, the bond influences the width and spacing of transverse cracks, tension stiffening, and curvature. At the ultimate limit state, the bond is responsible for the strength of end anchorages and lapped joints of reinforcement and influences the rotation capacity of plastic hinge regions [11].

The following considerations apply about the development of bond stresses:

- Reinforcement and concrete have the same strain in those areas where the steel is in compression and in those areas where steel is in tension in uncracked parts of the structure.
- In cracked cross-sections tension forces are transferred across the crack by the reinforcing steel. In general, the absolute displacements of the steel u_s and the concrete u_c adjacent to a crack are different. Due to the relative displacement (slip), $s = u_s - u_c$ bond stresses are generated between concrete and reinforcing steel [11].

The bond stress-slip relationship is modeled according to Figure 6.1-1 in the fib Model Code 2010 as seen in Figure 10. This is typically determined using standardized pull-out experiments, which must be viewed as a simplification in comparison to actual conditions within the slipping length [19]. The bond stress–slip relationship depends on a considerable number of influencing factors including rib geometry (relative rib area), concrete strength, position, orientation of the bar during casting, state of stress, boundary conditions and concrete cover. The bond stress–slip curves for confined and unconfined concrete presented in Figure 10 can be considered applicable as an average formulation for a broad range of cases [11].

The parameters of the bond-slip relationship are defined based on Table 6.1-1 in the fib Model Code 2010, which depends on the failure mode, pull-out, or splitting. Splitting failure will occur if splitting cracks can

reach the exterior surface before the steel rebar is pulled out. Two types of bond stress–slip laws can be defined for the splitting type bond failure in a specific bond condition, one is for unconfined anchorage conditions in concrete and the other is for confined anchorage conditions with stirrups [20]. Additional information about the bond-slip model can be contained in the fib Model Code 2010.
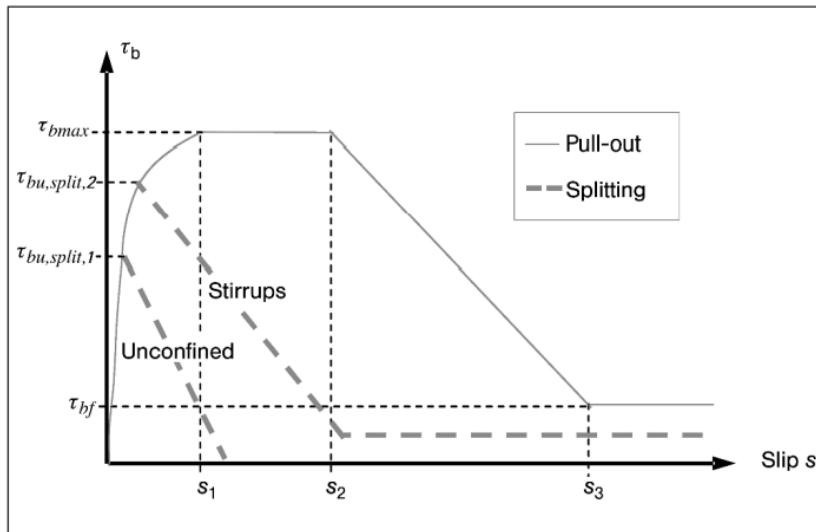
Figure 10. Bond-slip relationship according to the fib Model Code 2010

The bond-slip backbone curve consists of four sections. When pull-out failure is considered the first section spans from a slip of 0 up to s1, and it is expressed as a power function with an exponent α until it reaches the maximal bond stress τ_{bmax}. From s1 through s2, a constant value τ_{bmax} is used. The bond stress decreases linearly from s2 to s3 until it reaches the ultimate bond-slip stress τ_{bf}. Beyond s3, a constant value of τ_{bf} is considered. When spitting failure is considered the first section spans from a slip of 0 up to s1, and it is expressed as a power function with an exponent α until it reaches the peak value of the bond strength in a spitting failure mode denoted as $\tau_{bu,split}$. Additionally, s1 and s2 coincide, and the bond stress decreases linearly between s2 and s3. Beyond s3, a constant value of bond stress is considered. In the regions where the main reinforcement is located, good bond conditions and splitting is considered, and between the intersection of the wall and the floor, pull-out. The bond-slip parameters are determined in appendix II.

3
Conventional approach

In this chapter the concrete relief floor is modeled in a conventional way in 2D and 3D space. Modeling in two-dimensional space is done with beam elements, and in three-dimensional space, shell elements are used. The use of shell elements in three-dimensional space is also called 2.5D. Following that, the results of the internal forces of the two models are compared. The reinforcement is also calculated conventionally according to NEN-EN-1992-1-1. Also, the reports of Engie are used as reference for modeling the relieving platform.

3.1. Model description

The relieving platform consists of a hollow box system (wall A, wall B, deck), a concrete relieving floor, and a back wall (wall C). The substructure consists of a combi-wall and bearing piles to ensure vertical stability, and anchors to provide horizontal stability. Additionally, using a hollow box system reduces the soil weight on the combi-wall.

In Figure 11 the different structural elements in the model are shown.
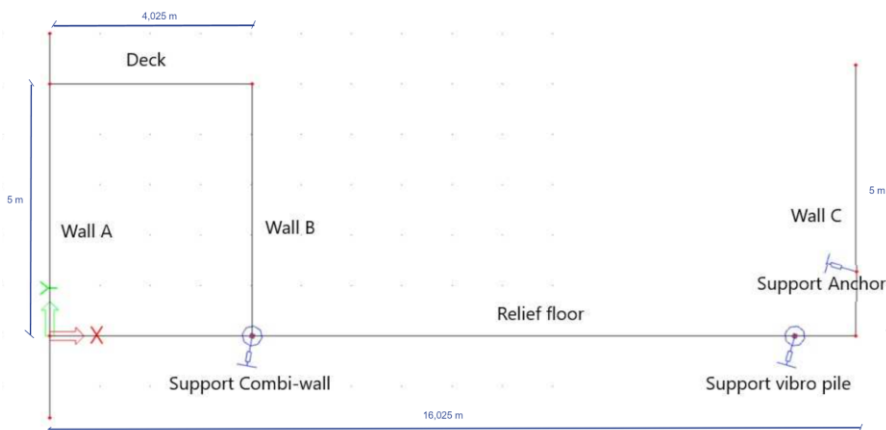
Figure 11. 2D cross-section conventional model (Scia)

In the case of Engie, the dimensions of the different concrete elements are given in Table 3, which will also be used in this thesis.

Table 3. Dimensions relieving platform

Structural element	Thickness [mm]	Length [m]
Wall A	750	5.000
Wall B	750	5.000
Wall C	600	5.000
Relief floor	1250	16.700
Deck	750	4.775

The top part of the tube is at NAP +5.00 m and the bottom at NAP -2.00 m. The top of the relief floor is at NAP +0.25 m and the bottom at NAP -1.00 with a thickness of 1.25 meters and a total width of 16.7 meters. In reality, the relieving platform consist of six sections with a total length of approximately 220 meters. For simplicity reasons, only one section is modeled with a length of 40 meters. The water levels are given in chapter 3.2.3.

In Figure 12 the geometry of the relieving platform with the dimensions is shown.
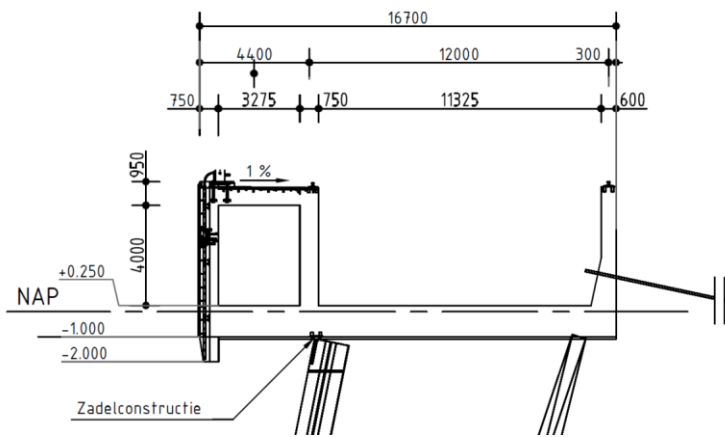
Figure 12. Geometry of Engie relieving platform

3.2. Modeling assumptions relieving platform

In this paragraph, the assumptions for modeling the relieving platform are explained. In reality, the retaining structure consist of six sections that are connected to one another with a joint in between. The joint effectively has a certain stiffness that transfer the forces to the adjacent sections. For simplicity reasons, one section has been modelled without a joint in between.

3.2.1. Material

Concrete

Concrete is a well-known material in the hydraulic engineering field because of its strength and resistance to extreme conditions. However, the development of cracks in hydraulic structures requires specific attention. These structures often have large dimensions, so extra care should be given to prevent significant temperature differences during the hardening period. Precautions should be taken to prevent or manage this phenomenon because this heat formation can cause cracks to emerge during the hardening process [12].

The concrete mix, execution, and curing affects the concrete's strength. During loading, the stiffness of concrete can change. Cracked concrete has an effective stiffness that is about 1/5-1/3 of uncracked concrete. 1/5 applies to the effective membrane stiffness, and 1/3 to the effective bending stiffness.

For the design of the quay wall of Engie, cracked concrete with concrete class C30/37 is used. As a starting point, this will also be used for the conventional approach in this thesis. In Table 4 the concrete properties are shown.

Table 4. Concrete properties

Concrete class	Volumetric weight [kg/m3]	E-Modulus [MPa]	Characteristic compressive strength (fck) [MPa]
C30/37	2500	32837	30
C30/37 (cracked)	2500	20000	30

The concrete requirements shown in Table 5 are based on NEN-EN 1992-1-1.

Table 5. Concrete requirements

	Requirement	Value
Environmental exposure conditions	Corrosion induced by carbonation	XC4
	Corrosion induced by chlorides	XD3
	Corrosion induced by chlorides from sea water	XS3
	Freeze-thaw attack with or without de-icing agents	XF4
	Chemical attack	XA2
Construction class		S4
Concrete cover	Minimum	45 mm
	In-situ	50 mm
Reinforcement steel		B500B
Crack width (norm)	Follows from environmental exposure conditions	0.22 mm

The concrete cover and crack width are determined using NEN-EN-1992-1-1, which is explained in Appendix I. In environmental class XC4, the National Annex to Eurocode 2 allow a maximum calculated crack width of 0.22 mm. If the relief floor is permanently under water (XS2), it is acceptable to depart from this standard. This is due to the extremely low probability and potential consequences of corrosion. Prof. Polder states that a maximum crack width of 0.4 mm as an upper limit is permissible [13]. In the case of Engie, the relief floor is not permanently under water (XS3) during extremely low water levels, so deviating from the norm is not permissible. In this thesis, the crack width of the National Annex to Eurocode 2 will be used, which is 0.22mm.

3.2.2. Interaction supports with the substructure

The substructure consists of combi-walls, bearing piles, and horizontal anchors spread over various distances. The interaction of the relieving platform with the substructure is modeled using inclined springs with a certain stiffness and different angles. The connection of the inclined spring supports with the superstructure is simulated by the forces occurring in the head of the combi-wall and vibro-pile. The stiffness, angle of the springs, and the forces resulting from the piles are calculated with the geotechnical software "Plaxis", obtained from the geotechnical report of the quay wall of Engie [14], and will be used in this thesis. In Table 6, the parameters of the substructural elements are given.

Table 6. Parameters substructure

Element	Angle (clockwise) [º]	Normal stiffness [MN/m]	Shear stiffness [MN/m]	C.t.c. distance [mm]
Combi- wall	10.2	240	24	3730
bearing pile	16	100	10	2280
Anchor	16	24	0	2735

3.2.3. Loading on the relieving platform

The loads acting on the relieving platform are obtained from Engie design report [2]. The loads acting on relieving platform of Engie are also applied to the relieving platform examined this thesis.

Earth pressure

The self-weight of the earth as well as surcharges are the sources of earth pressures.

In addition to horizontal earth pressures, possible vertical friction forces will develop. The maximum vertical friction force is related to the resultant of the maximum active earth pressure (Ea) and is directed downwards when passive and active pressures are activated. The maximum friction between "earth and structure" is $Ea \times \tan(\delta)$.

For determining the earth loads, the following assumptions are made:

Table 7. Assumptions for determining the earth loads

Parameters	
Volumetric weight earth dry (γ_{dry})	18 kN/m^3
Volumetric weight earth wet (γ_{wet})	20 kN/m^3
Volumetric water (γ_{water})	10 kN/m^3
Neutral earth pressure (λ_0)	0.5
Active earth pressure (λa)	0.33
Angle of the sliding plane (Φ)	30 °
Angle of the wall friction (δ)	2/3 δ

Water pressure

The magnitude of the water pressure difference over a quay wall strongly depends on the water level fluctuations at the outer side, the soil conditions, and the presence of a reliable drainage system. These loads are the result of differences between the outside water level (OWL) and the groundwater level (GWL). The water pressure difference can be minimized if the quay wall is equipped with a reliable drainage system [1].

In the case of the quay of Engie, the design is based on an existing drainage system that monitors groundwater levels on the quay's landward side. For simplicity reasons, only the fundamental and extremely low water levels are considered, because it is stated in the handbook of CUR 211 that these are often governing. In Table 8 the applied water level is shown.

![ARCADIS Design & Consultancy for natural and built assets]

Table 8. Applied water levels Engie

	OWL	GWL	Δh
Fundamental	NAP -1.00 m	NAP – 0.50 m	0.50 m
Accidental – extreme low water	NAP -2.35 m	NAP -1.35 m	1.00 m
Accidental – failure drainage	NAP -1.50 m	NAP +0.06 m	1.56 m

An example of how the water pressure is determined is shown below.

Fundamental case:
GWL: NAP – 0.50 m
OWL: NAP – 1.00 m
Top side floor: NAP + 0.25 m
Bottom side floor: NAP -1.00 m

Water pressure against bottom of the relief floor (behind combi wall): $(-0.50-1.00) \times 10 = 5 \frac{kN}{m^2}$

Water pressure against bottom of the relief floor (front combi wall): $(-1.00-1.00) \times 10 = 0 \frac{kN}{m^2}$

Water pressure against Wall C: $\frac{0.5 \times 5}{2} = 1.25 \frac{kN}{m}$
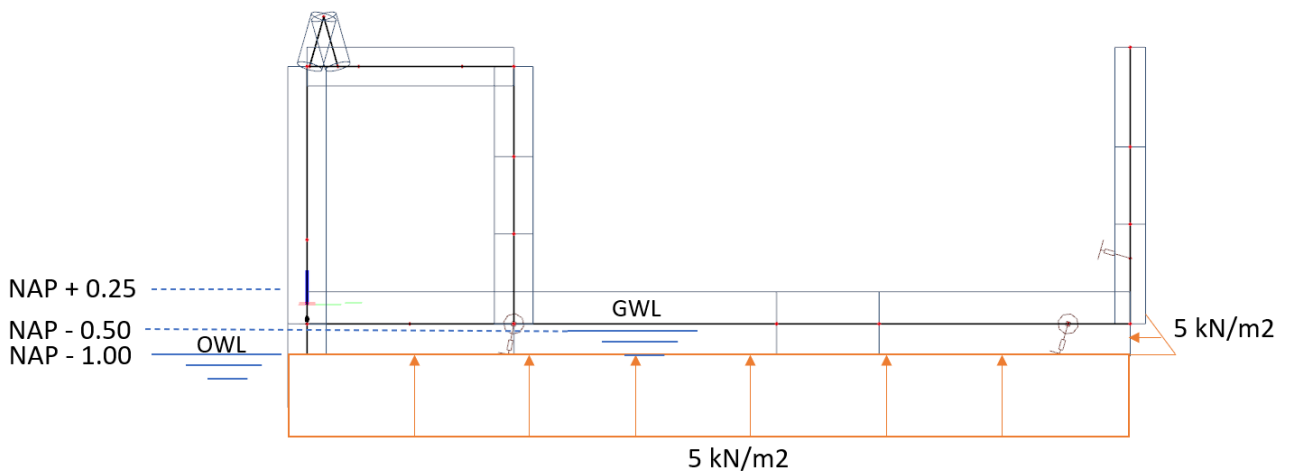
Figure 13. Water pressure relieving platform

Terrain loads
Terrain loads are active on the quay as a result of the cargo (containers and bulk products). In the case of Engie, a uniform distributed terrain load of 40 kN/m² from the front of the quay to 22.3 meters from the quay is used, followed by an increasing distributed terrain load ranging from 40 kN/m² to 230 kN/m² on 45.1 meters and then descending to 0 kN/m² at 72.7 meters, as illustrated in Figure 14.
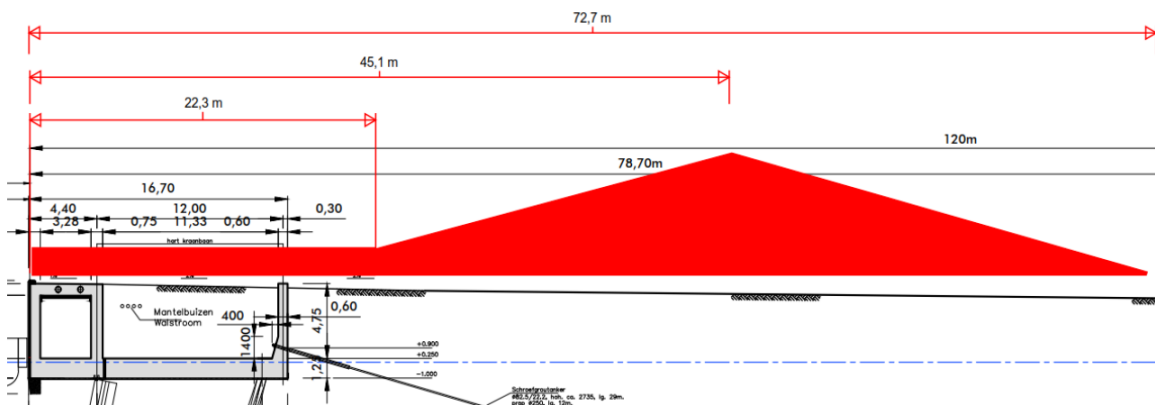
Figure 14. Surface loads assumed for "ENGIE" [2]

Also, in the case of Engie, the methodology of CUR 166[5] has been used to determine whether the increasing terrain load has an effect on the back wall of the concrete relieving platform. In Appendix 1, the calculation

[5] Handbook of CUR 166 - Chapter 4.5.4. Influence of top loads

procedure of the horizontal earth pressure is shown. From the results is stated that the earth's pressure on the back of the quay is limited. A uniform earth pressure of 20 kPa is therefore assumed across the entire height of the wall and a maximum vertical friction force of 7.28 kPa.
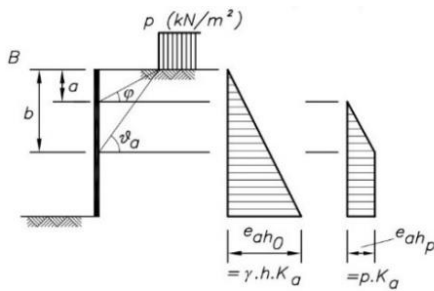
Figure 15. Horizontal ground pressure with limited top load [6](methodology of CUR 166)

Mooring loads
The mooring loads consist of bollard, and fender loads and do not occur together. Figure 16 shows a front view of the quay of Engie, including the distances between the bollards and fenders.
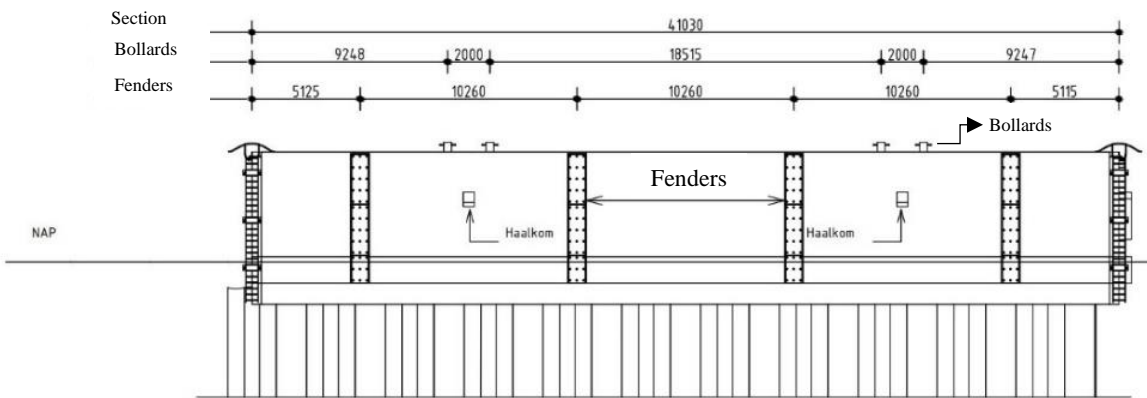
Figure 16. front view quay of Engie [2]

When a ship approaches, it is usually stopped by its own engines and partially by the use of spring hawsers. Mooring forces are thus transmitted to bollards located on the quay wall. The force on the bollards is determined by the water displacement caused by the ship. In Table 9 the characteristic values of the bollard load are given.

Table 9. Characteristic values of the bollard load[7] for ships

Water displacement [kN]	Bollard force [kN]
< 20,0000	100
< 100,000	300
< 500,000	600
< 1,000,000	1000
< 2,000,000	1500
>2,000,000	2000

The typical water displacement of ships at the Engie quay wall is less than 2,000,000 kN, resulting in a bollard force of 1500 kN per bollard. The bollards of the quay wall are placed in pairs with a horizontal load of 1500 kN. The first bollard is loaded for 100% and the second for 50 %.

When modeling in two-dimensional space, the redistribution of the loads should be considered. The bollard load is linearly redistributed through the superstructure over an angle of 45 °. The redistribution line load is

---

[6] Handbook of CUR 166 - Figure 4.40 - Horizontal ground pressure with limited top load
[7] Handbook of CUR 166 - Table 3.2 - Characteristic values of bolder loads

determined by the height of the wall, the width of the deck, and the distance between the two pairs of bollards, as shown in Figure 17.
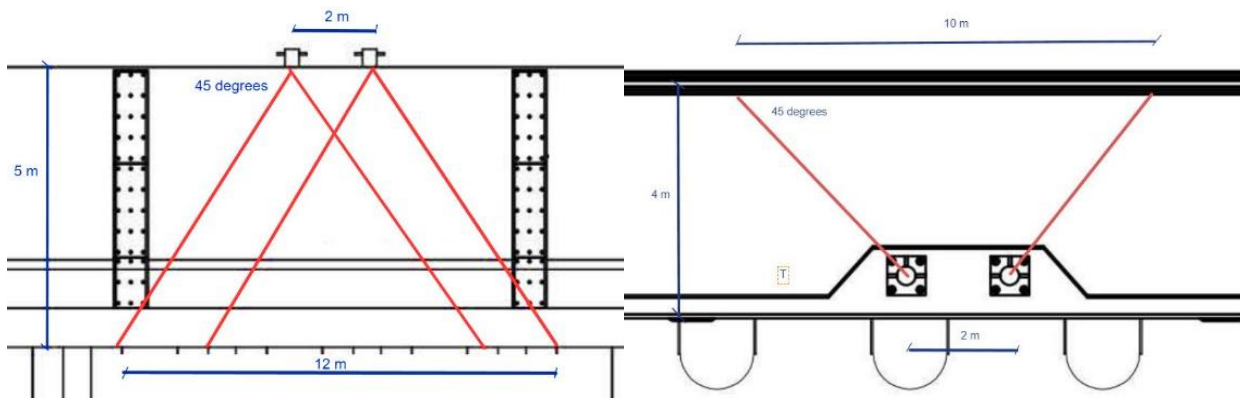
Figure 17. Redistribution of the bollard load in the wall and deck

The height of the wall is 5 meters, the height of the deck is 4 meters and the distance between the bollard pairs is 2 meters. This results in a line load of $\frac{(1500+750)kN}{((2\times5)+2)+((2\times4)+2)\ m} = 102.3\frac{kN}{m}$ spread in the wall over a distance of 22 meters.

The value of the fender loads is chosen according to the ROK standards. In the case of Engie, the fenders have a width of 0.76 meters with a uniform distributed load of 400 kN/m².

The distribution of the fender loads is almost identical to the distribution of the bollard loads. In the case of the fenders, the redistribution of the load is spread only over the wall of the superstructure over an angle of 45 °, as shown in Figure 18.
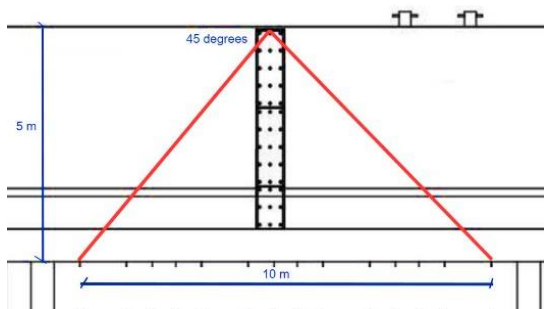
Figure 18. Redistribution of the fender loads

This results in a surface load of $\frac{(400\ \times0.76)\frac{kN}{m}}{(2\times5)m} = 30.4\frac{kN}{m^2}$ spread in the wall over a distance of 10 meters.

Crane loads
It is expected that future container cranes will be able to lift multiple containers at once. The foundation structure of such elements is crucial because the imposed loads are large. These loads include the weight of the crane, the weight of what is being lifted, wind loads, and dynamic loads produced by the crane moving and twisting. The swaying of the raised containers is the primary cause of the horizontal loads produced by the horizontal movements. The horizontal crane load ranges between 10% to 15% of the vertical crane load.

In the case of Engie, the rail of the crane is positioned 4.4 m and 16.4 meters from the front of the quay with a vertical line load of 600 kN/m and a horizontal load of 90 kN/m over a length of 20 meters parallel to the quay.
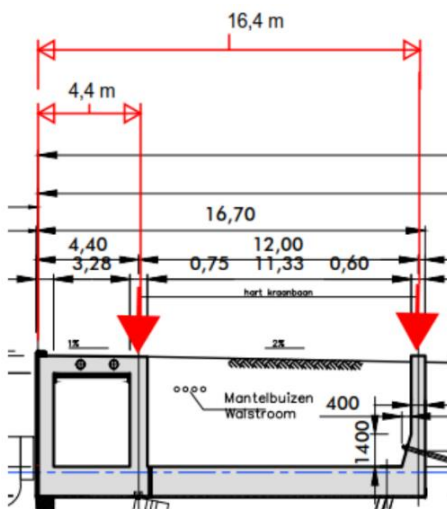
Figure 19. location of the vertical crane loads Engie [2]

Loads from substructure

The external forces resulting from the interaction of the substructure with the relieving platform are obtained from the geotechnical report of Engie [14]. In Table 63 of appendix I, the interaction loads that occur from the substructure are shown.

Wind loads

Wind loads occur at the quay's front wall. Due to the permanently available earth- and water pressure this load can be neglected.

Currents

Currents caused by passing ships are not taken into consideration (not governing). The quay wall can resist the resulting currents due to the slow vessel speeds.

Temperature loads

Seasonal influences and general climatic change are responsible for the temperature variances between the components of the structures.

Ice loads

The type of structure, the ice's features, and the environment in which the ice developed all affect how much force the ice generates. The value of the ice load is chosen according to the handbook of CUR 166[8]. In the case of Engie, an ice load of 250 kN/m is applied at the waterline.

Collison loads (ships)

In the case of Engie, the quay must bear a load of 10000 kN spread over an area of 5.0 x 5.0 meters (400 kN/m^2) operating at a level from NAP -2 m to NAP +5 m.

Seismic loads

Seismic or earthquake loads act at the center of gravity of the structure as a horizontal force equal to the design coefficient times the weight of the structure. In the calculated weight of the structure, half the live load should be added. The actual seismic load due to an earthquake will depend on the magnitude of the earthquake, the type of structure, and the soil conditions in the adjacent area. In the case of Engie, seismic loads are not considered at the location of the quay.

3.2.4. Summary loading

For simplicity reasons, only the fundamental and extremely low water levels are considered for this thesis. The water pressure resulting from the extremely low water levels is ignored, because the effect on the superstructure is limited. Also, the temperature loads, collision loads, ice loads, and seismic loads are neglected.

In appendix III, the loading on the relieving platform for the 2D-and 2.5D model is given. In the table below a summary of the vertical and horizontal loads that are used for modeling the concrete superstructure in 2D and 2.5D are shown.

---

[8] Handbook of CUR 166 – Chapter 3.2.5. Ice loads

Table 10. Summary applied loads (2D and 2.5D)

Vertical loads		2D	2.5D
	Terrain loads	40 kN/m²	40 kN/m²
	Earth pressures (due to terrain load - friction force)	7.28 kN/m²	7.28 kN/m²
	Crane loads	400 kN/m	600 kN/m
	Water pressure (uniform - upward)	5 kN/m²	5 kN/m²
	Earth pressure (fundamental - uniform)	85.50 kN/m²	85.50 kN/m²
	Earth pressure (fundamental – friction force)	11.26 kN/m²	11.26 kN/m²
	Earth pressure (accidental - uniform)	83.10 kN/m²	83.10 kN/m²
	Earth pressure (fundamental – friction force)	11.26 kN/m²	11.26 kN/m²
Horizontal loads			
	Earth pressures (due to terrain load)	20 kN/m²	20 kN/m²
	Crane loads	60 kN/m	90 kN/m
	Bollard loads	102.30 kN	1,500 kN / 750 kN
	Fender loads	30.4 kN/m	400 kN/m²
	Water pressure (triangular) (NAP -1,00 – NAP -0,50)	0 - 5 kN/m	0 - 5 kN/m
	Earth pressure (fundamental - triangular)	0 – 54 kN/m²	0 – 54 kN/m²
	Earth pressure (accidental - triangular)	0 – 54 kN/m²	0 – 54 kN/m²

3.2.5. Reliability classes

In NEN-EN 1990, the structure is divided into three consequence/reliability classes with different safety levels expressed as a reliability index. The safety class is characterized between structures that cause economic loss and those that cause human injury.

Table 11. Reliability classes and design life according to NEN-EN 1990 table B2 and table 2.1

Description of reliability classes	Reliability index (β)	Design life in years
RC1/CC1 **Consequence of failure:** - Risk of danger to life is negligible - Risk of economic damage is low	$\beta = 3.3$	50
RC2/CC2 **Consequence of failure:** - Risk of danger to life is negligible - Risk of economic damage is high	$\beta = 3.8$	50
RC3/CC3 **Consequence of failure:** - Risk of danger to life is high - Risk of economic damage is high	$\beta = 4.1$	50

Normally in the Port of Rotterdam quay walls are categorized with safety class RC2/CC2, which will be used in this thesis. The quay wall is predicted to last at least 50 years. The danger of human injury is quite low, but the chance of economic harm is extremely high due to the port's purpose (processing of cargo). At present, the Port of Rotterdam tends to move towards RC1/CC1.

3.2.6. Load combinations

The load combinations according to NEN-EN-1990 are applicable in the design of the quay wall. The characteristic value of the loads multiplied by a partial safety factor results in the design value of these loads. With these design values, the Ultimate Limit State (ULS) and Serviceability Limit State (SLS) loading

combinations can be determined. The Ultimate Limit State is the design for the safety of the structure and the Serviceability Limit State refers to the condition under which a building can still fulfil its function.

Table 12. Load combinations according to NEN-EN-1990

Limit state	Combination type	Case	Combination
ULS	Fundamental	6.10a	$\Sigma\gamma_G \cdot G_k + \Sigma\gamma_Q \cdot \psi_{0,i} \cdot Q_{k,i}$
		6.10b	$\Sigma\gamma_G \cdot G_k + +\gamma_Q \cdot Q_{k,1} + \Sigma\gamma_Q \cdot \psi_{0,i} \cdot Q_{k,i}$
	Accidental	6.11a/b	$\Sigma G_k + A_d + \psi_{1,1} \cdot Q_{k,1} + \Sigma\psi_{2,i} \cdot Q_{k,i}$
SLS	Frequent	6.15b	$\Sigma G_k + \psi_{1,1} \cdot Q_{k,1} + \Sigma\psi_{2,i} \cdot Q_{k,i}$
	Quasi-permanent	6.16b	$\Sigma G_k + \Sigma\psi_{2,i} \cdot Q_{k,i}$

G_k Characteristic value of the permanent loading
$Q_{k,1}$ Characteristic value of the variable loading
$Q_{k,i}$ characteristic value of the simultaneously occurring variable load i
A_d Accidental loading
γ_G Partial factor for permanent loads, which also considers model uncertainties and dimensional deviations
γ_Q Partial factor for variable loads
ψ_0 Reduction factor related to the combination value of the variable load
ψ_1 Reduction factor related to the frequent value of a variable load
ψ_2 Reduction factor related to the quasi-permanent value of the variable load factor
Σ Summation

Partial loading factors (γ)

For the fundamental combinations, the loading factors are based on consequence class 2 (CC2) and are determined according to NEN-EN 1997-1-1 and NEN-EN 1990[9].

Table 13. Partial loading factors (γ) fundamental combinations

Consequence class		A1 6.10a	A1 6.10b	A1 6.10a / b	A2 Other		A2 Retaining construction	
CC2		Unfavorable	Unfavorable	Favorable	Unfavorable	Favorable	Unfavorable	Favorable
Permanent	γ_G	1.35 [a]	1.20	0.90	1.00	1.00	1.00	1.00
Variable	γ_Q	1.5 [b]	1.5 [b]	0.00	1.30	0.00	1.10	0.00

Note: (a) For fluid pressure 1.2 is sufficient.
            (b) A load factor of 1.3 is recommended for horizontal loads such as the wind and horizontal crane loads.

The factors in column A1 applies to geotechnical loads on a geotechnical construction. These actions include forces from mooring, berthing and horizontal crane loads.

The factors in column A2 applies to geotechnical loads on geotechnical constructions, not being a foundation. With the factors under "other", the stability of the quay wall is checked and with the factors under "retaining construction" the strength itself (calculation and verifying of bending moment, shear force etc.) [15].

For the accidental combinations, the loading factors according to NEN-EN 1990 are applicable.

Table 14. Partial Loading factors accidental combinations[10]

Loading		6.11a/b	6.11 a/b
		Unfavorable	Favorable
Permanent	γ_G	1	1
Variable	γ_Q	1	1

Reduction factors (ψ)

The reduction factors (ψ) are given in Table 15 according to the handbook of CUR 211.

Table 15. Recommended values of ψ-factor for combinations of variable actions on quay walls[11]

Action	Combination factor (ψ_0)	Frequent value (ψ_1)	Quasi static value (ψ_2)
Uniform terrain load (cargo: containers, bulk goods)	0.7	0.5	0.3

---

[9] Table NB.4 – A1.2(B) – Design values of actions (STR/GEO) (set B)
[10] Table NB.10 – A1.3 – Design values of loads for use in accidental and earthquake load combinations.
[11] Handbook of CUR 211 - Table 6.5 Recommended values of ψ-factor for combinations of variable actions on quay walls.

Ship ramp loads (roll on roll of)	0.6	0.4	0
Traffic loads/actions (port of vehicles)	0.6	0.4	0
Crane loads (crane for cargo handling)	0.7	0.3	0
Ship berthing loads (reaction force fendering)	0.7	0.3	0
Earth pressures	1.0	1.0	1.0
(ground) water pressures	1.0	1.0	1.0
Differential settlement	1.0	1.0	1.0
Environmental/ Meteorological loads (wind, waves, current, temperature, ice)	0.7	0.3	0

The partial loading factors and reduction factors used for the quay wall of Engie will be used for this thesis. Also, a simplification of the load combinations is applied, where the surface load or mooring loads are governing, which is given in the table below. Notice that the mooring loads (bollard- and fender loads) do not occur together. Also, when the water level is extremely low, there is no upward water pressure working on the superstructure. In the table below, the load combinations applied to the conventional model are given.

Table 16. Load combinations (ULS)

Load combinations (ULS)	ULS 1-1	ULS 1-2	ULS 2-1	ULS 2-2	ULS 3 (accidental)
LC1- Self weight	1.20	1.20	1.20	1.20	1.00
LC2-1- Earth pressure (fundamental)	1.00	1.00	1.00	1.00	-
LC2-2- Earth pressure (Extreme low water)	-	-	-	-	1.00
LC3- Water pressure (fundamental)	1.00	1.00	1.00	1.00	-
LC4- Terrain load	1.50	1.05	1.50	1.05	0.30
LC5- Bollard load	1.05	1.50	-	-	-
LC6- Fender load	-	-	1.05	1.50	-
LC7- Crane load (towards water side + ground side or waterside rail)	0.90	0.90	0.90	0.90	0.60
LC8-loads substructure	1.20	1.20	1.20	1.20	1.00

Table 17. Load Combinations (SLS)

Load combinations (frequent)	SLS 1	SLS 2
LC1- Self weight	1.00	1.00
LC2-1- Earth pressure (fundamental)	1.00	1.00
LC3- Water pressure (fundamental)	1.00	1.00
LC4- Terrain load (governing)	0.50	0.50
LC5- Bollard load	0.30	-
LC6- Fender load	-	0.30
LC7- Crane load (towards water side + ground side or waterside rail)	0.60	0.60
LC8- loads substructure	1.00	1.00

3.3. 2D-model vs 2.5D-model

In this paragraph the concrete relief floor is modeled in a conventional way in 2D, and 3D space with the use of the software package SCIA-Engineering. Modeling in two-dimensional space is done with beam elements, and in three-dimensional space, shell elements are used. The use of shell elements in three-dimensional space is also called 2.5D. Following that, the results of the internal forces of the two models are compared. In paragraph 2.2 some background information about modeling with beam and shell- elements are given.
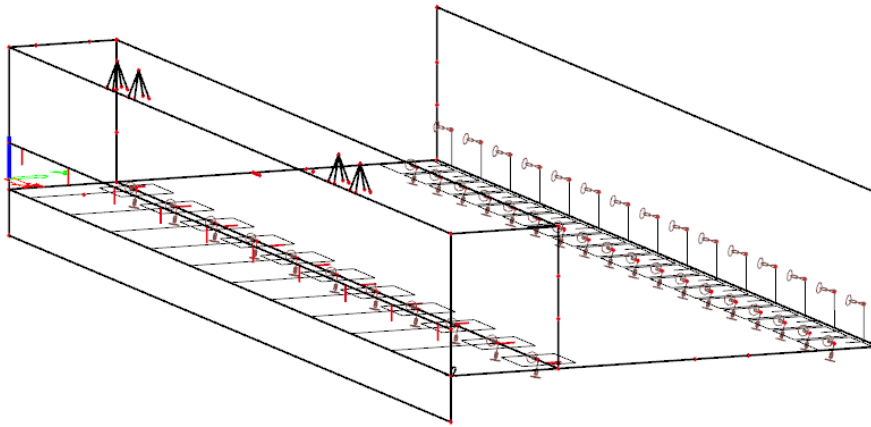
Figure 20. 2.5D-conventional model (Scia Engineering)

In the 2D model, the loads are applied per unit length, while in the 2.5D model it is spread over the entire length of the quay (40 meters). Modeling in two-dimensional space does not consider the redistribution of the loads, such as the bollard loads, fender loads, and crane loads acting on the quay wall. This is carried out by dividing the applied loads, which are redistributed through the superstructure over an angle of 45 °, with the redistribution distance.

The relief floor will be examined in this thesis, because of the significant internal forces that occur, it is the most crucial structural component of the relieving platform. For the applied load cases, the results of the reaction forces and bending moments for the 2D and 2.5D models are shown in appendix I. This is carried out to check the accuracy of the models. For simplicity reasons, the non-linear behavior of the anchors, combi-walls, and vibro-piles are ignored.

In the 2.5D model, the reaction force per unit length is calculated by dividing the result by the center-to-center distance of the substructural element to compare the accuracy with the 2D model. The center-to-center distances of the substructural elements are given in Table 6 of chapter 3.2.2.

The conclusions drawn from the data in appendix I indicates that the result of the 2D and 2.5D model are comparable. This means that the conventional 2.5D design of the relieving platform has been modeled correctly based on the reaction forces and bending moments.

Modeling in three-dimensional space gives a more accurate solution for determining the reinforcement. This is due to the fact that the loads are spread automatically, and also because the effect of torsion is considered in the formula of the design bending moment and design normal force.

3.4. Reinforcement conventional design

In this paragraph, the reinforcement is calculated conventionally based on the internal forces of the relief floor of the relieving platform according to NEN-EN-1992-1-1 with the use of the software package Idea-Statica.

In the 2D and 2.5D report given in appendix III, the figures and values of the bending moments, normal forces, and the shear forces of the conventional 2D and 2.5D model are shown.

In chapter 4, an advanced model 3D model per unit length is built. Because of the small depth of the model, the 3D model is most comparable to the 2D model. Implicitly it is assumed that when the entire quay wall is modelled, the 2.5D model will be the most comparable due to the extra torsion.

For the relief floor, the "positive" side of the moments creates tension at the bottom side of the floor (sagging bending moment), while the "negative" side creates tension at the top side (hogging bending moment).
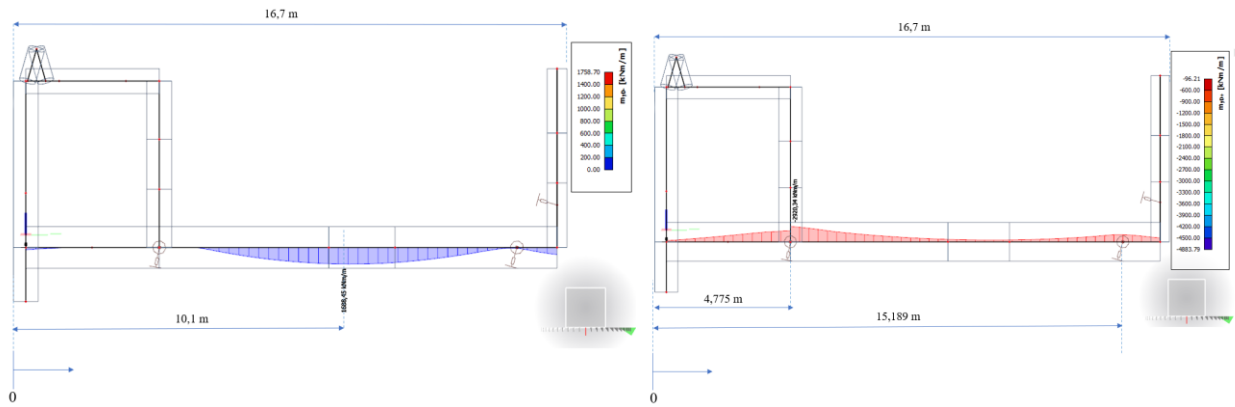
Figure 21. location governing sagging(left) and hogging (right) bending moments to determine the reinforcement (ULS)

The location of the maximum design bending moments of the relief floor for the Ultimate Limit State is shown in Figure 21. Here it can be noticed that the sagging bending moments govern at a distance of 10,1 meter from the exterior surface of wall A (location 1), and the hogging bending moments at the combi-wall (location 2) and vibro-piles (location 3). Locations 1 and 2 are the most critical part for the top and bottom reinforcement of the relief floor and will be modeled in an advanced way in chapter 5.

In the tables below, the ULS and SLS results of the internal forces for the 2D and 2.5D models at the critical locations are shown. For the 2.5D model, the average result of the design bending moments is used, and the governing result is used to calculate the normal and shear forces.

Table 18. Bending moment 2D model (ULS)

Structural element	Distance [m]	My+ [kNm]	My- [kNm]	Ned [kN]
Relief floor	4.775	-3200	0	530
	10.100	-327	1634	530
	15.189	-1500	0	530

Table 19. Bending moment 2D model (SLS)

Structural element	Distance [m]	My+ [kNm]	My- [kNm]	Ned [kN]
Relief floor	4.775	-1800	0	350
	10.100	0	1030	350
	15.189	-1000	0	350

Table 20. Shear force 2D model (ULS)

Structural element	Ved [kN]
Relief floor (Between wall A and B)	610
Relief floor (Between wall B and C)	1060

Table 21. Bending moment and normal force 2.5D model (ULS)

Structural element	Distance [m]	Myd+ [kNm/m]	Myd- [kNm/m]	Nyd [kN/m]
Relief floor	4.775	-3300	0	700
	10.100	-1200	1760	700
	15.189	-1600	800	700

Table 22. Bending moment and normal force 2.5D model (SLS)

Structural element	Distance [m]	Myd+ [kNm/m]	Myd- [kNm/m]	Nyd [kN/m]
Relief floor	4.775	-1850	0	450
	10.100	-200	1110	450
	15.189	-1200	280	450

Table 23.Shear force 2.5D model (ULS)

Structural element	Ved [kN/m]
Relief floor (Between wall A and B)	531
Relief floor (Between wall B and C)	800

In the tables below, the reinforcement for the 2D model is calculated at the critical locations. In appendix I an explanation is provided about which limit state condition is governing when determining the amount of reinforcement. The result indicates that the SLS condition (crack width) is governing when considering the crack width of 0.22 mm from National Annex of the Eurocode 2. When considering the crack width of 0.4 mm stated by Prof. Polder [13], the ULS condition (strength) is governing.

In this thesis, the crack width norm of the National Annex of the Eurocode 2 is considered and will be used to determine the amount of reinforcement needed.

As a starting point, a base main reinforcement layer has been modeled for the top and bottom of the relief floor. For the top layer Ø25 – 125 has been used and for the bottom layer Ø20 – 125 as base reinforcement. Hereafter, additional reinforcement has been added at crucial locations until the crack width conditions are satisfied. A strong enough shear reinforcement has been estimated to prevent shear failure in the optimization phase described in chapter 4. When determining the reinforcement, the technical execution is not considered.

Table 24. Main reinforcement relief floor per meter quay at the critical locations (conventional 2D model)

Relief floor	Distance [m]	Med [ULS]	Ned [ULS]	Med [SLS]	Ned [SLS]	Main reinforcement	Reinforcement area [mm2]	ULS unity check	SLS unity check
Top side	Combi-wall	-3200	550	-1800	350	Layer 1: Ø25– 125	10674	68%	100%
						Layer 2: Ø32– 120			
	Vibro-pile	-1500	550	-1000	350	Layer 1: Ø25 – 125	5580	60%	98%
						Layer 2: Ø16 – 110			
Bottom side	Between wall B and C	1630	550	1030	350	Layer 1: Ø20– 125	6485	59%	95%
						Layer 2: Ø25– 125			

Taking a look at Table 24 it can be noticed that the SLS conditions are governing, and less reinforcement is needed to satisfy the ULS conditions. Because the primary goal of this thesis is to optimize the amount of reinforcement and the geometry using an advanced calculation based on the ULS and the SLS, an artificial reinforcement set has been determined until the ULS conditions are between 95 and 100%. The SLS condition is neglected in this case. The SLS condition is likewise accomplished using the crack width of 0.4 mm stated by Prof. Polder [13].

In Table 25, the main reinforcement where the ULS condition is governing is given where it can be observed that no additional reinforcement is needed at the vibro-piles to satisfy this condition.

Table 25. Main reinforcement relief floor per meter quay at the critical locations (ULS governing)

Relief floor	Distance [m]	Main reinforcement	Reinforcement area [mm²]	ULS unity check	SLS unity check
Top side	Combi-wall	Layer 1: Ø25– 125	7944	96.1%	152%
		Layer 2: Ø25– 150			
	Vibro-pile	Layer 1: Ø25 – 125	3506	87%	170%
Bottom side	Between wall B and C	Layer 1: Ø20– 125	3853	95.6%	170%
		Layer 2: Ø16– 150			

Table 26. Shear reinforcement per meter quay (conventional 2D model)

	Ved [kN]	Shear reinforcement	Reinforcement area [mm²]	Shear capacity
Relief floor	1060	Ø20 – 300	1047	56%

Figure 23 illustrates the region over which the additional reinforcement of the relief floor is added. According to NEN-EN-1992-1-1, the spreading distance at the supports can be determined using the 'Shift rule' of the bending moment curve by summing up the distance a_l from the peak of the governing bending moment with the anchorage length (l_{bd}).

The following equations from the NEN-standards are used:

$$a_l = d \tag{3.1}$$

$$l_{bd} = \alpha_1 \alpha_2 \alpha_3 \alpha_4 \alpha_5 l_{b,rqd} \geq l_{b,min} \tag{3.2}$$

With,

$$d = h - c - \text{Ø}MR - \frac{1}{2}a \tag{3.3}$$

$$l_{b,rqd} = \frac{\text{Ø}}{4}\left(\frac{\sigma_s}{f_{bd}}\right) \tag{3.4}$$

$$f_{bd} = 2.25\,\eta_1 \eta_2 f_{ctd} \tag{3.5}$$

Where,

a_l = spreading distance from the peak
d = effective height
c = reinforcement cover
$\text{Ø}MR$ = diameter main reinforcement
a = distance between main and additional reinforcement
l_{bd} = anchorage length
$l_{b,rqd}$ = the required anchorage length
α_1 = the effect of the form of the bars assuming adequate cover
α_2 = the effect of concrete minimum cover
α_3 = the effect of confinement by transverse reinforcement
α_4 = the influence of one or more welded transverse bars along the design anchorage length
α_5 = the effect of the pressure transverse to the plane of splitting along the design anchorage length
η_1 = a coefficient related to the quality of the bond condition and the position of the bar during concerting
η_2 = related to the bar diameter
f_{bd} = the design value of the ultimate bond stress

The additional reinforcement at the bottom of the relief floor between walls B and C, which can be seen in Figure 23 is added throughout the whole region.

Table 27. Spreading distance from the peak at the top of the relief floor

Structural element	distance [m]	h [mm]	c [mm]	ØMR [mm]	a [mm]	d [mm]	a_l [mm]	l_{bd} [mm]	Spreading distance [mm]
Combi-wall	4.4	1250	50	25	25	1162.5	1308	894	2202
Vibro-pile	15.189	1250	50	25	25	1162.5	1308	572	1880
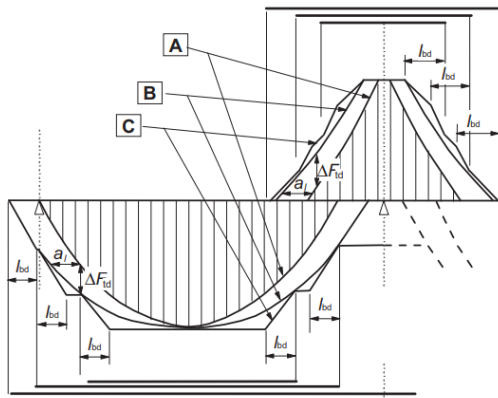
Figure 22. Illustration of the curtailment of longitudinal reinforcement [12]
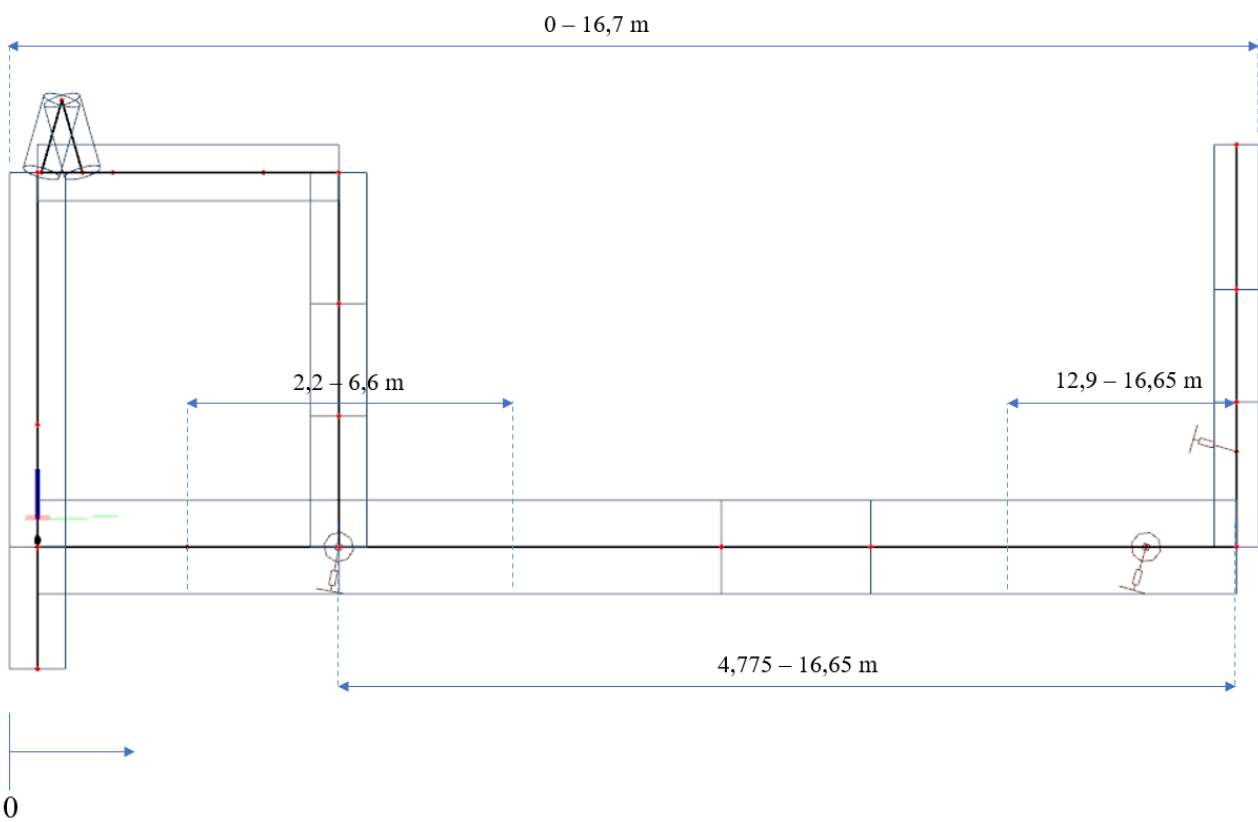
Figure 23. Reinforcement relief floor spreading distance of the additional reinforcement

---

[12] NEN-EN1992 – Figure 9.2 - Illustration of the curtailment of longitudinal reinforcement, considering the effect of inclined cracks and the resistance of reinforcement within anchorage lengths

4
Advanced approach

In this chapter, the concrete relief floor is modeled an advanced way in the three-dimensional space using volume elements. Modeling is done with the use of the software package "DIANA FEA".

DIANA stands for Displacement Method Analyzer and has been developed at the Dutch organization for applied scientific research (TNO) since 1972. DIANA is a multi-purpose finite element software package that is dedicated to a wide range of applications in Civil engineering including structural, geotechnical, tunneling, earthquake, and oil & gas engineering. A width variety of engineering problems can be solved with this program. Among other applications, the software is well equipped for the assessment of reinforced concrete. Material aspects such as the cracking of the concrete, plastic yielding of steel, creep and shrinkage, aging, and ambient influences, can also be considered in DIANA [7].

The relief floor is modeled per unit length in Diana FEA using volume elements with the same modeling assumptions as the 2D conventional model given in chapter 3.2.

First, a linear analysis is performed to check if the results of the advanced model are close to the conventional model. If this is the case, the advanced model has been modeled correctly. Hereafter, the reinforcement is modeled, and nonlinear analyses are performed with the focus on the most critical parts of the relief floor shown in chapter 4.3.

4.1. Linear elastic analysis advance model
To verify whether the structure has been modeled correctly and if the results of the conventional and advanced models are comparable, a linear analysis has been performed. The load cases applied to the 2D model are applied to the 3D model.
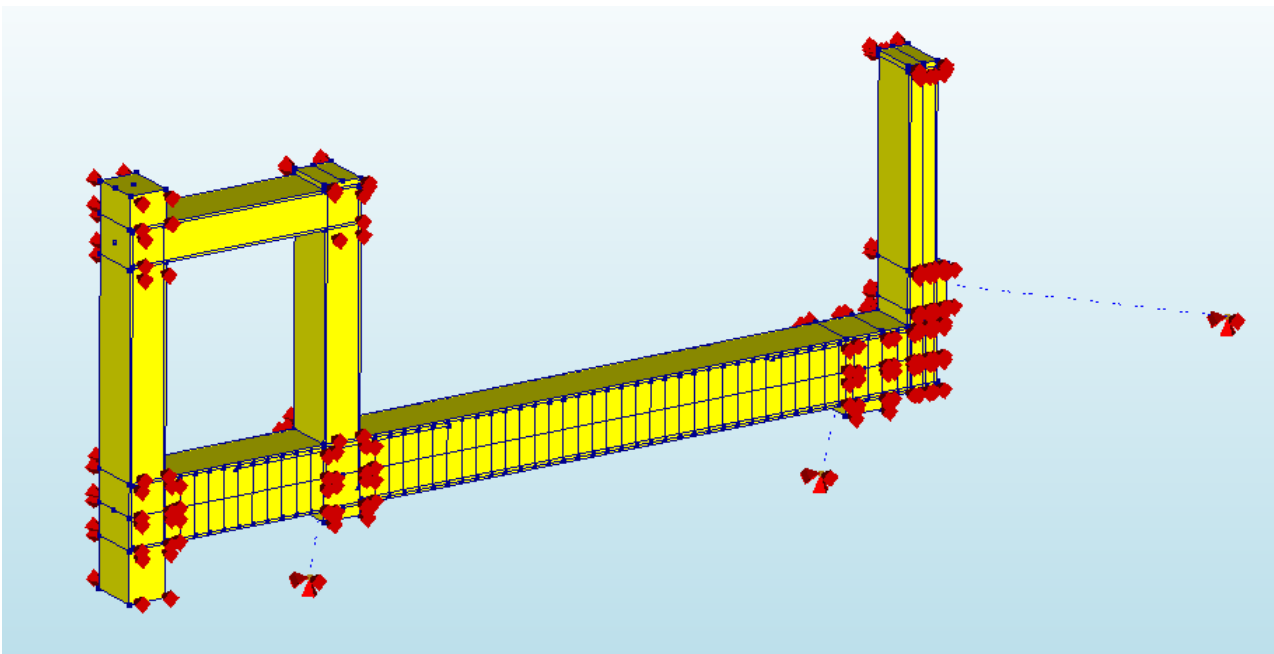
Figure 24. 3D model of the relieving platform (DIANA FEA)

4.1.1. Linear elastic modelling assumptions
In this paragraph, the modeling assumptions for performing the linear analysis are given. For the concrete and steel, a linear elastic behavior is assumed. The material properties are given in Table 28.
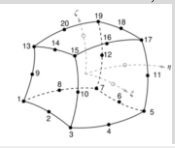
Table 28. material properties (concrete & steel)

Concrete	
Material class	Concrete and masonry
Material model	Linear elastic isotropic
E-modulus	20 GPa
Poisson's ratio	0.2
Mass density	2500 kN/m^3
Steel	
Material class	Steel
Material model	Linear elastic isotropic
E-modulus	200 Gpa
Poisson's ratio	0.3
Mass density	0

For modeling, solid/volume elements[13] have been used with an element size that is calculated with respect to the height of the relief floor. The element size is taken as 1/10 of the height (h), and results in 125 mm. The element properties are given in Table 29.
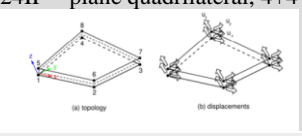
Table 29. Volume/solid element properties

Element class	Structural solid
Element type	CHX60 – Brick, 20nodes (quadratic)
Shape dimensions	3D
Topological dimension	3D
Assumed stress field	-
Displacement field	3D
Degree of freedom per node	Displacement (u_x,u_y,u_z)
Stress components	σxx, σyy, σzz, σxy, σyz, σzx
Interpolation scheme	Isoparametric mapping from global (xyz) coordinate system to a (ξηζ) local coordinate system.
Integration scheme	Numerical integration

Singularity problems can be prevented by spreading the point loads and boundary conditions over a larger surface. There are several ways to solve this, but in this case a distributed plate is used over the whole depth. Because the distributed plate needs to be sufficient stiff, steel plates are used.

The area of the concrete and steel plates are connected using plane interface elements. The structural interface elements[14] describe the interface behavior in terms of a relation between the normal and shear traction and the normal and shear relative displacements across the interface. The element and material properties of the structural interface are given in Table 30 and Table 31.

Table 30. Plane interface element properties

Element class	Structural plane interface
Element type	Q24IF – plane quadrilateral, 4+4 nodes, 3D
Shape dimensions	3D
Topological dimension	3D
Displacement field	3D
Degree of freedom per node	Displacement (u_x,u_y,u_z)
Integration scheme	Numerically integrated

---

[13] Diana manual 10.5 – Chapter 27. Solid elements
[14] Diana Manual 10.5 – Chapter 35. Structural interface elements

Table 31. Material properties plane interface element

Interface type	3D surface interface
Normal stiffness modulus	1e+07 kN/m³
Shear stiffness modulus	1e+06 kN/m³

In this thesis, the supports are modeled using spring connections[15]. The supports can be modeled using interfaces, boundary interfaces, or spring connections. Theoretically, the use of a spring connection will give the most accurate result compared to the conventional model, due to the units of the applied stiffness expressed in kN/m. Additionally, with a face-to-face connection between the concrete and the environment and a stiffness specified in kN/m³, boundary interfaces can be used. The element and material properties of the spring connections are given in Table 32 and Table 33.

Table 32. Spring element properties
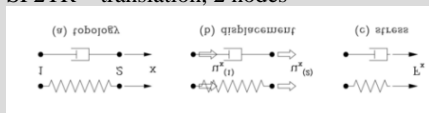
Element class	Discrete translation spring/dashpot
Element type	SP2TR – translation, 2 nodes
Degree of freedom per node	Displacement (u_x)

Table 33. Material properties spring element

Spring elements	Stiffness [MN/m]
Combi wall – vertical (z-direction)	240
Combi wall – longitudinal (y-direction)	24
Vibro- pile – vertical (z-direction)	100
Vibro- pile – longitudinal (y-direction)	10
Anchors (x-direction)	24

4.1.2. Comparison between 2D - conventional and 3D advanced model

In this paragraph, a comparison is made between the linear elastic results of the 2D-conventional and 3D-advanced models to determine the accuracy of the models.

In appendix II, the results of horizontal and vertical equilibrium of the external loading for the 2D-conventional model and 3D-smarter model are shown for each load case. Here it is noticed that the forces are near to being in equilibrium, indicating that the advanced model has been modeled correctly based on the load cases.

Also, the reaction forces, the bending moments, the normal forces, and the shear forces for the 2D and 3D-model that occur from the governing load combinations given in appendix I are shown in appendix II.

Table 34. Bending moments between 2D and 3D model (ULS)

Structural element	Bending moment	Location [m]	Load combination	2D – model	3D – model	Error
			[ULS]	[kNm]	[kNm]	
Relief floor A-B	Mz-	x=0.75 (At surface of wall A)	ULS 1-2/4	-309.5	235.1	24.1%
	Mz-	x=2.1 m (Bernoulli zone between wall A and B)	ULS 1-1/1	-982.8	909.4	7.5%
	Mz -	x=4.025 (At surface wall B)	ULS 1-1/1	-2084.7	1985.7	5.7%
	Mz+	x=0.75 (At surface of wall A)	ULS 2-2/5	152.5	-180.1	18.1%
Relief floor B-C	Mz-	x=4.775 (At surface wall B)	ULS 1-2/4	-2818	2737	2.9%

---

[15] Diana Manual 10.5 – Chapter 29. Spring and dashpot elements

	Mz-	x=6.025 (Bernoulli zone between wall B and C)	ULS 1-2/12	-1781	1764.2	0.9%
	Mz-	x=10.1(Bernoulli zone between wall B and C)	ULS 1-2/12	-327	326.3	0.2%
	Mz-	x=14.814 (At vibro-pile)	ULS 1-2/3	-1499	1582.9	5.6%
	Mz-	x= 16.1 (At surface of wall C)	ULS 1-1/23	-778.2	815.9	4.8%
	Mz+	x=10.1 (Bernoulli zone between wall B and C)	ULS 2-1/16	1633.9	-1635.2	0.1%

4.1.3. Evaluation and discussion

The inaccuracy of the reaction forces between the 2D and 3D model is less than 5%. This concludes that the reaction forces are equivalent between the models.

Looking at Table 34, it can be observed that the inaccuracy of the bending moments of the relief floor between walls B and C is below 1%. In this region, the Bernoulli hypothesis of plane strain distribution applies (also called B-region). At the surface of the walls, the inaccuracy is higher. This is due to the fact that in the 3D-smart model Bernoulli's hypothesis is inactive in the zone between the wall and the floor. This inactive zone is called the discontinuity or distortion region (D-region) and is determined by taking the distance D (thickness of the floor) from the wall. In this zone, there is a direct transfer of the loads to the floor with a compression diagonal. Aside from the D-zones, there is also the fact that the dimensions of all structural elements are realistically modeled, which causes the structure to react differently.

Also, notice that the inaccuracy of the bending moment of the relief floor between walls A and B in the Bernoulli zone is below 10%. In appendix II, a comparison is made on load combination level where the ULS result has been calculated analytically. Here it can be noticed that the inaccuracy of 10% is a summation of small differences that occur per load case. In Figure 25 the Bernoulli and distortion zones of the relief floor are identified.
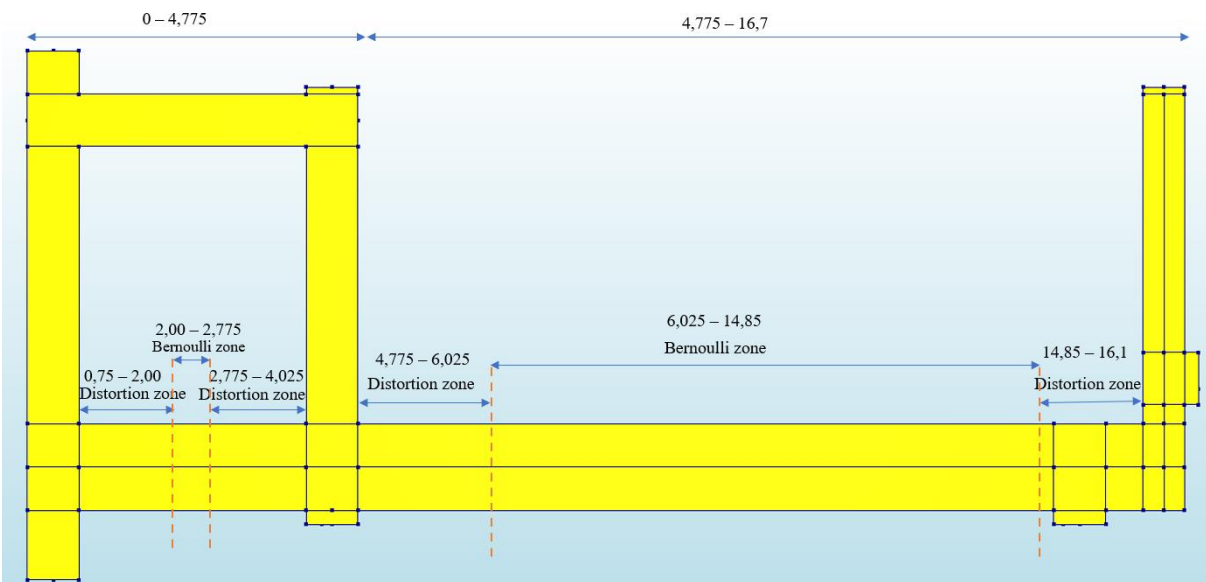
Figure 25. Bernoulli and distortion zone 3D model

4.2. Nonlinear approach

In this paragraph, the modeling assumptions for performing a nonlinear analysis is explained.

The Dutch Road Authority (Rijkswaterstaat) issued guidelines for nonlinear analysis of concrete structures provided in RTD 1016-1:2020. These recommendations cover all forms of bridges (girder bridges, slab bridges, box girder bridges, etc.), reinforced concrete, prestressed concrete, tunnels, and culverts. The safety formats applied in RTD 1016-1:2020 and the fib Model Code 2010 are the same [16].

4.2.1. Reinforcement modeling approach smart model

A reinforced concrete structure in DIANA can be represented by plain concrete elements and steel reinforcement bars or grids, each with its specific material properties. Cracking failure under tensile stresses and crushing failure under compressive and shear stresses have been considered in the concrete material model. For the steel reinforcement, Von Mises type elastic-plastic material models with user-defined hardening are considered.

The following types of reinforcements is offered by DIANA:

- *Embedded reinforcement[16]*
  The reinforcements are fully embedded in the elements in which they are located taking up no space in the so-called mother element (do not allow relative slip). Additionally, neither do they influence the mass of the element, nor do they have any degree of freedom of their own. Based on the displacement of the mother element, the strains in the reinforcement are calculated. Between the steel reinforcement and the concrete, a perfect bond is assumed, meaning that the displacement of the reinforcement node is the same as the concrete element (no-slip). Also, after a crack develops, the tension in the steel is transferred to the next element, causing another crack to develop.
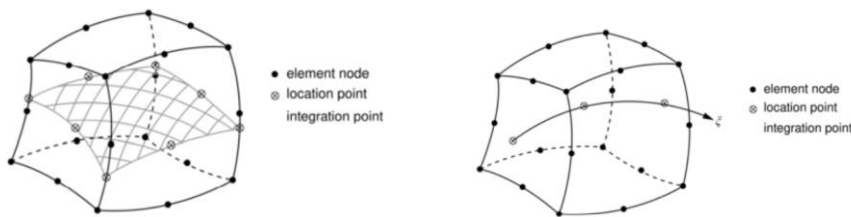
Figure 26. Grid and bar reinforcement in solid element

- *Bond-slip reinforcement[17]*
  The deformation of the reinforcements may be different than the mother element in which they are located (relative slip is allowed). This means that after a crack develops, tension transfer in steel is restricted due to the slip. A certain distance is needed until a second crack is developed. The bond-slip bars need to be specified for both the bond-slip interaction between the bar and the concrete as well as the material behavior of the reinforcement bars [7].

4.2.2. Constitutive model concrete and steel

Constitutive models, also known as material models, are used in the finite element environment to specify the constitutive behavior (stress-strain relationship) that is expected for the materials in the structure. The recommendations for the constitutive model of concrete are determined according to guidelines provided in RTD 1016-1:2020.

In Diana, cracking in concrete can be modeled using a smeared and discrete modeling approach. The advantage of this smeared cracking model over a discrete cracking model is that cracks can form anywhere and in any direction in the mesh. Within the smeared crack approach distinction can be made between fixed and rotating crack models. In the fixed smeared crack model, the direction of the normal to the crack is fixed upon initiation of cracks. Rotating crack models on the other hand allow the normal to the crack to rotate during the fracture process [17].

According to the guidelines a total strain-based crack model (smeared cracking approach) with a rotating crack is preferred for concrete, because it is not known in advance where the crack will start to develop in the model.

---

[16] DIANA manual 10.5 – chapter 38.1. Embedded Reinforcement
[17] DIANA manual 10.5 – chapter 38.2. Bond-slip Reinforcement

In this model, the stress-strain relationship is based on the total strain and is evaluated in the principal direction of the strain vector.

Tensile behavior
The tensile behavior of concrete is modeled in Diana using a prescribed tension softening curve. According to the guidelines it is recommended to use an exponential softening diagram. The following parameters need to be defined:

- The Tensile strength (f_t)
- The fracture energy (G_F)
- The equivalent length (h_{eq})
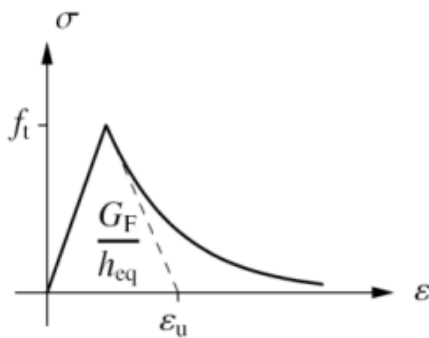
Figure 27. Exponential softening diagram [18]

The ultimate strain parameter for exponential softening is given by:

$$\varepsilon_u = \frac{G_F}{h_{eq} \times f_t} \qquad (4.1)$$

When the equivalent length is too large for softening materials, the post-peak response can show a snap-back behavior. The descending branch of the softening diagram should not be too straight. The equivalent length influences the softening behavior and should limited to:

$$h_{eq} < \frac{G_F E_c}{f_t^2} \qquad (4.2)$$

Fracture energy (G_F)
The energy required to create a crack with unit area is known as fracture energy. It is a physical characteristic that is independent of the size of the structure. The fracture energy is determined using the following equation from the fib Model Code 10:

$$G_F = 73 \times f_{cm}^{0,18} \qquad (4.3)$$

The equivalent length (h_{eq})[18]
The equivalent length, also known as the crack-band width, is an important quantity in constitutive models describing a softening stress-strain relationship.
Diana FEA offers three methods to determine the crack bandwidth (h_{eq}):

- Rots' element-based method: The crack bandwidth depends on the size, shape, and interpolation function of the used finite element. The default value for solid elements is $heq = \sqrt[3]{V}$, where V is the element's volume.
- Govindjee's projection method: The crack bandwidth (h_{eq}) is defined as the projected length of the element containing the crack onto the crack plane.
- Direct input: To guide the cracking algorithm, the user may directly input the crack bandwidth.

According to the guidelines it is recommended to use the method based on the initial direction of the cracks and the element dimensions (Govindjee's projection method).

---

[18] Diana 10.5 Manual: Chapter 46.17.1.1. Crack bandwidth

Compressive behavior

According to the guidelines it is recommended to use a parabolic stress-strain diagram with a softening branch. The softening branch is based on the compressive fracture energy (G_c) in order to reduce mesh size sensitivity during compressive strain localization [18]. In order to account for tension-compression interaction and lateral cracking, Vecchio and Collins' reduction model is adopted. The reduction curve's lower bound value is indicated by the parameter β_σ.
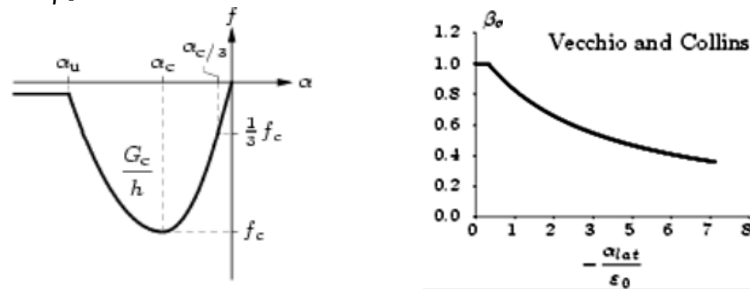
Figure 28. Parabolic compression diagram and reduction of the compressive strength diagram [18]

The Compressive fracture energy is determined using the following equation from the fib Model Code 2010:

$$G_C = 250 \times G_F \tag{4.4}$$

For the steel reinforcement, an elastic-plastic material model with hardening has been used.

Material properties for the ULS and SLS verification

The material properties of concrete and steel for the ULS and SLS verification are determined according to the guidelines provided in RTD 1016-1:2020. For the Ultimate Limit State verification, the global resistance method is used, which is explained in paragraph 4.3.1. The objective of the nonlinear analysis is to simulate the real structural behavior and to evaluate the representative value of the resistance. A task of this type can alternatively be expressed as a prediction of the most likely real resistance, which is the mean value of resistance. When performing the GRF method the mean material properties (mean GRF) for calculating the resistance are used [11]. For the calculation of the crack width in the Serviceability Limit State, the characteristic value of the material properties has been used.

The correct input values of concrete and reinforcement steel are determined with the use of Table 85 and Table 86 given in appendix II. The concrete and steel reinforcement material parameters for the ULS and SLS verification are summarized below.

Table 35. Concrete material parameters for the ULS and SLS verification

Concrete	C30/37	C30/37
Safety format	Characterstic	Mean GRF
E-modulus (E_c)	31008 MPa	29373 MPa
Tensile strength (f_{ct})	2.02 MPa	2.6 MPa
Tensile fracture energy (G_f)	0.135 N/mm	0.131 N/mm
Compressive strength (f_c)	30.0 MPa	25.5 MPa
Compressive fracture energy (G_c)	33.7 N/mm	32.7 N/mm

Table 36. Reinforcement steel material parameters for the ULS and SLS verification

Reinforcement	B500	B500
Safety format	Characteristic	Mean GRF
E-modulus	200000 MPa	200000 MPa
Characteristic yield strength (f_{yk})	500 MPa	550 MPa
Yield strain strain (ε_{yk})	0.002	0.00275
Characteristic ultimate strength (f_t)	540 MPa	594 MPa
Ultimate strain (ε_{uk})	0.05	0.05

In Table 37 and Table 38 a summary is given of the mechanical properties of the concrete and the steel reinforcement.

Table 37. Summary mechanical properties of concrete
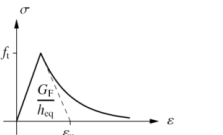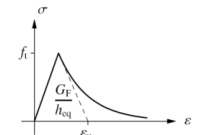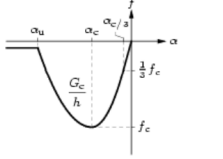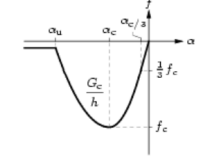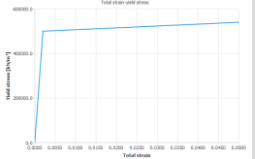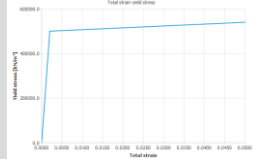
Concrete	C30/37	C30/37
Safety format	Characteristic	Mean GRF
Material class	Concrete and masonry	Concrete and masonry
Material model	Total strain-based crack model	Total strain-based crack model
E-modulus	31008 MPa	29373 MPa
Poisson's ratio	0.2	0.2
Mass density	2500 kN/m^3	2500 kN/m^3
Crack orientation	Rotating	Rotating
Tensile curve	Exponential	Exponential
Tensile strength	2.02 MPa	2.6 MPa
Tensile fracture energy	0.135 N/mm	0.131 N/mm
Crack bandwidth	Govindjee's	Govindjee's
Residual tensile strength	0.1 MPa	0.1 MPa
Compressive curve	Parabolic	Parabolic
Compressive strength	30.0 MPa	25.5 MPa
Compressive fracture energy	33.7 N/mm	32.7 N/mm
Reduction model	Vecchio and Collins 1993	Vecchio and Collins 1993
Lower bound reduction curve	0.4	0.4
Stress confinement	Selby and Vecchio	Selby and Vecchio

Table 38.Summary mechanical properties of steel reinforcement

Reinforcement	B500	B500
Safety format	Characteristic	Mean GRF
Material class	Reinforcement	Reinforcement
Material model	Von Mises plasticity	Von Mises plasticity
E-modulus	200000 MPa	200000 MPa
Plastic hardening	Total strain-yield stress	Total strain-yield stress
Characteristic yield strength (fyk)	500 MPa	550 MPa
Yield strain strain (εyk)	0.002	0.00275
Characteristic ultimate strength (ft)	540 MPa	594 MPa
Ultimate strain (εuk)	0.05	0.05

4.2.4. Solution procedure nonlinear analysis

The equilibrium path is a graphical representation of the response (load-deflection) diagram that characterizes the overall behavior of the problem. Each point on the equilibrium path represents an equilibrium point or equilibrium configuration.

To find the solution to the non-linear analysis, a standard full Newton-Raphson algorithm is used to achieve equilibrium between internal and external forces. This method is commonly used and updates the stiffness for every iteration. The Newton-Raphson iteration method requires at least one iteration for determining when equilibrium has been reached. In general, the unbalance forces will not be decreased exactly to zero, but a tolerance must be established at which convergence is accomplished. The criterion is often a norm of the unbalance force vector, the incremental displacement vector, or a norm based on energy [18].

According to the guidelines provided in RTD-1016-2020, the convergence criteria, energy-norm together with force-norm, is recommended. Load increments that satisfy at least one of the two norms are referred to as being converged

Table 39. Convergence tolerance criteria according to guidelines provided in RTD-1016-2020

Convergence criteria	Tolerance
Norm of the unbalance force	0.01
Energy Norm	0.001

Load increments that do not fully comply with the convergence criterion may nevertheless be acceptable if they are followed by converged load increments and a reasonable explanation for the temporally non-convergence is supplied [18].

4.3. Limit state calculation using the advanced approach

In this paragraph, numerical analyses are carried out using Diana FEA. The calculation is done based on the ULS and SLS-conditions according to the RTD-1016-2020 guidelines.

At the governing critical locations of the relief floor, which is explained in chapter 3.2, a nonlinear analysis is carried out.

These locations are:

- Location 1: at a distance of 10,1 meter from the exterior of wall A (tension bottom side of the floor)
- Location 2: at the Combi-wall (tension topside of the floor)

The governing load combinations for the bending moment at the critical locations and the reinforcement calculated in chapter 4 is modelled in Diana FEA. The optimization is done based on the strength verification (ULS) and the crack width (SLS), which will be examined in the following chapters.

In Table 40 a summary is given of the governing load combinations at the critical locations.

Table 40. Governing load combination for the bending moment at the critical locations

Structural element	Relief floor			
Bending moment (Mz)	Mz+	Mz-	Mz+	Mz-
Location [m]	Location 1	Location 2	Location 1	Location 2
Load combination	ULS 2-1/16	ULS 1-2/4	SLS 1-2/11	SLS 1-1/3
LC1	1.20	1.20	1.00	1.00
LC2-1	1.00	1.00	1.00	1.00
LC2-2				
LC3	1.00	1.00	1.00	1.00
LC4-1		1.05		
LC4-2	1.50	1.05	0.5	0.50
LC4-3	1.50		0.5	
LC5		1.50		0.30
LC6	1.05		0.3	
LC7-1	0.90		0.6	
LC7-4		0.90		0.60
LC8	1.20	1.20	1.00	1.00

4.3.1. Strength advanced verification

The ULS verification is done according to the GRF method explained in RTD-1016-2020. The consequences of numerous uncertainties (of material properties, geometrical dimensions, etc.) are integrated into a global design resistance and expressed by a global resistance factor. The design value of the ultimate load is regarded as the design resistance R_d and is computed as follows:

$$R_d = P_d = \frac{P_u}{\gamma_0} \tag{4.5}$$

Where P_u represents the ultimate load that was determined by inputting the mean GRF mechanical parameters into the analysis and the global resistance factor γ_0. According to the fib Model Code 2010, global resistance factor is a multiplication of the partial safety factor of resistance (γ_R) and the model uncertainty factor (γ_{RD}). The partial safety factor of the resistance is equal to 1.2.

The RTD-1016-2020 guidelines refers to a publication of Allaix (2020), who stated that "the global resistance factor (γ_0) is equal to 1.4 and is based on a partial factor that accounts for uncertainties of the resistance model of 1.15". In the fib Model Code 2010, a lower value of 1.06 is used for the model uncertainty factor and results in a global resistance factor of 1.27.

In the case of bending (flexural) failure, a global resistance factor of 1.27 can be used, provided that shear failure is not established at a global resistance factor of 1.4. Because a sufficient reinforcement set for shear has been chosen, only bending failure is expected. In a nonlinear analysis different strength for the concrete and steel are used, which can cause sudden concrete crushing before yielding, or failure of the steel reinforcement before crushing.

Strength verification location 1

The strength capacity at location 1 is examined followed by the strength capacity at location 2.

For the advanced strength verification, the conventionally designed reinforcement to meet the ULS has been modeled in Diana FEA. The result of the physical non-linear analysis in terms of the load-displacement diagram is shown in Figure 29.
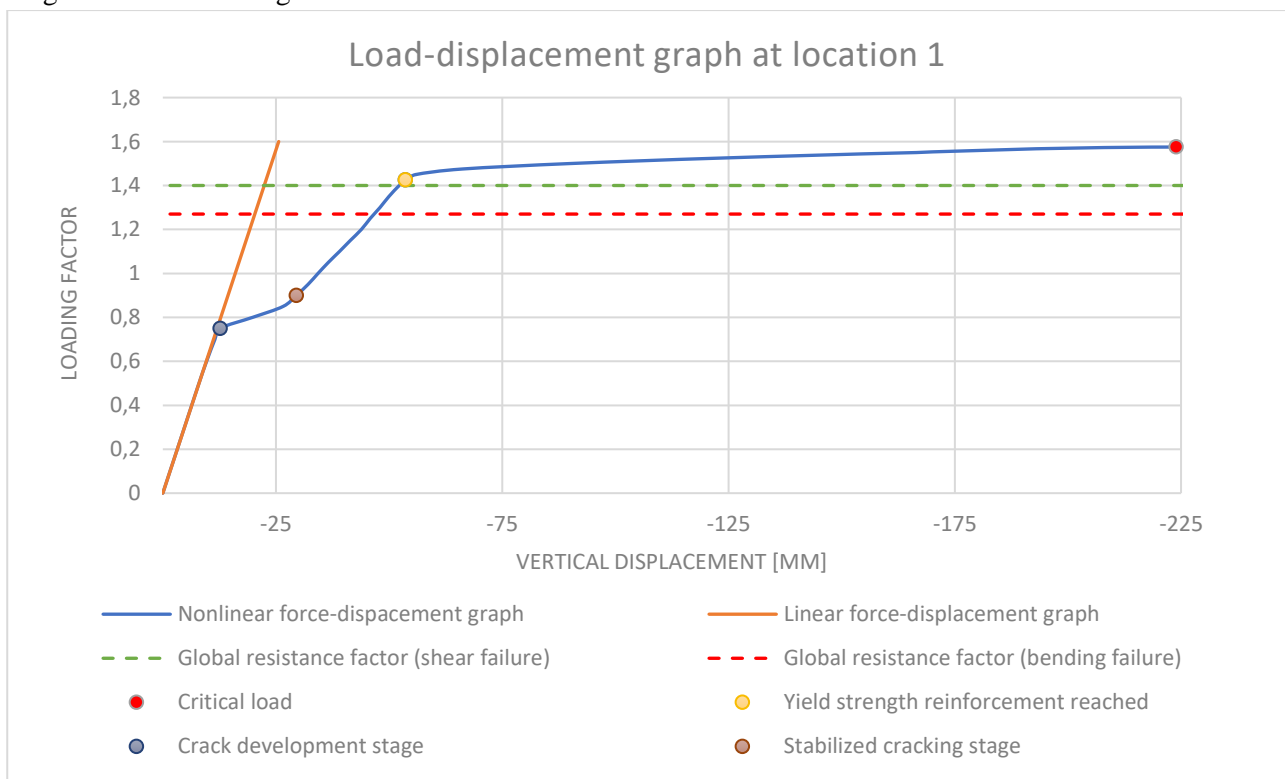
Figure 29. Load - displacement graph at location 1 (Ø20-125 + Ø16-150)

In Figure 29 it can be noticed that when the load stage of 75% is reached, the nonlinear effects are observed in the structure. At a load stage of 75% the structure starts to crack and increasing the load to 142.5% the reinforcement starts to yield. The maximal load is reached at a loading factor of 157.5%, which is 17.5% above

the global resistance factor of 1.4 for shear failure and 30.5% above the global resistance factor of 1.27 for bending failure. The structure does not fail in shear, but in bending. This is established by taking a look at the behavior of the stirrups, which do not yield when the maximal load is reached.

The maximum load exceeds the global resistance factor of 1.27, which means that the structure is safe, and that there is room for optimization. The ULS condition can be satisfied with less reinforcement. The ULS unity check is equal to $\frac{1.27}{1.575} \times 100\% = 81\%$, which means that the structure can be optimized by about 19%.

Strength verification location 2

For the advanced strength verification, the conventionally designed reinforcement to meet the ULS has been modeled in Diana FEA. The result of the physical non-linear analysis in terms of the load-displacement diagram is shown in Figure 30.

In Figure 30 it can be noticed that the nonlinear effect is observed once a load stage of 35% is reached. Hereafter, the structure begins to crack and increasing the load until 125% the reinforcement starts to yield. The maximal load is reached at a loading factor of 1.4125%, which is 1.25% above the global resistance factor of 1.4 for shear failure and 14% above the global resistance factor of 1.27 for bending failure. The structure does not fail in shear, but in bending. The maximum load exceeds the global resistance factor of 1.27, which means that the structure is safe, and that there is room for optimization. The ULS condition can be satisfied with less reinforcement.

The ULS unity check is equal to $\frac{1.27}{1.4125} \times 100\% = 90\%$, which means that the structure can be optimized by about 10%.
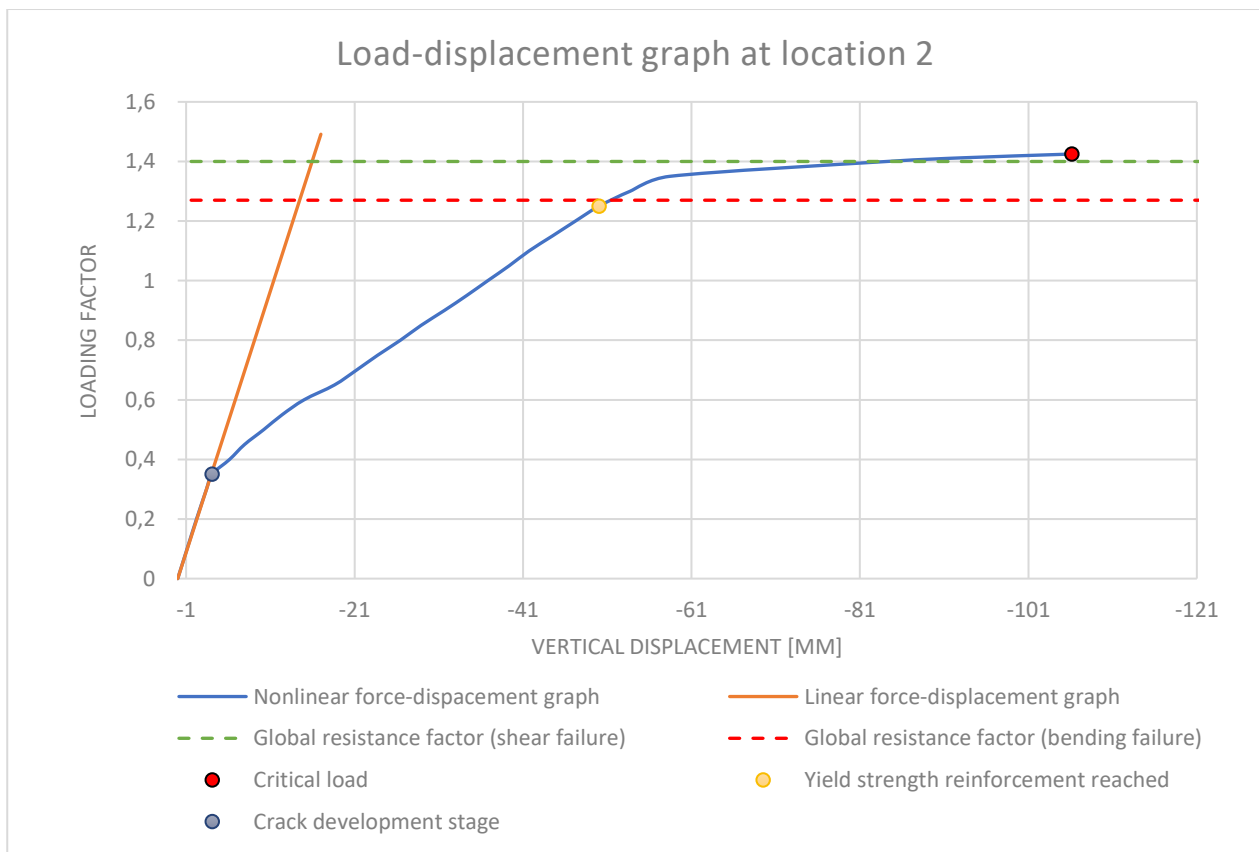
Figure 30. Load-displacement graph at location 2 (Ø25-125 + Ø25-150)

TUDelft

4.3.2. Crack width advanced verification

The crack width verification is based on the procedure given in the RTD-1016-2020 guidelines, which is also referred to as the indirect method. When flexural cracks are present, the crack opening is calculated as follows:

$$w = S_{r,max}\bar{\varepsilon}_s \qquad (4.6)$$

Where $\bar{\varepsilon}_s$ is the average strain value of the main reinforcement in the cracked zone following from the analysis and $S_{r,max}$ is the maximum crack spacing obtained using NEN-EN 1992-1-1. In appendix I the calculation of the crack spacing is explained.
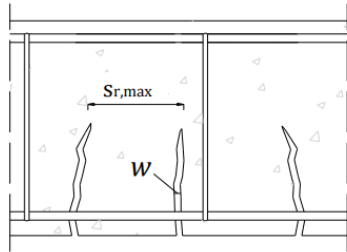
Figure 31. Crack spacing ($S_{r,max}$) and crack width (wk)

Crack width verification at location 1

The crack width development at location 1 (Sagging bending moment) is examined followed by the crack width development at location 2 (hogging bending moment).

For the crack width verification, the conventionally designed reinforcement to meet the SLS has been modeled in Diana FEA. The result of the physical non-linear analysis in terms of the crack width development diagram is shown in Figure 33.

In Table 41 the result of the crack width using formula 4.6 is shown. Between the two governing cracks in the center of the relief floor, the mean reinforcement strain (ε_s) value is determined for each load level. Hereafter, the reinforcement strain (ε_s) is multiplied by the distance between the cracks ($S_{r,max}$) to get the crack width (wk).
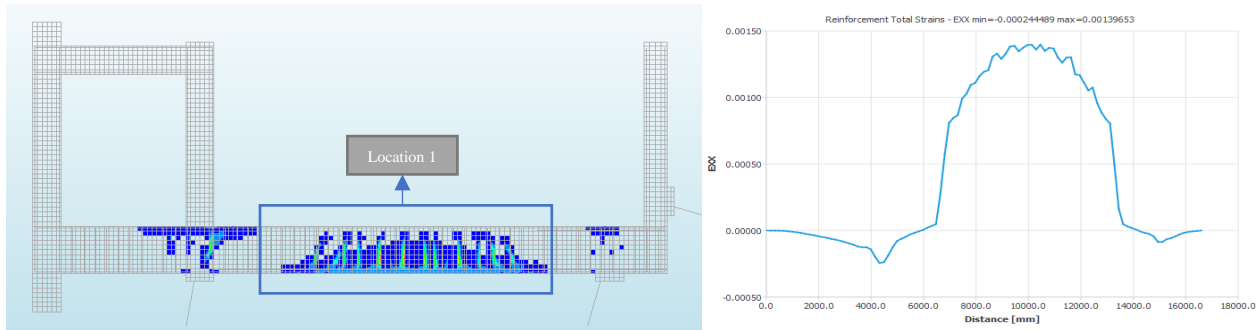
Figure 32. Stabilized cracks at location 1 (left) and strain at the bottom reinforcement (180% loading)

Figure 32 shows the crack development at location 1, where flexural cracks are developed.

Table 41. Advanced crack width calculation at location 1 (reinforcement set Ø20-125 + Ø25-125)

load factor	ε_s (mean)	$S_{r,max}$ [mm]	wk [mm]
0,2	2.08E-05	307	0.006
0,4	4.16E-05	307	0.013
0,6	6.29E-05	307	0.019
0,8	9.89E-05	307	0.030
1	1.82E-04	307	0.056
1,1	2.69E-04	307	0.083
1,2	5.50E-04	307	0.169
1,3	9.32E-04	307	0.286
1,4	1.04E-03	307	0.319
1,5	1.13E-03	307	0.346
1,6	1.21E-03	307	0.372
1,7	1.30E-03	307	0.398
1,8	1.38E-03	307	0.424
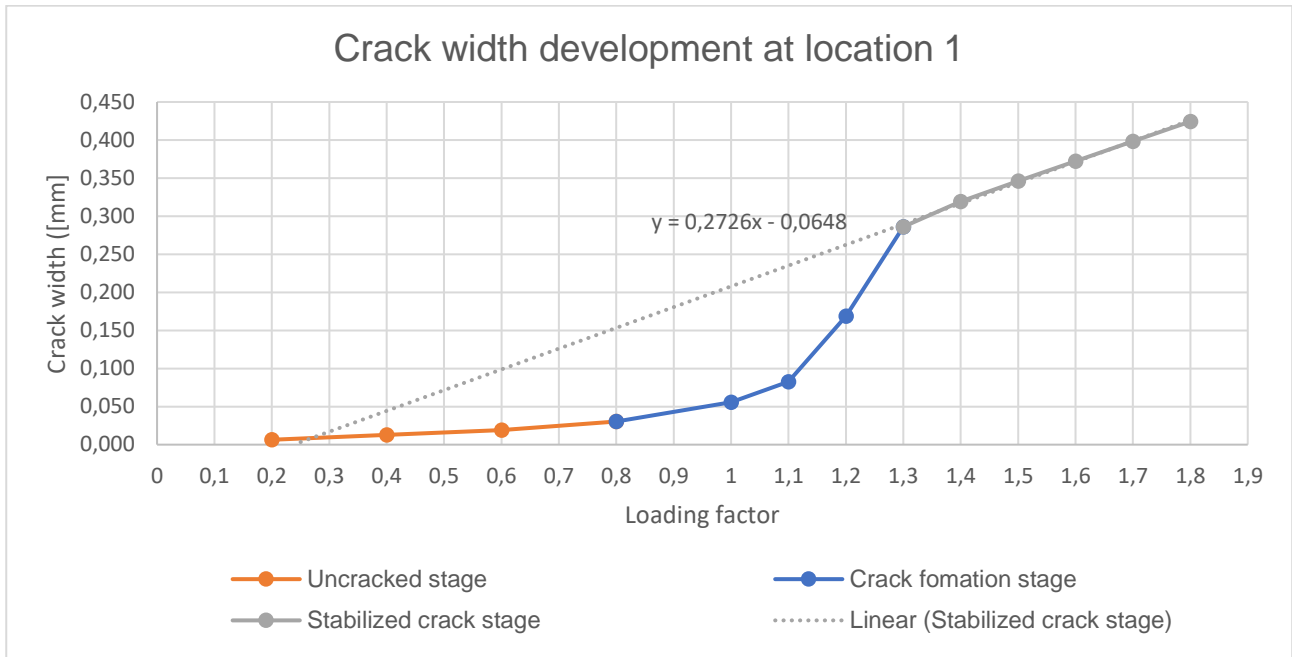
Figure 33. Crack width development graph at location 1 (reinforcement set Ø20-125 + Ø25-125)

Figure 33 shows that the cracks have not yet been fully developed when the structure is loaded at 100%. After 130% loading, there is a linear relationship between the crack width and the loading factor, indicating that the cracks are fully developed.

Because the cracks have not yet been fully developed when the structure is loaded at 100%, the crack width at this loading stage can be calculated as follows:

- Using linear extrapolation
- Reducing the tensile strength of concrete.
  Using this method, the crack width will be stabilized at an earlier stage (at 100% loading).

The crack width at 100% has been calculated using linear extrapolation, shown in Figure 33.

For example, using the linear equation given in Figure 33 results in a crack width of $0.2726 \times 1 - 0.00648 = 0.2078 \ mm$ at a loading stage of 100%.

Table 42. Crack width comparison IDEA and DIANA at location 1 (reinforcement set Ø20-125 + Ø25-125)

Calculation method	Reinforcement set	Reinforcement area [mm²]	wk [mm]	wk (norm) [mm]	SLS unity check
IDEA	Ø20-125 + Ø25-125	6484	0.208	0.22	95%
DIANA	Ø20-125 + Ø25-125	6484	0.2078	0.22	94%

In Table 42 the crack width value using the conventional and advanced approach is shown. From these results, it can be concluded that the crack widths of both methods are comparable at location 1. To be sure that this is the case a second analysis is performed with a different reinforcement set explained in appendix II.
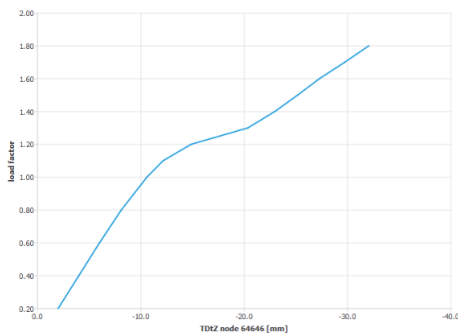
Figure 34. Load displacement graph location 1 (SLS)

In Figure 34 the load displacement graph is shown where can be noticed that when the structure is loaded at 100%, the nonlinear effects are not yet active. The cracks are not yet fully developed at this loading stage.

Crack width verification at location 2

For the crack width verification, the conventionally designed reinforcement to meet the SLS has been modeled in Diana FEA. The result of the physical non-linear analysis in terms of the crack width development diagram is shown in Figure 36. For the crack width determination at location 2 the same procedure as for location 1 has been used. Between the two governing cracks close to the surface of the wall of the relief floor, the mean reinforcement strain (ε_s) value is determined for each load level. Hereafter, the reinforcement strain (ε_s) is multiplied by the distance between the cracks ($S_{r,max}$) to get the crack width (w_k).
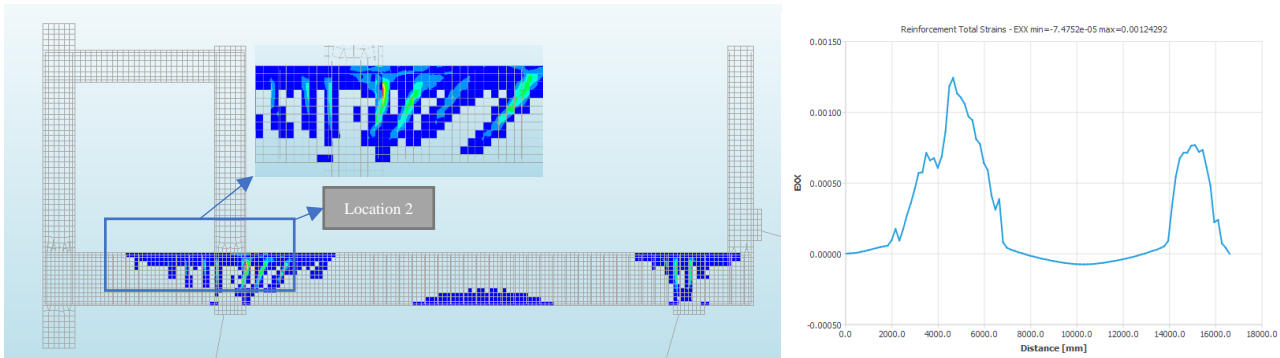
Figure 35. Stabilized cracks at location 2 (left) and strain at the top reinforcement (right) (150% loading)

Figure 35 shows the crack development at location 2, where first a flexural crack is developed followed by inclined flexural-shear cracks.

Table 43. Advance crack width calculation at location 1 (reinforcement set Ø25-125 + Ø32-120)

load factor	ε_s (mean)	$S_{r,max}$ [mm]	wk [mm]
0,1	1.42E-05	280	0.0040
0,2	2.83E-05	280	0.0079
0,3	4.24E-05	280	0.0119
0,4	5.75E-05	280	0.0161
0,5	7.49E-05	280	0.0210
0,6	1.04E-04	280	0.0291
0,7	2.21E-04	280	0.0619
0,8	4.25E-04	280	0.1190
0,9	5.45E-04	280	0.1526
1	6.45E-04	280	0.1806
1,1	7.42E-04	280	0.2078
1,2	8.33E-04	280	0.2332
1,3	9.20E-04	280	0.2575
1,4	1.01E-03	280	0.2817
1,5	1.09E-03	280	0.3054

Table 44. Crack width comparison IDEA and DIANA at location 2 (reinforcement set Ø20-125 + Ø25-125)

Calculation method	Reinforcement set	Reinforcement area [mm²]	wk [mm]	wk (norm) [mm]	SLS unity check
IDEA	Ø25-125 + Ø32-120	10629	0.219	0.22	100%
DIANA	Ø25-125 + Ø32-120	10629	0.186	0.22	85%

In Table 44 it can be noticed that the crack width using the advanced approach is 15% less than the conventional approach, which means that there is room for optimization. The SLS condition can be satisfied with less reinforcement.
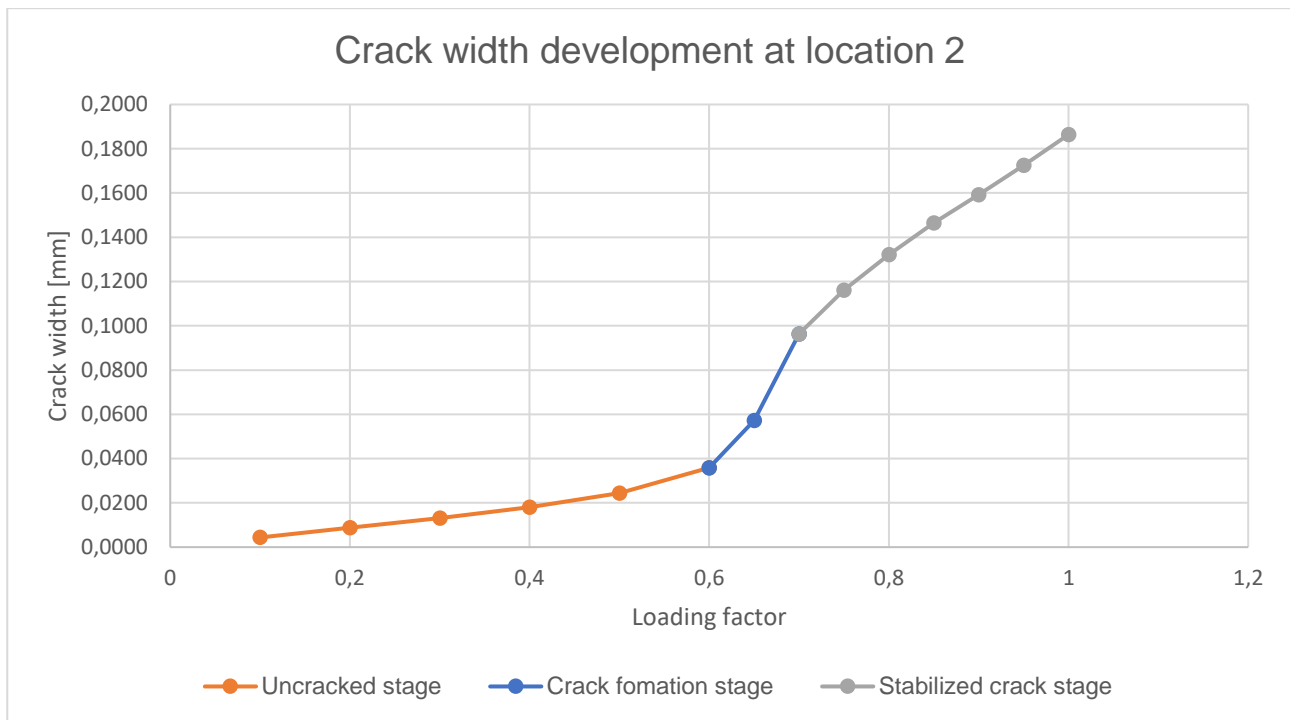
Figure 36. Crack width development graph at location 2 (reinforcement set Ø25-125 + Ø32-120)

Figure 36 shows that the cracks have been fully developed when the structure is loaded at 100%. Figure 37 illustrates that non-linear effects are active at a loading stage of 100%. It can also be noticed that cracks started to develop at a loading stage of 60%.
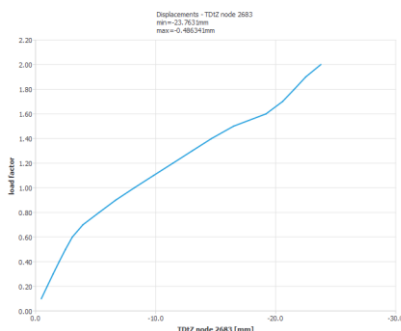
Figure 37. Nonlinear behavior at SLS stage (location 2)

4.4. Crack width advanced calculation using bond-slip model

In this paragraph, a numerical analysis is performed at locations 1 and 2 using a bond-slip model instead of assuming a perfect bond between the reinforcement and the concrete. The difference is that slip is allowed considering bond slip. The method for calculating the crack width using the guidelines provided in RTD-1016-2020 is indirect. Using a bond-slip model and by summing the relative displacement at both sides of the cracks results in a more direct estimation of the crack width. The bond-slip parameters are determined according to the fib Model Code 2010, and the results are given in appendix II.

The crack width is calculated using the indirect method provided in the RTD-1016-2020 guidelines at locations 1 and 2, followed by the direct method by summing the relative displacement (slip) at both sides of the cracks.

The indirect method has been carried out using the following two approaches for obtaining the maximum crack spacing ($S_{r,max}$):

- Using the formula provided in the Eurocode 2, as explained in appendix I.
- Measuring the distance between the two governing cracks in Diana FEA.

TUDelft

Additionally, a mesh refinement is carried out to get as close as possible to the exact value of the crack spacing. Initially, a mesh size of 100 mm (h/1.25) is used, and then the mesh is locally refined to 62.5mm (h/20). At location 2 the calculation is carried out with a refined mesh size of 62.5 mm.

The crack width at 100% at location 1 has been calculated using linear extrapolation, shown in Figure 44.

Table 45. Comparison indirect method no bond slip vs using bond slip at location 1

Calculation method	Reinforcement	Reinforcement area [mm²]	$S_{r,max}$ [mm]	wk (diana) [mm]	wk (norm) [mm]	SLS unity check
Indirect method (No Bond slip)	Ø20-125+ Ø25-125	6484	307	0.208	0.22	94%
Indirect method using Bond slip ($S_{r,max}$ Eurocode 2)	Ø20-125+ Ø25-125	6484	307	0.203	0.22	92%
Indirect method using Bond slip ($S_{r,max}$ measured)	Ø20-125+ Ø25-125	6484	301	0.1917	0.22	87%
Indirect method using Bond slip ($S_{r,max}$ measured + mesh refinement)	Ø20-125+ Ø25-125	6484	281	0.1856	0.22	84%

According to Table 45, adopting a bond-slip model with crack spacing ($S_{r,max}$) determined in accordance with Eurocode 2 results in a slight decrease of the crack width, which is almost equivalent to the model without bond slip. Measuring the crack spacing in Diana FEA results in a value of 301 mm, and adjusting the mesh gives a value of 281 mm. Using bond slip and refining the mesh yields a value of 0.1856 mm for the crack width and an SLS unity check that is 10% less than the conventional approach.

For the crack width determination at location 2 the same procedure as for location 1 has been used.

Table 46. Comparison indirect method no bond slip vs using bond slip at location 2

Calculation method	Reinforcement	Reinforcement area [mm²]	$S_{r,max}$ [mm]	wk (diana) [mm]	wk (norm) [mm]	SLS unity check
Indirect method (No Bond slip)	Ø25-125 + Ø32-120	10629	280	0.1864	0.22	85%
Indirect method using Bond slip ($S_{r,max}$ Eurocode 2)	Ø25-125 + Ø32-120	10629	280	0.1827	0.22	83%
Indirect method using Bond slip ($S_{r,max}$ measured + mesh refinement)	Ø25-125 + Ø32-120	10629	250	0.1631	0.22	74%

According to Table 46, adopting a bond-slip model with crack spacing ($S_{r,max}$) determined in accordance with Eurocode 2 results in a crack width slightly less than the model without bond slip. Measuring the crack spacing in Diana FEA gives a value of 250 mm, which yields a value of 0.1631 mm for the crack width. This results in an SLS unity check that is 11% less than using a model without bond slip.
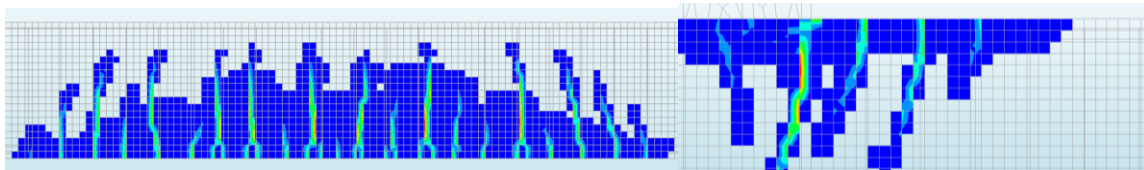
Figure 38. Crack width at location 1(150% loading) and location 2 (100% loading) using bond-slip model
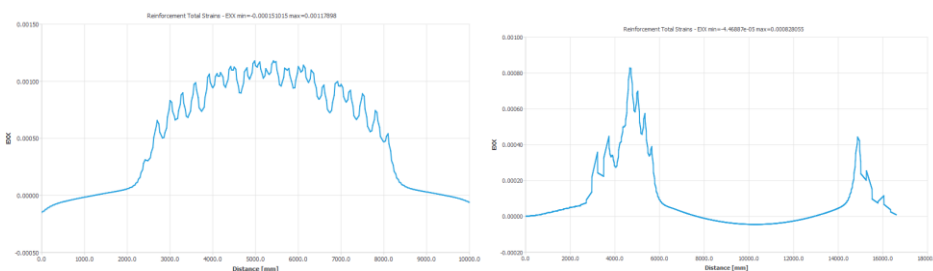
Figure 39. Steel strain at the bottom reinforcement (150% loading) and top reinforcement (100% loading)

In Figure 38 it can be noticed that using a bond-slip model and reducing the element size gives a better understanding of the crack development. At location 1, flexural cracks are developed and at location 2 flexural cracks followed by inclined flexural – shear cracks.

In the previous results the indirect calculation of the crack width according to the guidelines provided in RTD-1016-2020 is used. A direct estimation of the crack width is achieved by summing the relative displacement (slip) at both sides of the cracks. Using this method will give the exact result of the crack width.
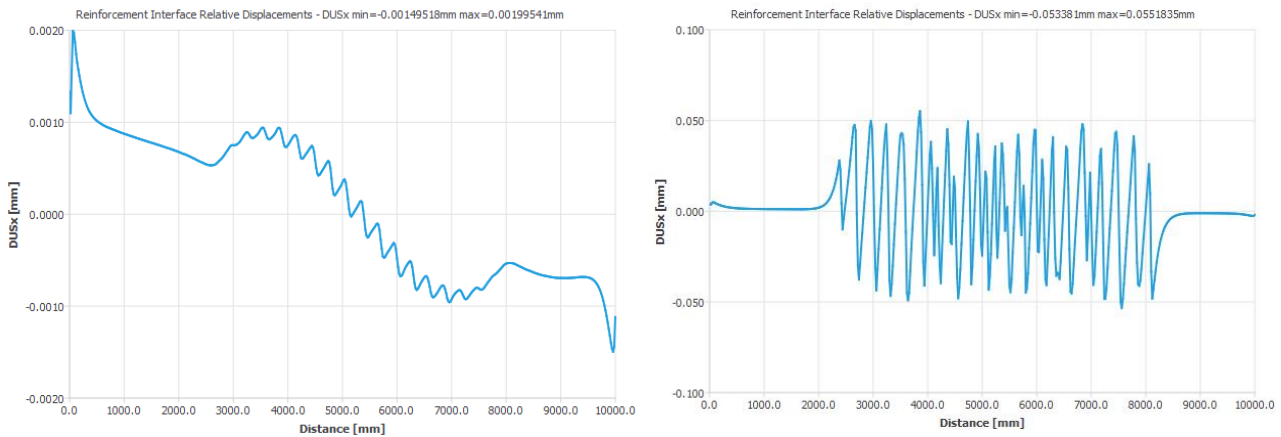
Figure 40. Slip of the bottom reinforcement rebar (100% loading vs 150% loading)

In Figure 40 the slip curve of the bottom reinforcement rebar is shown, where it can be noticed that cracks are not yet fully developed when the structure is loaded 100%. This can be established due to the very small value of the slip at the bottom reinforcement.
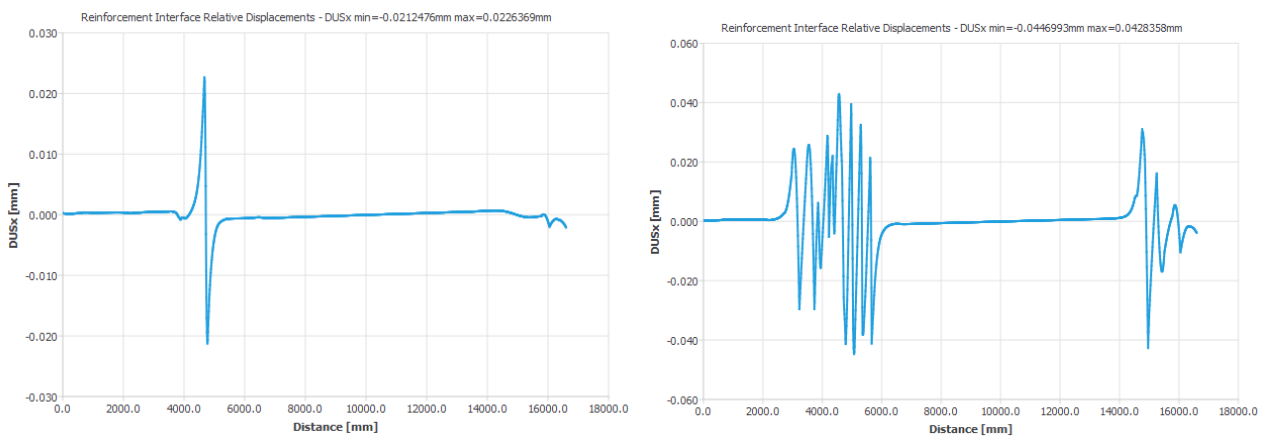
Figure 41. Slip of the top reinforcement rebar (60% loading vs 100% loading)

Looking at Figure 41 it can be established that cracks occur at the supports. A single crack occurs followed by the development of more cracks when the load increases.

The crack width according to the slip-curve is determined at location 1, then at location 2. At location 1, the cracks have not yet been fully developed when the structure is loaded 100%. The crack width is therefore calculated using linear extrapolation, as described in chapter 4.3.2.

TUDelft
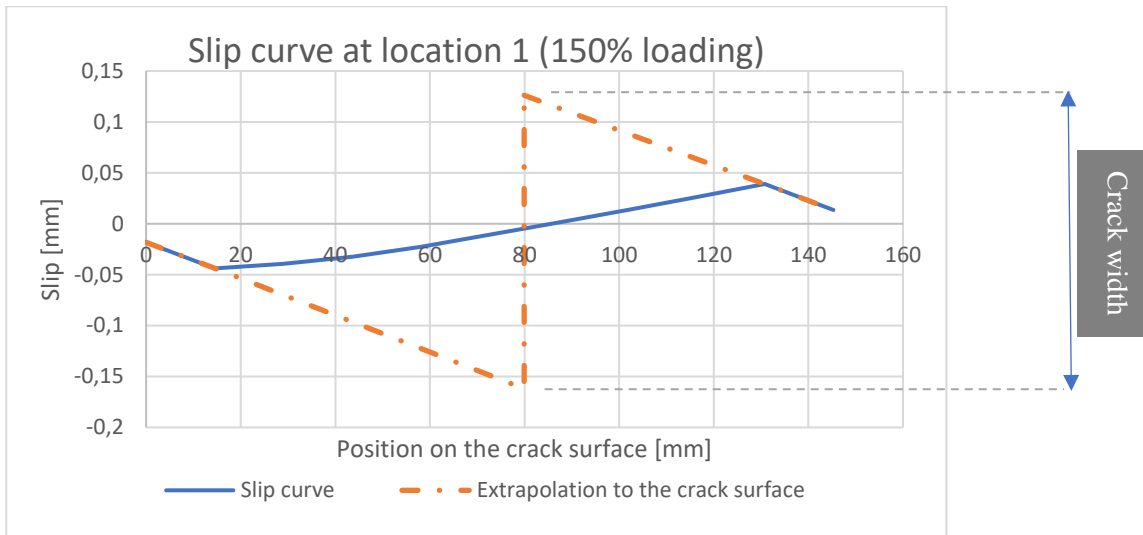
Figure 42. Slip-curve of the bottom reinforcement at location 1 (150% loading)

In Figure 42 the slip curve at a loading stage of 150% between the governing cracks at location 1 is given. Using the finite element analysis with a smeared cracking model, the slip is spread over at least one element. This causes the slip between the cracks to be connected with an ascending or descending line. In reality, the crack is concentrated in the center of the crack surface, so instead of a gradual transition between positive and negative slip values, both branches continue up to the center of the crack surface (middle). This is carried out by extrapolating the slip curve to the crack surface. The crack width is the sum of the slip at both sides of the crack, which yields a value of 0.2881 mm.

The same procedure described above is carried out at a loading stage of 140% and 130% to obtain the crack width at 100% loading. Hereafter, the crack width at 100% loading is calculated using linear extrapolation, which yields a result of 0.14 mm, illustrated in Figure 44. In comparison to adopting a model without bond slip, this yields an SLS unity check of 62%, which is 32% less.

In Figure 43 the slip curve between the governing cracks at location 2 is given. The same procedure by extrapolating the slip curve to the center of the crack surface is carried out. The crack width is the sum of the slip at both sides of the crack, which yields a value of 0.155 mm. This results in an SLS unity check of 70% which is 15% less than using a model without bond slip.
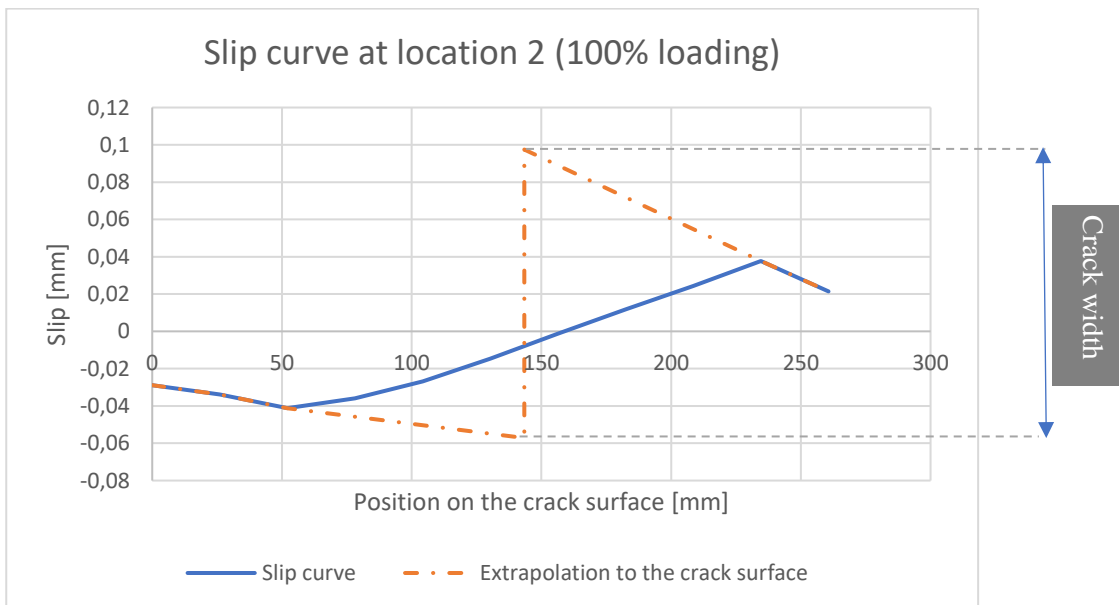
Figure 43. Slip curve at the top reinforcement at location 1 (100% loading)

In Figure 44 and Figure 45 the crack width development at locations 1 and 2 between the no bond slip and bond-slip model are shown.
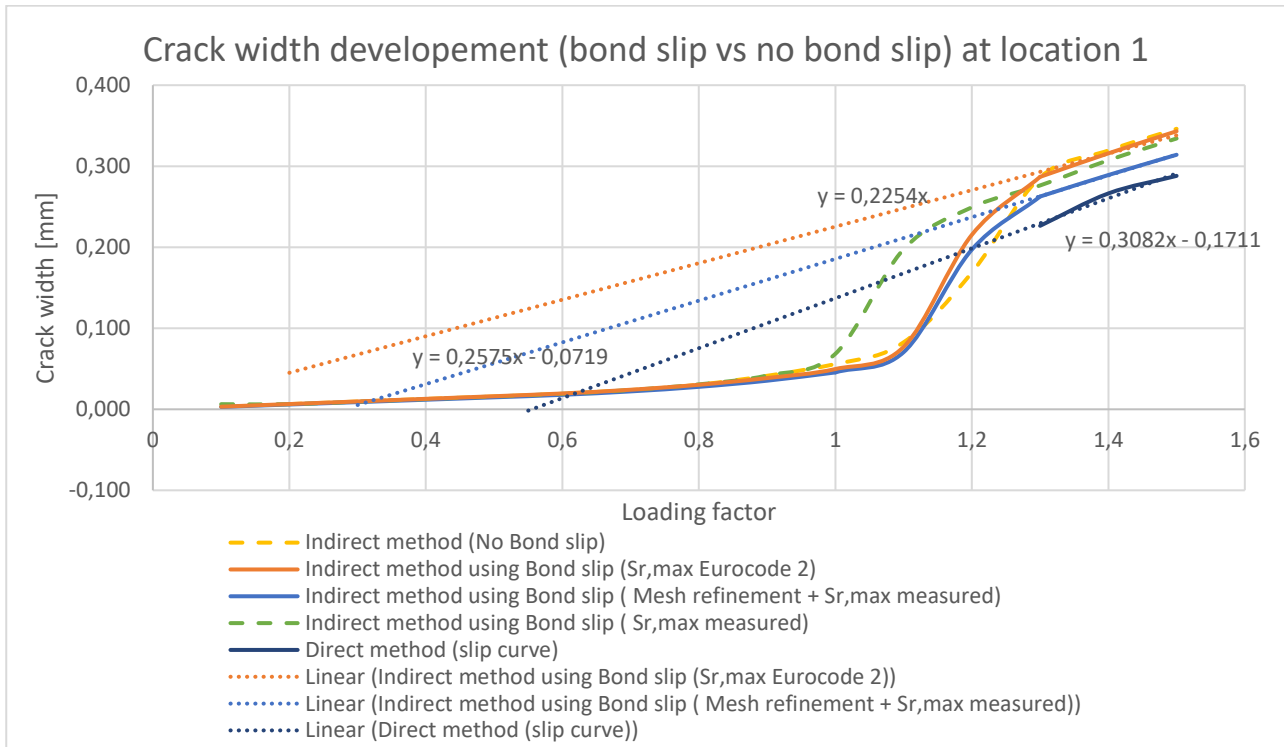
Figure 44. Crack width development using bond slip and no bond slip at location 1
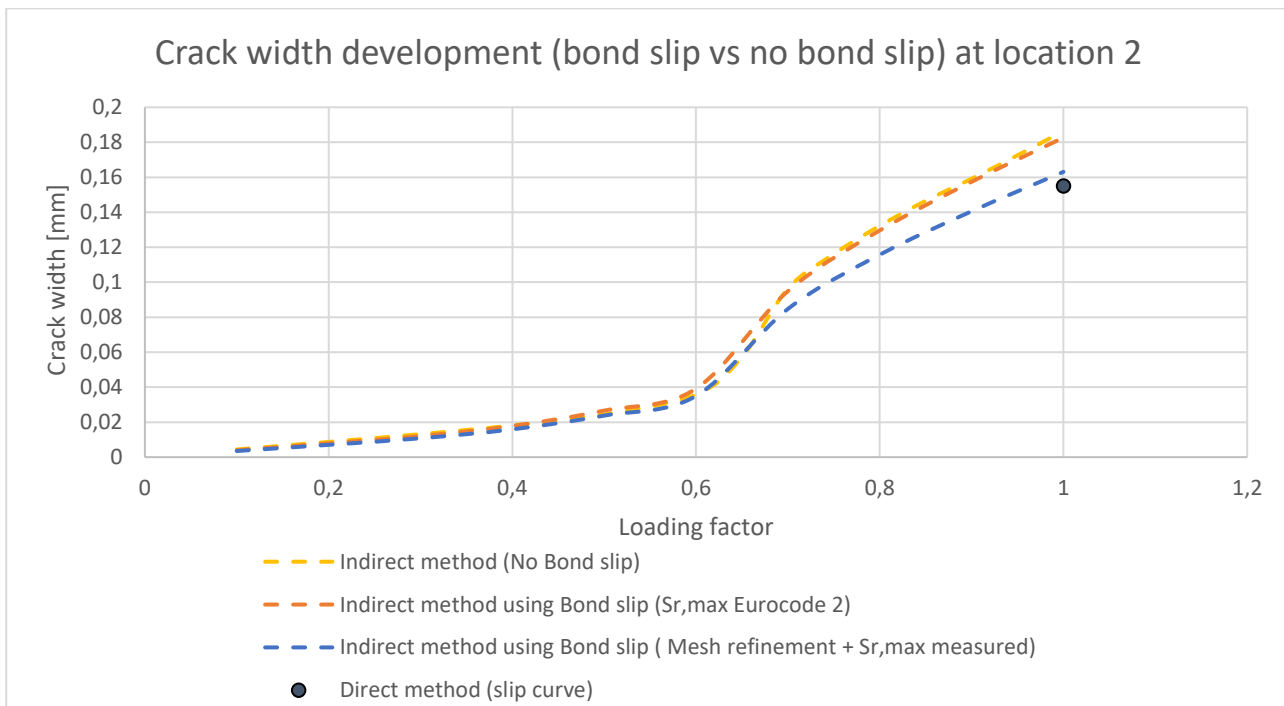
Figure 45. Crack width development using bond slip and no bond slip at location 2

4.5. Summary of the results

In this paragraph, a summary of the ULS and SLS unity check between the conventional and advanced approach is given.

In Table 47 a summary of the ULS unity check between the conventional and advanced approach at locations 1 and 2 is shown.

Table 47. Summary ULS unity check (conventional vs advanced)

	Reinforcement	Reinforcement area [mm2]	ULS unity check (conventional)	ULS unity check (advanced)
Location 1	Ø25-125 + Ø25-150	7944	96%	90%
Location 2	Ø20-125 + Ø16-150	3853	96%	81%

In Table 48 and Table 49 a summary of the SLS unity check between the conventional and advanced approach at locations 1 and 2 is shown.

Table 48. Summary SLS unity check at location 1 (conventional vs advanced)

Calculation approach	Reinforcement set	Reinforcement area [mm2]	$S_{r,max}$ [mm]	w_k [mm]	w_k (norm) [mm]	SLS unity check
Conventional	Ø20-125+ Ø25-125	6484	307	0.207	0.22	94%
Advanced (No Bond slip)	Ø20-125+ Ø25-125	6484	307	0.208	0.22	94%
Advanced using bond slip (Indirect method + Sr,max Eurocode 2)	Ø20-125+ Ø25-125	6484	307	0.203	0.22	92%
Advanced using bond slip (Indirect method + Sr,max measured)	Ø20-125+ Ø25-125	6484	281	0.1856	0.22	84%
Advanced using bond slip (direct method)	Ø20-125+ Ø25-125	6484	-	0.14	0.22	62%

Table 49. Summary SLS unity check at location 2 (conventional vs advanced)

Calculation approach	Reinforcement set	Reinforcement area [mm2]	$S_{r,max}$ [mm]	w_k [mm]	w_k (norm) [mm]	SLS unity check
Conventional	Ø25-125 + Ø32-120	10629	280	0.219	0.22	100%
Advanced (No Bond slip)	Ø25-125 + Ø32-120	10629	280	0.1864	0.22	85%
Advanced using bond slip (Indirect method + Sr,max Eurocode 2)	Ø25-125 + Ø32-120	10629	280	0.1827	0.22	83%
Advanced using bond slip (Indirect method + Sr,max measured)	Ø25-125 + Ø32-120	10629	250	0.1631	0.22	74%
Advanced using bond slip (direct method)	Ø25-125 + Ø32-120	6484	-	0.155	0.22	70%

4.6. Evaluation and discussion

Using the conventional approach results in an ULS unity check of 96% at both locations. Using the advanced approach, the ULS unity check is reduced to 81% at location 1 and to 90% at location 2. This means that 19% less reinforcement or concrete is needed at location 1 and 10% less at location 2. Compared to the conventional approach, this is a reduction of the ULS unity check by 15% at location 1 and by 6% at location 2. The optimization rate that is achieved is based on the assumptions of the quay wall of Engie.

It can also be noticed that at location 1 the ULS reduction is higher compared to location 2. In Diana FEA the optimization percentage is directly related to the ULS unity check, which is directly related to the strength that Diana FEA shows. In both cases it concerns bending, but in location 1 it is almost pure bending (V ~ 0), while at location 2 the moment/shear ratio is different. Also, at location 1 the bending moment is spread over a wider region compared to location 2. In the conventional approach, the shear force (V) and the course of the moment line are not considered for checking the cross-section, while in the advanced approach, these factors are considered. As a result, the maximum load at location 1 is reached at a later stage compared to location 2. Based on the calculated ULS conditions the structure can be optimized at locations 1 and 2, which is numerically examined in the next chapter.

Using the indirect method provided in RTD-1016-2020, the SLS unity check is reduced at location 2, but not at location 1. This is because the nonlinear behavior of the structure is not completely active at location 1 when the structure is loaded 100%, which is verified based on the load-displacement graph shown in Figure 46.
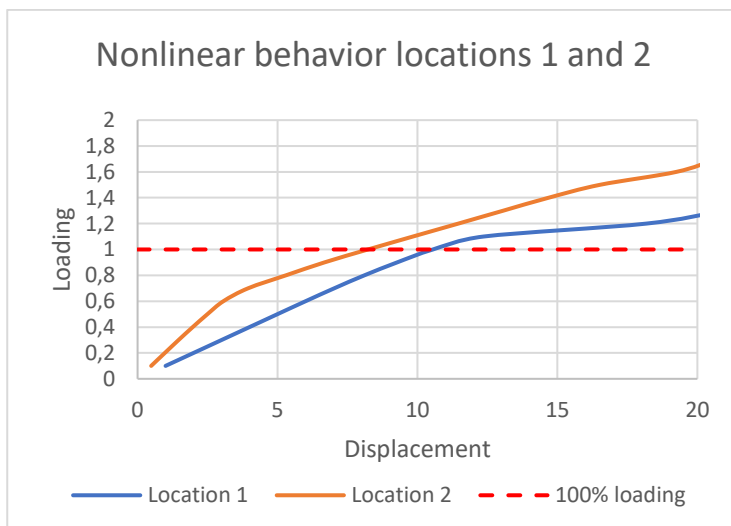
Figure 46. Load-displacement graph at locations 1 and 2 using the SLS

The conventional approach assumes a fully cracked cross-section when the tensile strength of the concrete is reached. This is not the case for the advanced approach, which uses a tension-softening behavior, meaning that the concrete still contributes after the tensile strength is reached. In Figure 47 the tensile behavior of the concrete at locations 1 and 2 is shown.
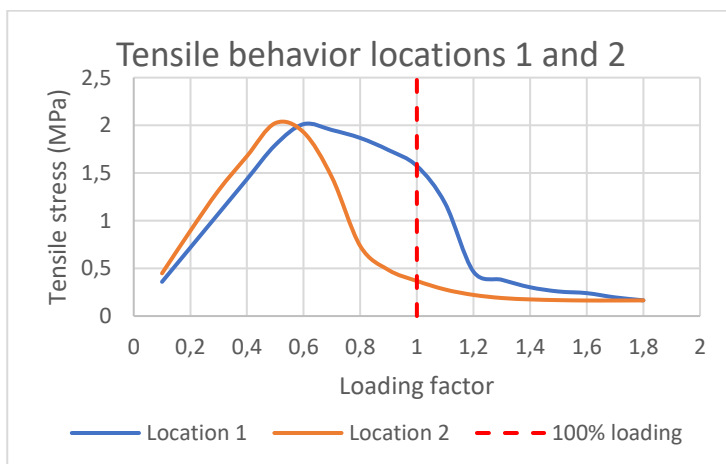
Figure 47. Tensile behavior of concrete at locations 1 and 2

TUDelft

Although the tensile strength has been reached at location 1, due to the softening behavior the concrete still contributes when the structure is loaded 100%. The incomplete nonlinear behavior and the contribution of the concrete results in cracks that are not yet fully developed. At location 2, the SLS unity check is 15% less than the conventional approach, meaning about 15% less reinforcement is needed to satisfy this condition. Based on the SLS conditions the structure can only be optimized at location 2, but not at location 1.

When using a bond-slip model, the crack width decreases. This results in a reduced SLS unity check at both locations, implying that the structure can be further optimized with bond slip. When considering the crack spacing of the Eurocode 2, the crack width between the bond-slip and no bond-slip models is comparable at both locations. The optimization possibility is due to the measured crack spacing in Diana FEA. Also, directly estimating the crack width based on the slip curve (direct method) provides the most favorable outcome. More research should be carried out by further reducing the element size to get the exact crack spacing and also by adjusting the bond-slip relationship curve of Figure 6.1-1 from the fib Model Code 2010. It is also recommended that a different bond-slip model is used to investigate what the impact between the different models is on the crack width.

Convergence of nonlinear analysis is not reached at every step. This is because many cracks are being formed over the entire structure, while the critical cracks are only developed at one location. It is a possibility that convergence is reached at the location of the critical cracks, which can be considered for further study. By reducing the load steps or using a different iterative procedure should result in convergence. However, reducing the load step will drastically increase the computational time. Because of insufficient capacity, the analysis has not been performed with smaller load steps until convergence. This should be performed to get an accurate result. It is not necessary to reach convergence at every step but is it preferable.

5

Optimization phase

In this chapter, numerical analyses are carried out using the optimization rate for the ULS and SLS that is established in the previous chapter. This is carried out to ensure that the optimization rate is correct and that this result can be trusted. The analyses are done based on the optimization of the reinforcement and geometry for the ULS, and the optimization of the reinforcement for the SLS based on the indirect method provided in RTD-1016-2020 without using bond slip. The numerical analyses are not carried out using the optimization rate obtained from using a bond-slip model, because more research should be done to obtain the exact crack width. Also, the geometry is optimized for the SLS based on the direct method using Idea Statica.

5.1. Reinforcement optimization

In this paragraph, the reinforcement is optimized based on the ULS and the SLS using the optimization rate that is calculated in the previous chapter.

5.1.1. Reinforcement Optimization based on the ULS

In this paragraph, a numerical analysis is performed where reinforcement at location 1 and location 2 is optimized based on the ULS conditions. The reinforcement is optimized at location 1 followed by location 2. From the results of the previous chapter, the reinforcement can be reduced by 19% at location 1 and by 10% at location 2. The optimized reinforcement with the optimization rate for that reinforcement set is given in Table 50.

Table 50. Optimized reinforcement set at location 1 and location 2

	Reinforcement set	Reinforcement area [mm²]	Optimization rate
Location 1	Ø16-125 + Ø16-125	3215	17%
Location 2	Ø25-125 + Ø20-120	6581	9%

At location 1, 17% less reinforcement has been used, which should give an ULS unity check close to 98%. For the advanced strength verification, the optimized designed reinforcement to meet the ULS has been modeled in Diana FEA. The result of the physical nonlinear analysis in terms of the load-displacement diagram is shown Figure 48.
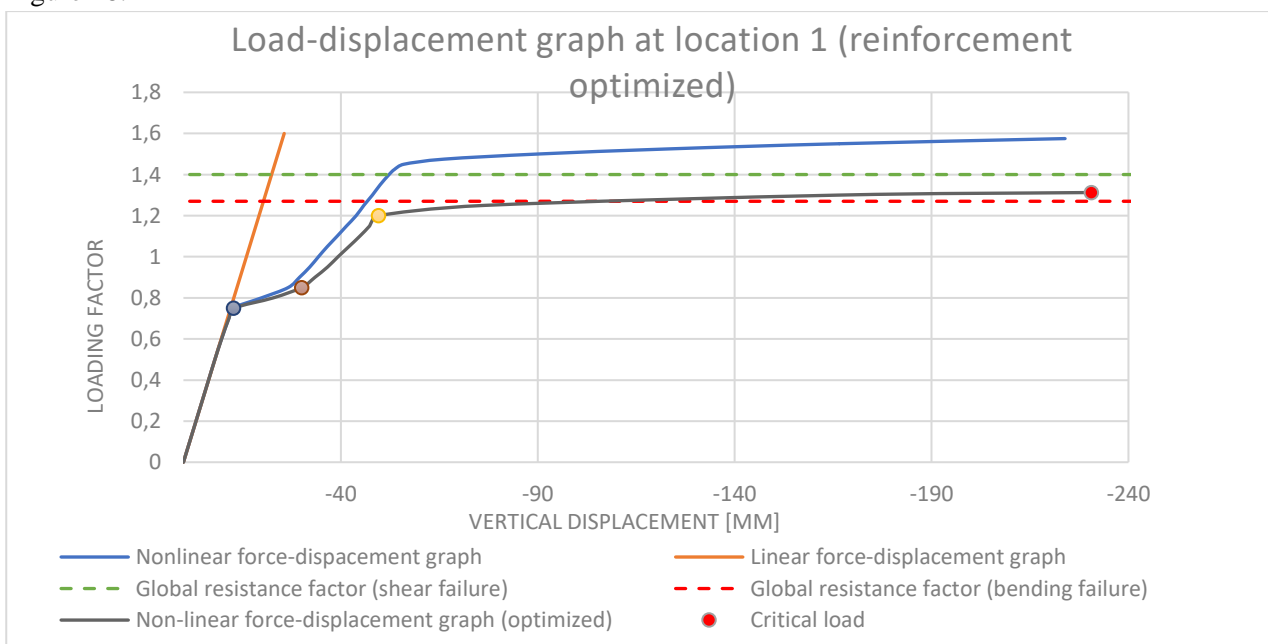
Figure 48. Optimized load-displacement graph at location 1 (reinforcement set Ø16-125 + Ø16-125)

In the figure above the load-displacement graph for the optimized reinforcement set is shown. The maximum load is about 3% above the GRF and the ULS unity check is $\frac{1.27}{1.30} \times 100\% = 98\%$. The same procedure has been carried out at location 2 with 9% less reinforcement.
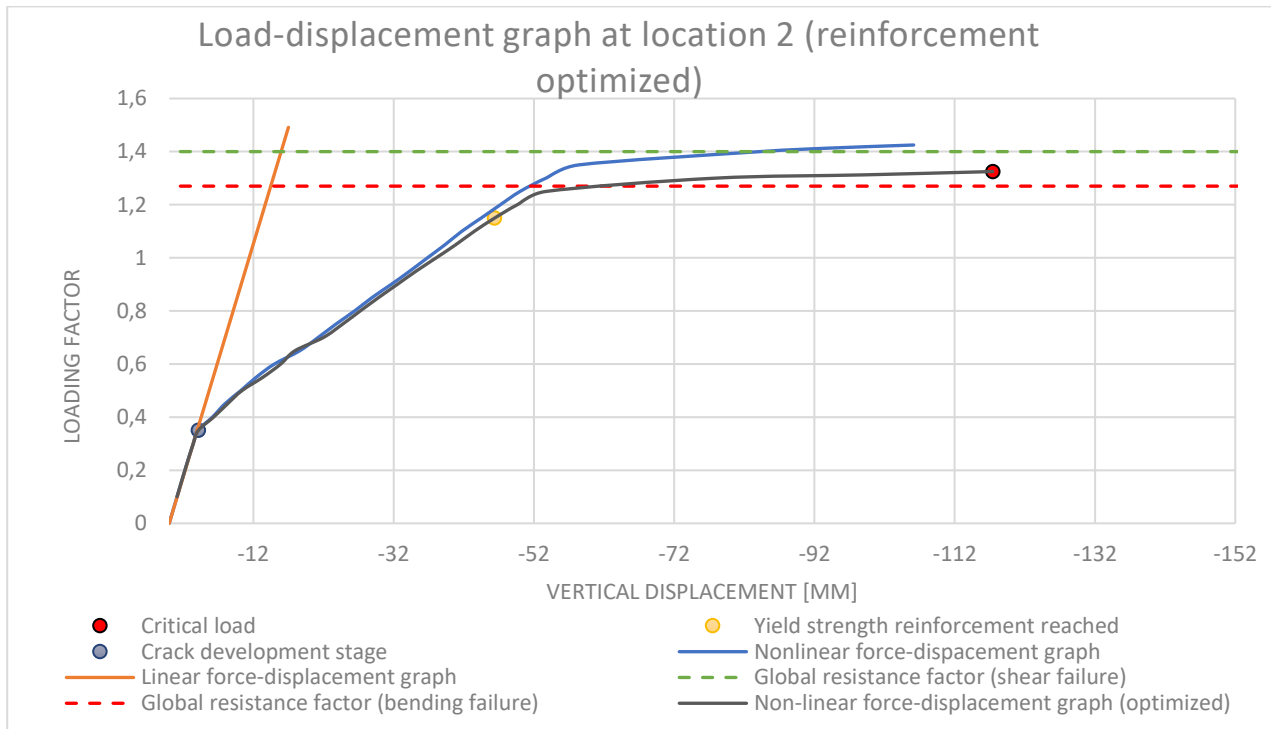
Figure 49. Optimized load-displacement graph at location 2 (reinforcement set Ø25-125 + Ø20-120)

In Figure 49 the load-displacement graph for the optimized reinforcement set is shown. The maximum load is about 3% above the GRF and the ULS unity check is $\frac{1.27}{1.3125} \times 100\% = 97\%$.

5.1.2. Reinforcement optimization based on the SLS

In this paragraph, a numerical analysis is performed where the reinforcement is optimized at location 2 based on the SLS conditions. The previous chapter stated that the reinforcement can be optimized by 15% at location 2, which means 15% less reinforcement can be used. A reinforcement set of Ø20-125 + Ø32-150 is considered, which is about 13% less than the previous set. An SLS unity check close to 98% should be obtained using this reinforcement set. For the crack width verification, the optimized designed reinforcement to meet the SLS has been modeled in Diana FEA. The result of the physical nonlinear analysis in terms of the crack width development diagram is shown in Figure 50.
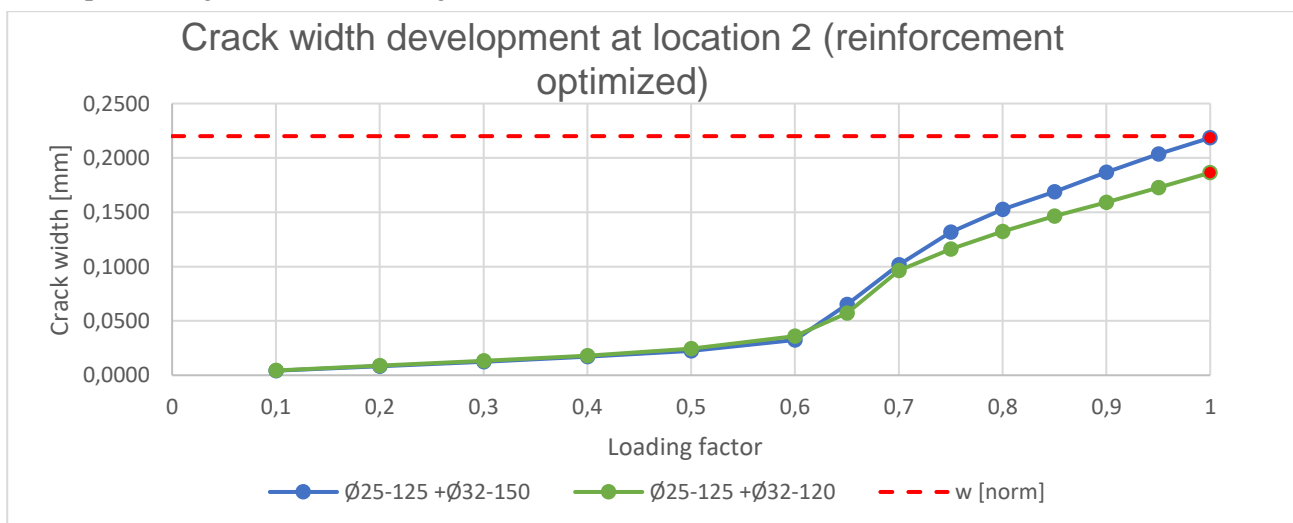
Figure 50. Optimized crack-development graph at location 2

Table 51. Optimized crack width at location 2

Reinforcement	Reinforcement area [mm2]	wk (diana) [mm]	wk(norm) [mm]	SLS unity check
Ø25-125 +Ø32-120	10629	0.186	0.22	85%
Ø25-125 +Ø32-150	9289	0.219	0.22	99%

In Table 51 the value of the crack width is shown for the optimized reinforcement set. The SLS condition of the optimized reinforcement set is 99%, which is close to the predicted value.

5.2. Geometry optimization

5.2.1. Geometry optimization based on the ULS

In this paragraph, a numerical analysis is performed where the geometry of the structure at location 1 and location 2 is optimized based on the ULS conditions instead of the reinforcement. At location 1, a maximal loading factor of 1.575 is achieved, which results in a ULS unity check of 81%. To optimize the geometry an opposite approach has been used where the height of the geometry has been reduced by about 18% instead of the amount of reinforcement. The same procedure is carried out at location 2 with a reduction of the geometry by about 8%. The internal forces change along with the geometry's dimensions.

In Table 52 the ULS unity check for the reduced geometry are shown. Also, a comparison is made between the ULS unity check of the conventional, and advanced methods based on this reduction.

Table 52. Optimized geometry at location 1 and location 2 based on the ULS

Location	Height [mm]	Optimization rate	Reinforcement set	Reinforcement area [mm²]	ULS unity check (IDEA)	ULS unity check (Diana)
1	1250	-	Ø20-125 + Ø16-150	3853	96%	81%
	1025	18%	Ø20-125 + Ø16-150	3853	111%	96%
2	1250	-	Ø25-125 + Ø25-150	7199	96%	90%
	1150	8%	Ø25-125 + Ø25-150	7199	105%	99%

From the result of Table 52 can be noticed that when the geometry decreases using the conventional approach, the ULS unity check increases and becomes insufficient. The load-displacement graphs based on the optimized geometry are shown in the figures below. As seen in Figure 51, the maximum load is 3.25% above the GRF, resulting in an ULS unity check of 96%. In Figure 52, the maximum load is 2% above the GRF, resulting in an ULS unity check of 99%.
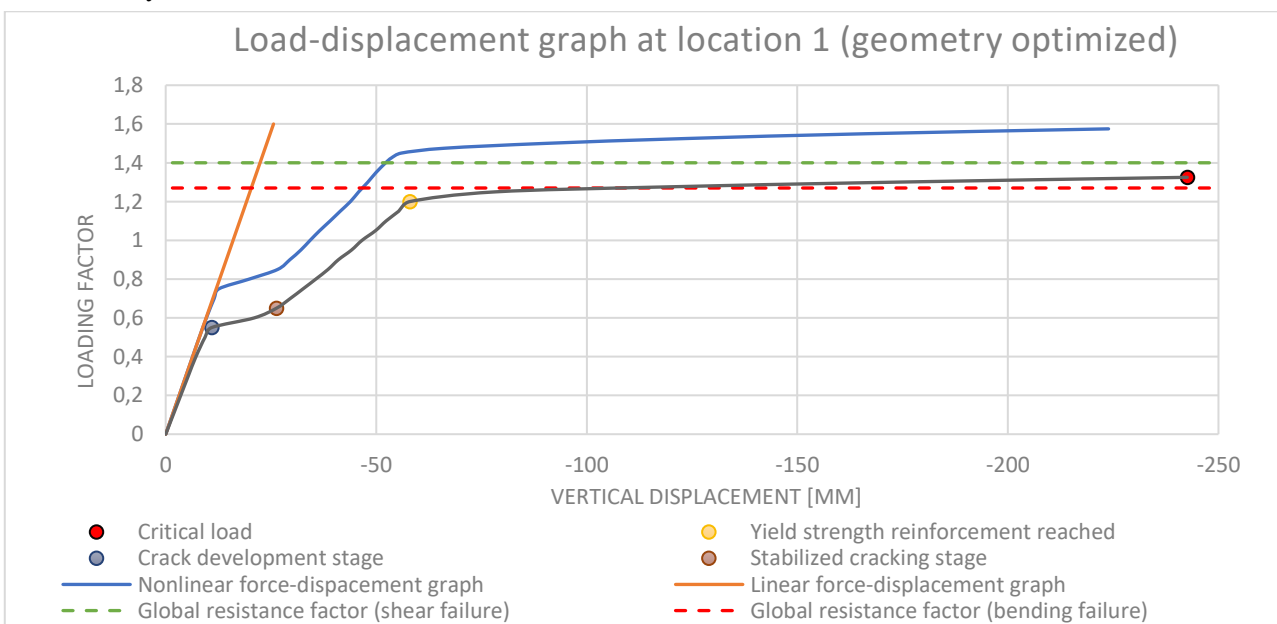
Figure 51. Optimized load-displacement graph at location 1 (h=1025 mm)
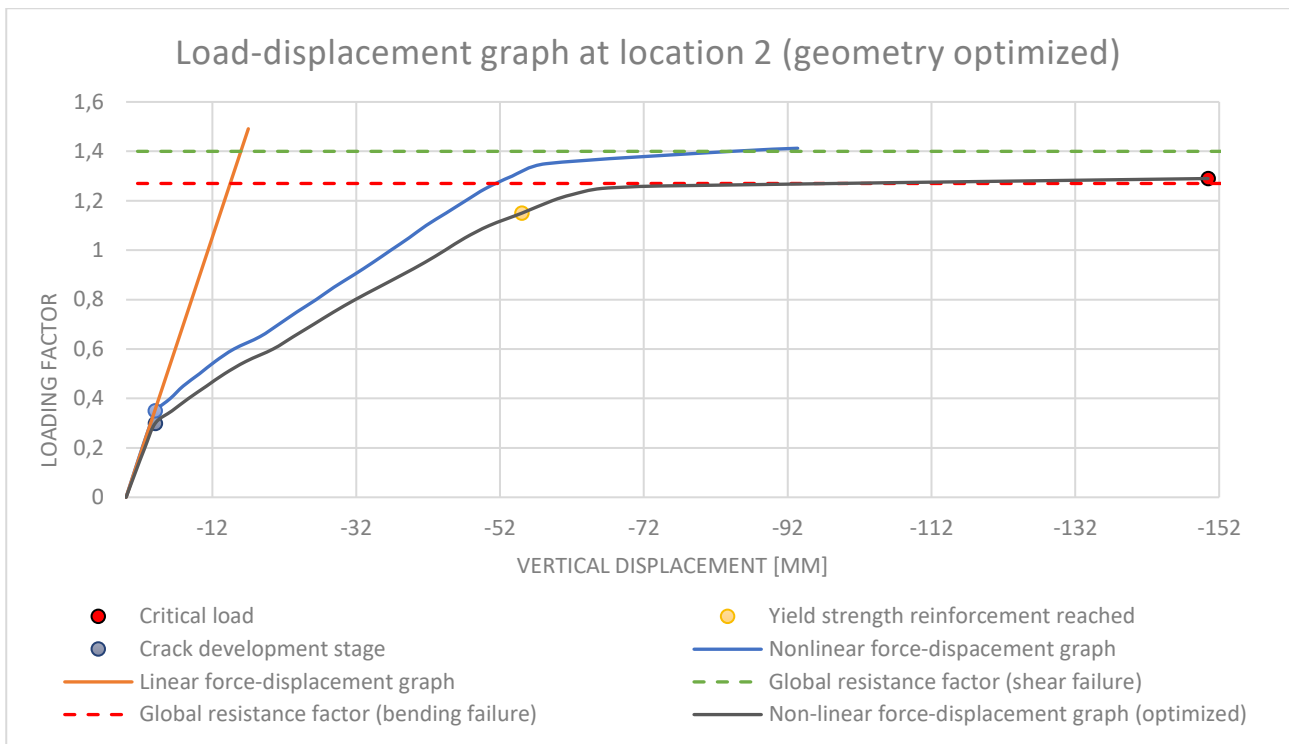
Figure 52. Optimized load-displacement graph at location 2 (h=1150 mm)

5.2.2 Geometry optimization based on the SLS

In this paragraph, the geometry of the relief floor at location 1 and location 2 is not numerically examined but optimized using Idea Statica based on the SLS conditions instead of the reinforcement. Using the advanced approach based on the direct method results in the most favorable outcome for the crack width. This results in an SLS unity check of 63% at location 1 and 70% at location 2. The unity check using the conventional approach is 95% at location 1, which is a difference of 32% compared to the advanced approach. At location 2 the unity check using the conventional approach is 100%, which is a difference of 30% compared to advanced approach.

An assumption is made that the SLS unity check using the conventional approach should increase by 32% at location 1, and by 30% at location 2 to achieve an SLS unity check of 100% using the advanced approach. As a result, the SLS unity check using the conventional approach should be about 132% at location 1, and about 130% at location 2. The geometry is optimized until the SLS unity check mentioned above is achieved using Idea Statica.

Table 53. Optimized geometry at location 1 and location 2 based on the SLS

Location	Height [mm]	Optimization rate	Reinforcement set	Reinforcement area [mm²]	SLS unity check (IDEA)	SLS unity check (Diana)
1	1250	-	Ø20-125 + Ø25-125	7899	95%	63%
	875	30%	Ø20-125 + Ø25-125	7899	132%	-
2	1250	-	Ø25-125 + Ø32-120	10674	100%	70%
	975	22%	Ø25-125 + Ø32-120	10674	128%	-

Look at Table 53 it can be noticed that the geometry can be optimized by 30% at location 1, and by 22 % at location 2.

5.3. Evaluation and discussion

From the result above it can be concluded that the optimization rate gives a good indication. Using the advanced approach based on the ULS, reducing the reinforcement or geometry results in a maximal load close to the GRF. To obtain an exact outcome on the GRF level, the structure must be precisely optimized depending on the optimization rate.

Using the advanced approach based on the SLS, the reinforcement can be reduced by 15% at location 2. Because the structure can only be optimized at location 2 and not at location 1 when a perfect bond is assumed, the geometry is not optimized for the SLS. This is because the SLS condition at location 1 becomes insufficient if the geometry is optimized based on the optimization rate at location 2.

Using the advanced approach based the SLS and the direct method result in the most favorable outcome. For the optimization of the height of the geometry the governing value of 975 mm is used, which is a reduction of 22%. This is because the SLS unity check at location 2 becomes insufficient if the geometry is optimized based on the optimization rate at location 1.

Optimizing the reinforcement causes the bending moment resistance (M_{Rd}) in the ULS to decrease when yielding is reached. As a result, the yield strength of steel is achieved at an earlier loading stage in Diana FEA, which causes the maximum load to decrease. Additionally, the steel stress (σ_s) in the SLS increases, which results in an increase of the reinforcement strain (ε_s) in Diana FEA. As a result the crack width increases.

Optimizing the geometry influences the internal forces, bending stiffness (EI), and section modulus (W) of the structure. Due to the smaller level arm, the bending moment resistance (M_{Rd}) in the ULS reduces when yielding is reached. As a result, the yield strength of steel is achieved at an earlier loading stage in Diana FEA, which causes the maximum load to decrease. The optimization of the geometry also has an impact on the shear reinforcement, but since it is strong enough, failure does not occur. This is examined by verifying the stresses of the shear reinforcement when the maximum load is reached.

In Figure 53 the principle for determining the bending moment resistance using the equilibrium of forces when yielding is reached is shown.
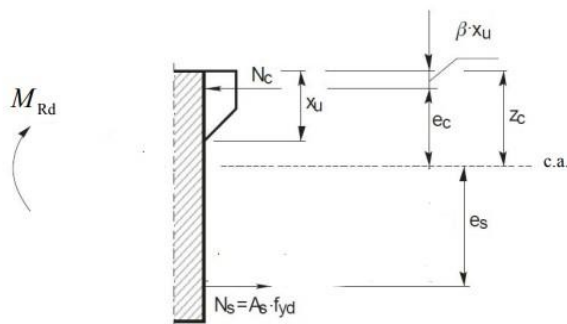
Figure 53. Bending moment resistance using the equilibrium of forces

The optimization rate is utilized in the next chapter to compare the amount of steel and concrete used in the conventional and advanced approaches.

6

Comparison phase

In this chapter, a comparison is made between the advanced and conventional approach in the terms of the amount of steel and concrete and the CO_2 footprint. Two design approaches are carried out: one that reduced the quantity of steel by optimizing the reinforcement and another that reduces the amount of concrete by optimizing the geometry. The optimization is carried out based on the ULS and the SLS, which consist of an artificial and actual designed reinforcement explained in chapter 3.4. For the SLS, the optimization rate gained using the direct method is used.

6.1. Comparison amount of concrete and steel

In the previous chapter, the optimized reinforcement and optimized geometry rate are given which will be used in this paragraph. For the reduction of the geometry, the governing value is used.
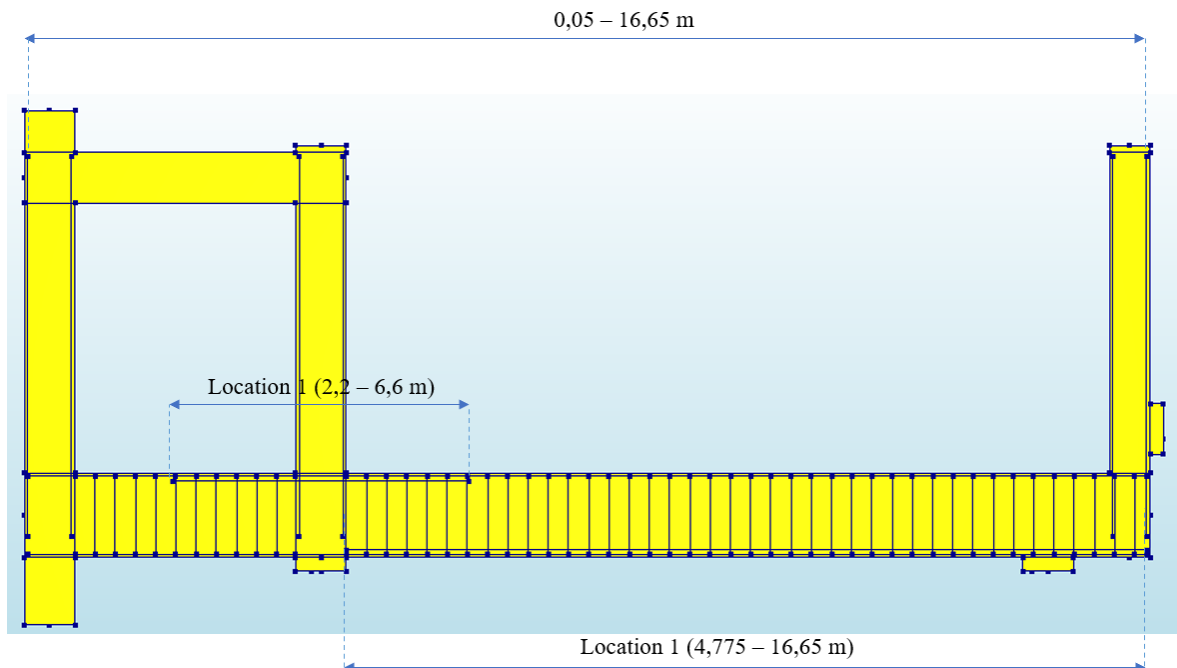
Figure 54. Reinforcement set distribution over the transverse direction of the platform

In this thesis the main reinforcement and the dimensions of the relief floor has been optimized. The total amount of concrete and steel is determined based on the optimization of the main reinforcement at the critical locations and the geometry. The amount of longitudinal reinforcement and stirrups has been neglected to get a clearer understanding of the reduction rate.

For the conventional model, the main reinforcement at the top and bottom of the relieving platform runs along the full length of the structure. The additional reinforcement at location 1(bottom side relief floor) is spread over a distance of 11.875 meters and at location 2 (top side relief floor) over a distance of 4.4 meters. In the advanced model, the reinforcement at locations 1 and 2 is optimized based on the ULS and the SLS while the reinforcement is distributed similarly to the conventional model. In appendix II, the calculation of the amount of reinforcement steel for the conventional and advanced approach is given.

The amount of steel is calculated based on the optimization of the main reinforcement, followed by the amount of concrete based on the optimization of the geometry.

In Table 54 and Table 55 the total amount of steel and concrete used expressed in cubic meters and kilograms for the conventional and advanced model by optimizing the reinforcement based on the ULS is shown. To get the weight of the steel, the steel volume is multiplied by the weight of the steel per cubic meter, which is 7850 kg/m³. To get the weight of the concrete, the volume of the concrete being used is multiplied with the weight

of the concrete per cubic meter, which is 2500 kg/m^3. In the tables below, the amount of concrete and steel being used expressed in cubic meters and kilograms is shown.

Table 54. Amount of concrete and steel based on 40-meter quay (reinforcement optimized based on the ULS)

	Total Volume[m3]	Amount of steel [m^3]	Amount of concrete [m^3]	Total weight of the steel [kg]	Total weight of concrete [kg]
Conventional approach	835	5.49	829.51	43100.6	2073773.70
Advanced approach	835	5.13	829.87	40287.0	2074669.74
		0.36	-0.36	2813.6	-896.04

Table 55. Amount of concrete and steel based on 220-meter quay (reinforcement optimized based on the ULS)

	Total Volume[m3]	Amount of steel [m3]	Amount of concrete [m3]	Total weight of the steel [kg]	Total weight of concrete [kg]
Conventional approach	4593	30.20	4562.30	237053.2	11405755.36
Advanced approach	4593	28.23	4564.27	221578.6	11410683.57
		1.97	-1.97	15474.6	-4928.20

According to the results in Table 54, the advanced approach uses 2814 kg less steel than the conventional approach. Using less steel results in additional space for concrete. Here it is clear that using less steel results in 896 kg more concrete due to the additional open space. In Table 55 the amount of concrete and steel is calculated using the entire length of the quay wall. The advanced approach uses 15474.6 kg less steel and 4982.2 kg more concrete compared to the conventional approach. This is 7% less steel being used compared to the conventional approach.

For the optimization of the geometry, an opposite approach where the reinforcement remains constant has been used, which is explained in the previous chapter.

Table 56. Amount of concrete and steel based on 40-meter quay (geometry optimized based on the ULS)

	Height of the geometry [m]	Amount of steel [m3]	Total weight of the steel [kg]	Amount of concrete[m3]	Total amount of concrete [m3]	Total Weight of concrete [kg]
Conventional approach	1.25	5.49	43100.58	835	829.51	2073773.70
Advanced approach	1.15	5.49	43100.58	768	762,71	1865023.70
					66,80	167000.00

Table 57. Amount of concrete and steel based on 220-meter quay (geometry optimized based on the ULS)

	Height of the geometry [m]	Amount of steel [m3]	Total weight of the steel [kg]	Amount of concrete[m3]	Total amount of concrete [m3]	Total Weight of concrete [kg]
Conventional model	1.25	30.20	237053.17	4593	4562.30	11405755.36
Advanced model	1.15	30.20	237053.17	4225	4194.90	10487255.36
					367.40	918500.00

According to the results in Table 56, it is clear that reducing the height of the geometry results is 167000 kg less concrete. In Table 57 the amount of concrete and steel is calculated using the entire length of the quay wall. The advanced approach uses 918500 kg less concrete compared to the conventional approach. This is 8% less concrete being used.

TUDelft

For optimization based on the SLS, the same approach carried out for the ULS explained above has been used.

Table 58. Amount of concrete and steel based on 220-meter quay (reinforcement optimized based on the SLS)

	Total Volume[m3]	Amount of steel [m3]	Amount of concrete [m3]	Total weight of the steel [kg]	Total Weight of concrete [kg]
Conventional model	4593	39,58	4552,92	310700,8	11382300,69
Advance model	4593	30,53	4561,97	239623,4	11404936,83
		9,05	-9,05	71077,5	-22636,13

According to the results in Table 58, the advanced approach uses 71078 kg less steel, which is a reduction of 23% compared to the conventional approach.

Table 59. Amount of concrete and steel based on 220-meter quay (geometry optimized based on the SLS)

	Height of the geometry [m]	Amount of steel [m3]	Total weight of the steel [kg]	Amount of concrete[m3]	Total amount of concrete [m3]	Total Weight of concrete [kg]
Conventional model	1,25	39,58	310700,8246	4593	4552,92	11382300,69
Advanced model	0,975	39,580	310700,8246	3582	3542,57	8856425,69
					1010,35	2525875,00

According to the results in Table 59, the advanced approach uses 2525875 kg less concrete, which is a reduction of 22% compared to the conventional approach.

6.2. Comparison CO_2 footprint

In this paragraph, a life cycle assessment (LCA) is performed to calculate the CO_2 footprint of the concrete and steel. A life cycle assessment is a tool to quantify the environmental impact, in this case, the "global warming potential", which is expressed in "CO_2-equivalents". The global warming potential is defined as the effect of emissions due to human activities on the 'heat radiation absorbing capacity' of the lower atmosphere [3].

To calculate the environmental cost indication (ECI) value, a specific value in Euros is allocated to the unit equivalent. The unit equivalent value for global warming potential is 0.05 €/kg CO_2 equivalents. This is the value related to the costs required to compensate for the damage done to the environment. The total environmental cost of a product is referred to as the "shadow costs" of the product [3]. The environmental impact value of concrete C30/37 and reinforced steel are given in appendix II, which is multiplied by the amount expressed in kg.

A comparison is made between the CO_2 footprint of the concrete, and the steel based on ULS and SLS optimization. The comparison is made between the conventional and advanced approaches, where the reinforcement and the geometry are optimized. This provides knowledge on the best design procedure in terms of the CO_2 footprint. The comparison is made between the conventional and advanced approaches where the designed reinforcement is optimized.

In the tables below the calculated shadow costs for the ULS expressed in Euros are given.

Table 60. Shadow cost concrete and steel (conventional approach (ULS))

Shadow prize (Euro) per kg equivalents		€	0.05
Impact category	**Unit**	Global warming (GWP100)	Total Shadow costs
Unit		kg CO_2 eq	Euro (€)
Concrete C30/37 (CEM III)	kg	1077770.265	€ 53.888,51
Steel reinforcement for concrete	kg	424649.3081	€ 21.232,47
			€ 75.120,98

Table 61. Shadow cost concrete and steel (advanced approach (ULS)- reinforcement optimized)

Shadow prize (Euro) per kg equivalents		€ 0.05	
Impact category	Unit	Global warming (GWP100)	Total Shadow costs
Unit		kg CO_2 eq	Euro (€)
Concrete C30/37 (CEM III)	kg	1078235.949	€ 53.911,80
Steel reinforcement for concrete	kg	396928.6812	€ 19.846,43
			€ 73.758,23

Table 62. Shadow cost concrete and steel (advanced approach (ULS) - geometry optimized)

Shadow prize (Euro) per kg equivalents		€ 0.05	
Impact category	Unit	Global warming (GWP100)	Total Shadow costs
Unit		kg CO_2 eq	Euro (€)
Concrete C30/37 (CEM III)	kg	969279.8631	€ 48.463,99
Steel reinforcement for concrete	kg	424649.3081	€ 21.232,47
			€ 69.696,46
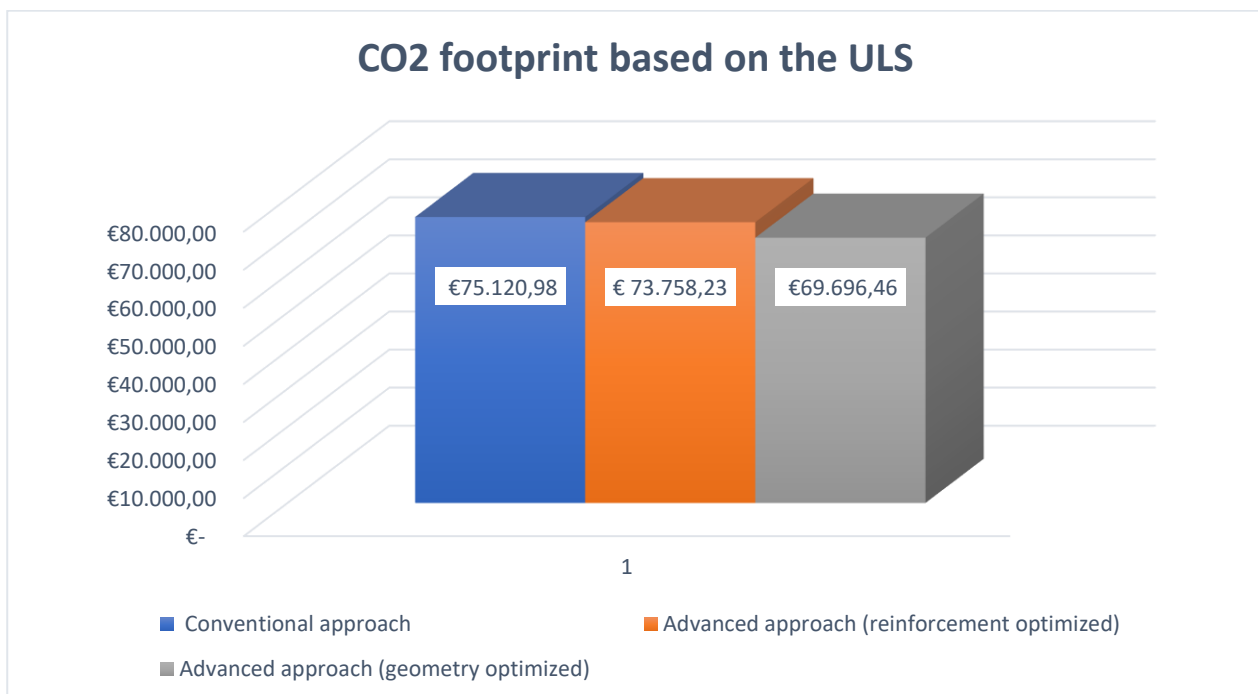
Figure 55. CO_2-footprint between the conventional and advance approach based on the ULS optimization

From the results of Figure 55, it is clear that optimizing the reinforcement or the geometry results in a reduction of the CO_2 footprint. Although the environmental impact of steel is greater than that of concrete, the reduction in footprint achieved by optimizing the geometry is greater. This is because much more concrete is used than steel. When compared to the conventional approach, optimizing the geometry results in €5.424,52 (6%) less CO_2 emission, and optimizing the reinforcement in €1.362,75 (2%) less emission. This result is based on a relieving platform with a length of 220 meters. If the platform's length is doubled, the environmental cost will rise by a factor of two as well.

Also, a comparison is made between the CO_2 footprint of the concrete, and the steel based on the SLS optimization, given in appendix II.
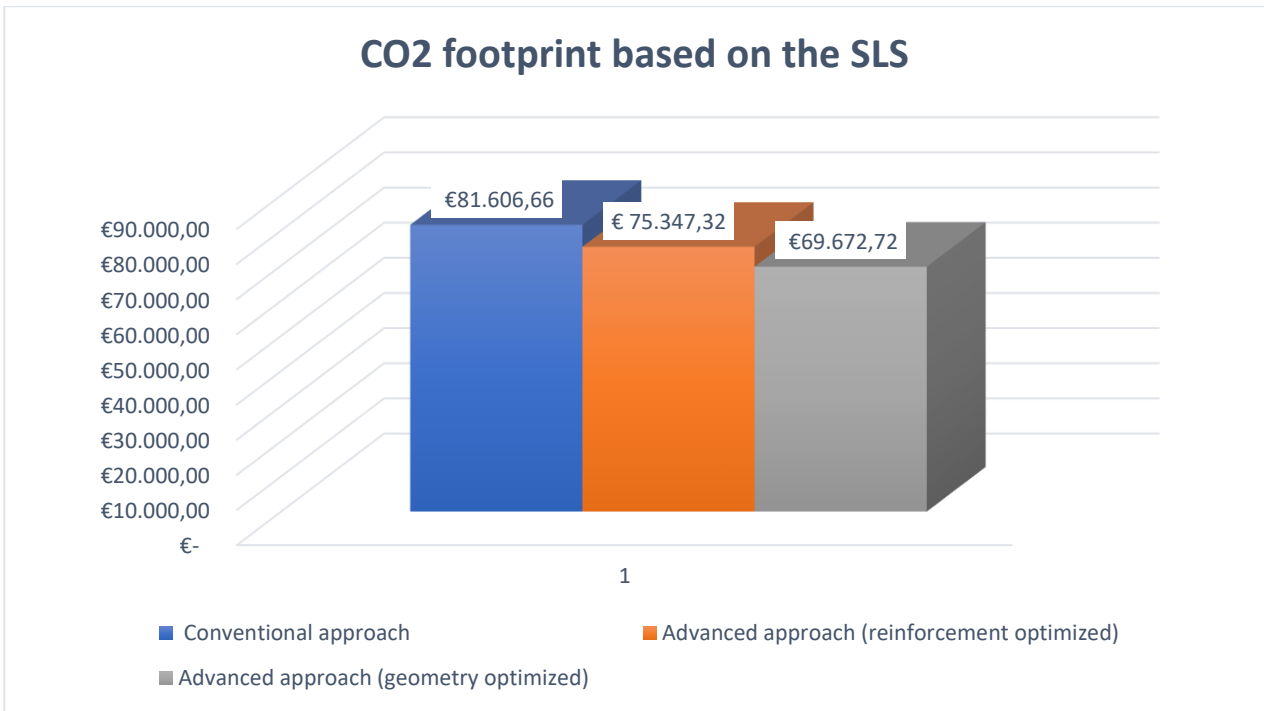
Figure 56. CO₂-footprint between the conventional and advance approach based on the SLS optimization

Looking at Figure 56, optimizing the reinforcement results in €6260 (8%) less CO$_2$ emission, and optimizing the geometry in €11934 (15%) less emission. This result is based on a relieving platform with a length of 220 meters.

7

Conclusion

The main goal of this thesis is to determine to what extent the use of concrete and steel is reduced by further optimizing the reinforcement or the dimensions of the specific quay wall of Engie. The optimization is performed using advanced calculations in Diana FEA with volume elements and by performing nonlinear analyses based on the ULS and SLS. The expectation is that by using less material, the CO_2 emission will also decrease.

The conventional approach consists of general assumptions, such as plane sections remaining plane, etc., which do affect the amount of steel and concrete being used. The conventional calculation is carried out by performing a Linear Elastic Analysis, meaning that the yield stress does not exceed. The reinforcement is calculated using the internal forces and is based on the NEN-EN-1992-1-1.

The results of this study lead to the following conclusions:

- The critical locations for the top and bottom reinforcement of the relief floor are identified, which are at a distance of 10.1 meters from the exterior surface of wall A (location 1), and at the combi-wall (location 2).

- When the reinforcement is calculated using the crack width of the National Annex of the Eurocode 2, which is 0.22 mm, the SLS unity check governs. Using the conventional approach for designing the reinforcement results in an SLS unity check of 95% at location 1, and 100% at location 2. Additionally, an artificial reinforcement set is designed where the ULS unity check governs by neglecting the SLS conditions. This is carried out to check whether the structure can be optimized based on the ULS. The artificial designed reinforcement results in an ULS unity check of 96% at locations 1 and 2.

- The advanced approach for verifying the strength is done according to the GRF method explained in paragraph 4.3. The design value of the ultimate load is regarded as the design resistance R_d and is computed by dividing the ultimate load P_u with the global resistance factor γ_0. In the case of bending (flexural) failure, a global resistance factor of 1.27 can be used, provided that shear failure is not established at a global resistance factor of 1.4. The advanced approach for verifying the crack width is done according to indirect and direct method explained in paragraph 4.3 and paragraph 4.4. The indirect method is a multiplication of the average strain ($\bar{\varepsilon}_s$) with the maximum crack spacing ($S_{r,max}$), and the direct method a summation of the relative displacement (slip) by adopting a bond-slip model.

- Performing the advanced approach based on the strength verification, the maximum load exceeds the global resistance factor of 1.27, which means that the structure is safe, and that there is room for optimization. The ULS unity check is reduced by 15% at location 1 and by 6% at location 2 compared to the conventional approach. Based on these results it can be concluded that the structure can be optimized at both locations based on the ULS.

  Performing the advanced approach using the indirect method for verifying the crack width, the SLS unity check at location 1 is comparable to the unity check of the conventional approach. At location 2, the SLS unity is reduced to 85%, which is a reduction of 15% compared to the conventional approach. From these results it can be concluded that the structure can be optimized at location 2, but not at location 1.

  Adopting a bond-slip model, measuring the crack spacing, and using the indirect method for verifying the crack width results in a SLS unity check of 84% at location 1 and 74% at location 2. This is a reduction of 12% at location 1, and of 26% at location 2 compared to the conventional approach. Using the direct method for verifying the crack width yields a SLS unity check of 62% at location 1 and 70% at location 2. This is a reduction of 32% at location 1, and of 30% at location 2 compared to the conventional approach. The direct method using the slip curve provides the most favorable outcome

when used to determine the crack width. Based on the result above it can be concluded that structure can only be optimized at location 2 when bond slip is not considered. However, when bond slip is considered, the structure can be optimized at both locations.

- A comparison is made between the advanced and conventional approach in the terms of the amount of steel and concrete based on the ULS and SLS optimization rate. For the SLS, the optimization rate gained from the direct method is used. When optimizing the reinforcement based on the ULS, 7% less steel is used, and when optimizing the geometry instead of the reinforcement, 8% less concrete compared to the conventional approach. When optimizing the reinforcement based on the SLS, 23% less steel is used, and when optimizing the geometry, 22% less concrete compared to the conventional approach.

- Taking a look at the CO_2 footprint, optimizing the reinforcement based on the ULS results in 2% less emission and optimizing the geometry in 7% less emission. Optimizing the reinforcement based on the SLS results in 8% less emission and optimizing the geometry in 15% less emission. These results are based on a relieving platform with a length of 220 meters. If the platform's length is doubled, the environmental cost will rise by a factor of two as well. Based on the CO_2 emissions, it can be concluded that optimizing the geometry instead of the reinforcement offers a more effective design strategy.

The main conclusion is that, based on the specific analyzed quay wall, optimization to reduce amounts of reinforcement steel and concrete is possible using advanced calculations with volume elements and nonlinear approaches.

8 Recommendations

The following recommendations are made based on the research presented in this thesis.

Failure mode and optimization

In this thesis, the main reinforcement is optimized based on bending failure. It is recommended for future research to also optimize the longitudinal reinforcement based on bending failure and the shear reinforcement based on shear failure.

In this thesis, for simplicity reasons only the relief floor is optimized. Future research can be performed if it is also possible to optimize the walls. Also, when the cracks have not yet been fully developed, the crack width is calculated using linear extrapolation. Another method to determine the crack width is to decrease the tensile strength of the concrete, which can be performed in the future. By doing this, a comparison can be made between the two methods.

In this thesis, the reinforcement has been optimized based SLS without bond slip. It is recommended for future research to also optimize the reinforcement with a bond-slip model to determine if the optimization rate gives a good indication. Also, the optimization of the geometry based on the SLS is not numerically examined. It is recommended for future research to also examine the geometry numerically.

In this thesis, the optimization results are based on a specific analyzed quay wall. It is recommended for future research to investigate if the same optimization rate is obtained if a different quay wall is examined.

Convergence criteria

Convergence is not reached for every step, and non-convergence is ignored based on engineering judgment. Using a different iteration method and decreasing the load step should result in convergence. However, reducing the load step will drastically increase the computational time. Because of insufficient capacity, the analysis has not been performed with smaller load steps until convergence. This should be performed in the future to get an accurate result.

Bond-slip model

More research should be carried out by further reducing the element size to get the exact crack spacing and also by adjusting the bond-slip relationship curve of figure 6.1-1 from the fib Model Code 2010. It is also recommended that a different bond-slip model is to be used to investigate what the impact between the different models is on the crack width.

3D finite element model of the entire platform

In this thesis, a 3D model is built based on a relieving platform with a length of one meter. Although optimization is possible, it is recommended for future research to build a 3D model of the entire length of the relieving platform. By doing this, the spreading of the loads will be considered automatically, improving the outcome of the internal forces in real-world applications.

References

[1] Cur 211 - Handbook of Quay walls, Cur, 2013.

[2] M. Welsink and F. Kesting, "Uitgangspunennota Biomasskade ENGIE," Arcadis, Rotterdam, 2016.

[3] H. Jonkers, "Reader CIE4100 Materials and Ecological Engineering," TU Delft Faculty of Civil Engineering & Geosciences, Delft, 2020.

[4] M. Welsink, "Ontwerpnota bovenbouw hoofdconstructie Biomassakade ENGIE," Arcadis , Rotterdam, 2017.

[5] J. Erochko, "Learn about structures," 2020. [Online]. Available: https://learnaboutstructures.com/Bernoulli-Euler-Beam-Theory#:~:text=The%20two%20primary%20assumptions%20made,angles%20(slopes)%20are%20small..

[6] D. Broekaart, "Simulatio by technia," 5 March 2015. [Online]. Available: https://info.simuleon.com/blog/why-should-you-consider-performing-non-linear-finite-element-analysis.

[7] D. Ferreira and J. Manie, "DIANA Documentation release 10.5," DIANA FEA BV, The Netherlands, 2021.

[8] F. Engineering, "In Fea, what is linear and nonlinear analysis?," May 2017. [Online]. Available: https://www.femto.eu/stories/linear-non-linear-analysis-explained/#:~:text=A%20nonlinear%20analysis%20is%20an,plastic%20material)%2C%20and%20contact..

[9] M. Hendiks, R. Esposito and J. Rots, "CIE5148 - Introduction to nonlinear finite element analysis," Tu Delft , The Netherlands, 2019.

[10] D. Haarsma, "Modelling compressive membrane action and geometrical nonlinearity in one way concrete slabs," Tu Delft, Delft, 2021.

[11] P. Beverly, "fib Model Code for concrete structures 2010," International Federation for structural concrete, Lausanne, 2013.

[12] J. L. Gumucio, "Master of science thesis - Design of Quay Walls using the Finite element method," Gemeente Rotterdam, Rotterdam, 2013.

[13] R. B. Polder, "Advisering m.b.t. toelaatbare scheurwijdte ontlastvloer L-vormige," TNO, 2020.

[14] M. Welsink, "Ontwerpnota onderbouw Biomassakade ENGIE," Arcadis, Rotterdam, 2017.

[15] B. Gouda, GTB 2013, Gouda: Betonvereniging, 2013.

[16] A. de Boer, E. O. Lantsoght, C. van der Veen and D. A. Hordijk, "Optimizing Finite Element Models for concrete bridge assessment with proof load testing," Tu Delft, The Netherlands, 2019.

[17] L. Sluys and R. de Borst, Computational mehods in non-linear solid mechanics, Delft: Tu Delft, 2015.

[18] A. de Boer, B. Belletti and M. A. Hendriks, "Guidelines for Nonlinear Finite Element Analysis of concrete structures. RTD 1016-1:2020," Rijkswaterstaat Centre for Infrastructure, Utrecht, Netherlands, 2020.

[19] D. Schlicke, E. M. Dorfmann, E. Fehling and N. V. Tue, "Calculation of maximum crack width for practical design of reinforced concrete," Graz University of Technology, institute of Structural Concrete, Germany, 2021.

[20] M. H. Mazumber and R. l. Gilbert, "Finite element modelling of bond–slip at anchorages of reinforced concrete members subjected to bending," 04 October 2019. [Online]. Available: https://link.springer.com/article/10.1007/s42452-019-1368-5.

[21] "Design of reinforced concrete sections according to EN 1992-1-1 and EN 1992-2," Idea Statica, 2022.

[22] E. d. h. o. building, "Brightspace," 2021. [Online]. Available: https://brightspace.tudelft.nl/d2l/le/content/288949/viewContent/2026948/View.

[23] Cur 166 - Damwandconstructies (6e herziene druk, deel 2), Cur, 2012.

[24] Cur 166 - Damwandconstructies (6e herziene druk, deel 1), Cur, 2012.

[25] "Stress-strain curve for steel rebars," [Online]. Available: https://theconstructor.org/structural-engg/stress-strain-curve-steel/3514/.

[26] "Stress–strain curve," 2022. [Online]. Available: https://en.wikipedia.org/wiki/Stress%E2%80%93strain_curve.

[27] Rijkswaterstaat, "Richtlijnen Ontwerp Kunstwerken 1.4," Rijkswaterstaat, Utrecht, Netherlands, 2017.

[28] A. de Boer, M. A. Hendriks, C. Damoni and B. Belleti, "Validation of the Guidelines for nonlinear finite element analysis of Concrete structures - Part 3A:Reinforced Beams. RTD 1016-3A:2017," Rijkswaterstaat Centre of Infrastructure, Utrecht, Netherlands, 2017c.

[29] A. Singer, "Sustainable shear design of quay walls - Reducing the CO2 emissions of relieving structures of quay walls," Tu Delft, Delft, 2022.

[30] "National Annex to NEN-EN 1992-1-1+C2," 2016.

[31] "Grafieken en Tabellen voor beton gebaseerd op de Europese Normen voor Ontwerp, Materiaal en Uitvoering (GTB)," Betonvereniging, Gouda, 2013.

[32] "NEN-EN 1990 - Eurocode: Basis of structural design," CEN (European Committee for Standardisation), Brussel, 2019.

[33] "Richtlijnen Ontwerp Kunstwerken (ROK 1.4)," Rijkswaterstaat Technische Document (RTD), 2017.

[34] "NEN-EN 1997-1+C1, Eurocode 7: Geotechnical design -Part 1: General rules," CEN (European Committee for Standardisation), Brussel, 2012.

[35] "NEN-EN 1992-1-1+C2, Eurocode 2: Design of concrete structures – Part 1-1: General rules and rules for buildings," CEN (European Committee for standardisation), Brussel, 2011.

Appendices

Appendix I. Conventional part

In Appendix I, addition information about the conventional part is added that has been used in this thesis.

1.1. Conventional loading assumptions

The conventional modeling assumptions are derived from the reports of Engie. In this chapter, additional information about the terrain load and substructural loads is described.

<u>Terrain load</u>

The horizontal load at the back wall of the quay is calculated using the formulas below, which is derived from the report of Engie.

$$p(l_1) := \begin{vmatrix} \left[40\text{kPa} + \dfrac{(230\text{kPa} - 40\text{kPa})}{(45.1 - 22.3)} \cdot (l_1 - 22.3 + 16.7)\right] & \text{if } l_1 < (45.1 - 16.7) \\ 40\text{kPa} & \text{if } l_1 < (22.3 - 16.7) \\ (0\text{kPa}) & \text{if } l_1 \le 0 \end{vmatrix}$$

$$\varphi := 30°$$

$$\upsilon_a := 45.° + \frac{\varphi}{2} = 60°$$

$$\lambda_a := \sin\left(45.° - \frac{\varphi}{2}\right) = 0.5$$

$$a(l_1) := \tan(\varphi) \cdot l_1 \qquad b(l_1) := \tan(\upsilon_a) \cdot l_1$$

$$q_{n2}(z) := \sum_{i=1}^{28400} \begin{vmatrix} \dfrac{\lambda_a \cdot \left(p\left(\frac{i}{1000}\right) - p\left(\frac{i-1}{1000}\right)\right)}{b\left(\frac{i}{1000}\right) - a\left(\frac{i}{1000}\right)} \cdot \left(z - a\left(\frac{i}{1000}\right)\right) & \text{if } z < b\left(\frac{i}{1000}\right) \\ 0 & \text{if } z < a\left(\frac{i}{1000}\right) \\ \left[\lambda_a \cdot \left(p\left(\frac{i}{1000}\right) - p\left(\frac{i-1}{1000}\right)\right)\right] & \text{otherwise} \end{vmatrix}$$

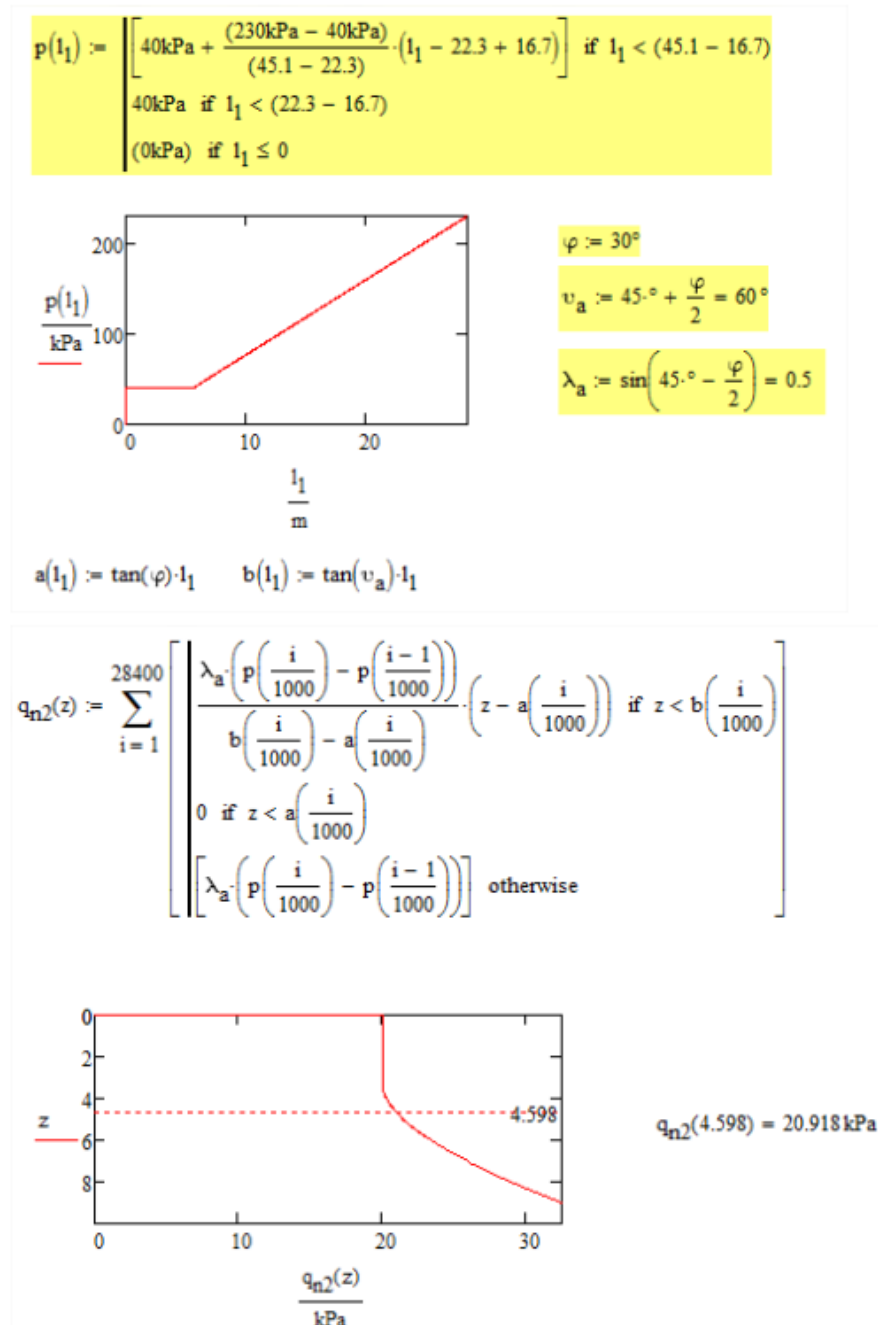$$q_{n2}(4.598) = 20.918 \text{ kPa}$$

Figure 57. Horizontal load against the back of the quay [2]

Loading substructures

In the tables below, the loads from the substructure are given. These results are derived from the substructural report of Engie.

Table 63. Loading of the substructure [14]

Belasting uit combiwand op bovenbouw — Systeemmaat: 3,73 m

BC [-]	u1 combi BGT [m/m]	Ncombi UGT [kN/m]	Ncombi UGT [kN]	N combi BGT [kN/m]	N combi BGT [kN]	Veer [MN/m]	Veer punt [MN/m]	Veer tot [MN/m]	UGT/BGT [-]	V combi BGT [kN/m]	V combi BGT [kN]
I	0,0041	2562	9556	2059	7680	506	350	207	1,24	-349	-1302
II	0,0042	2689	10030	2078	7751	497	350	205	1,29	-337	-1257
III	0,0034	2310	8616	1881	7016	558	350	215	1,23	-332	-1238
IV	0,0022	1825	6807	1604	5983	736	350	237	1,14	-326	-1216
V	0,0028	2130	7945	1752	6535	617	350	223	1,22	-316	-1179
VI	0,0021	1815	6770	1561	5823	756	350	239	1,16	-313	-1167
VII	0,0040	2629	9806	2027	7561	512	350	208	1,30	-330	-1231
VIII	0,0040	2512	9370	2039	7605	514	350	208	1,23	-331	-1235
Average								218		-329	-1228
Max								239		-313	-1302
							Te hanteren veer:	240		Dwarskracht:	-1302

Belasting uit vibropalen E= 10000 Mpa op bovenbouw — h.o.h.: 2,565 m

BC [-]	Δu1 combi BGT [m/m]	Nvibro UGT [kN/m]	Nvibro UGT [kN]	N vibro BGT [kN/m]	N vibro BGT [kN]	Veer paal [MN/m]	Veer punt [MN/m]	Veer tot [MN/m]	UGT/BGT [-]	V vibro BGT [kN/m]	V vibro BGT [kN]	M vibro BGT [kN/m]	M vibro BGT [kN]
I	0,0116	1529	3922	1383	3547	120	400	92	1,11	-76	-195	60	154
II	0,0119	1462	3750	1438	3688	121	400	93	1,02	-74	-190	57	146
III	0,0108	1445	3706	1308	3355	121	400	93	1,10	-67	-172	54	139
IV	0,0103	1360	3488	1306	3350	126	400	96	1,04	-57	-146	50	128
V	0,0111	1464	3755	1336	3427	120	400	93	1,10	-65	-167	49	126
VI	0,0099	1294	3319	1281	3286	129	400	98	1,01	-53	-136	46	118
VII	0,0121	1458	3740	1470	3771	122	400	93	0,99	-100	-257	95	244
VIII	0,0117	1529	3922	1413	3624	121	400	93	1,08	-100	-257	94	241
Average								94		-74	-190	63	162
Max								98		-100	-257	95	244
							Te hanteren veer:	100		Dwarskracht:	-257	Moment:	244

Belasting uit vibropalen E= 20000 Mpa op bovenbouw — h.o.h.: 2,565 m

BC [-]	u1 combi BGT [m/m]	Nvibro UGT [kN/m]	Nvibro UGT [kN]	N vibro BGT [kN/m]	N vibro BGT [kN]	Veer paal [MN/m]	Veer punt [MN/m]	Veer tot [MN/m]	UGT/BGT [-]	V vibro BGT [kN/m]	V vibro BGT [kN]	M vibro BGT [kN/m]	M vibro BGT [kN]
I	0,0116	1528	3919	1401	3594	121	400	93	1,09	-88	-226	73	187
II	0,0119	1462	3750	1458	3740	122	400	94	1,00	-85	-218	68	174
III	0,0108	1448	3714	1337	3429	124	400	95	1,08	-78	-200	67	172
IV	0,0103	1382	3545	1329	3409	129	400	97	1,04	-66	-169	62	159
V	0,0111	1463	3753	1355	3476	122	400	94	1,08	-75	-192	58	149
VI	0,0099	1309	3358	1308	3355	132	400	99	1,00	-60	-154	59	151
VII	0,0121	1455	3732	1494	3832	124	400	95	0,97	-117	-300	124,5	319
VIII	0,0117	1531	3927	1435	3681	123	400	94	1,07	-117	-300	122	313
Average								95		-86	-220	79	203
Max								99		-60	-300	125	319
							Te hanteren veer:	100		Dwarskracht:	-300	Moment:	319

Veer anker

BC [-]	u1 combi BGT [m/m]	Nanker BGT [kN/m]	Nanker BGT [kN]	Veer tot [MN/m]
I	0,0360	572	1467	16
II	0,0220	480	1231	22
III	0,0240	524	1344	22
IV	0,0460	689	1767	15
V	0,0260	538	1380	21
VI	0,0290	597	1531	21
VII	0,0140	248	636	18
VIII	0,0150	356	913	24
Average				20
Max				24
			Te hanteren veer:	24

1.2. Results 2D vs 2.5D model

In the tables below, the result of the reaction forces per load case and the bending moments for the ULS between the 2D and 2.5D models are shown.

Table 64. Reaction forces per unit length (2D vs 2.5D)

Load case	Substructural element	Vertical reaction force (2D)	Vertical reaction force (2.5D)	Vertical reaction force per unit length (2.5D)	Horizontal reaction force (2D)	Horizontal reaction force (2.5D)	Horizontal per unit length (2.5D)
		[kN]	[kN]	[kN]	[kN]	[kN]	[kN]
Self-weight (LC1)	Combi-wall	672,3	2508,2	672,4	121,0	451,8	121,1
	Vibro-pile	129,9	317,2	139,1	40,1	92,2	40,4
	Anchor	46,2	125,6	45,9	-161,1	-440,9	-161,2
Ground pressure (LC2-1)	Combi-wall	448,0	1694,0	454,1	80,6	307,5	82,4
	Vibro-pile	553,5	1264,0	554,4	158,7	358,8	157,4
	Anchor	22,23	59,4	21,7	-77,5	-209,4	-76,6
Water pressure (LC3-1)	Combi-wall	-28,8	-107,8	-28,9	-5,2	-19,6	-5,3
	Vibro-pile	-27,2	-62,6	-27,5	-7,8	-18,5	-8,1
	Anchor	-4,1	-11,1	-4,1	14,2	38,9	14,2
Terrain load above duct profile (LC-4-1)	Combi-wall	230,8	863,0	231,4	41,6	155,3	41,6
	Vibro-pile	-47,8	-111,2	-48,8	-13,7	-31,1	-13,6
	Anchor	8,0	22,0	8,0	-27,8	-76,3	-27,9
Terrain load above relief floor (LC4-2)	Combi-wall	212,2	806,0	216,1	38,2	145,0	38,9
	Vibro-pile	209,8	478,5	209,9	60,2	137,2	60,2
	Anchor	28,8	77,0	28,2	-100,3	-268,6	-98,2
Terrain back of the quay (LC4-3)	Combi-wall	7,2	26,4	7,1	1,3	4,74	1,3
	Vibro-pile	60,1	140,7	61,7	17,5	39,7	17,4
	Anchor	-29	-79,5	-29,1	101,2	277,1	101,3
Bollard load (LC5)	Combi-wall	42,1	174,3	46,7	7,6	31,4	9,3
	Vibro-pile	-13,8	-39,3	-17,2	-4,0	-11,3	-5,0
	Anchor	-28,3	-83,0	-30,3	98,7	289,6	105,9
Fender load (LC6)	Combi-wall	-7,3	-30,0	-8,0	-1,3	-5,4	-1,4
	Vibro-pile	-49,3	111,0	48,7	-14,3	-29,9	-13,1
	Anchor	56,6	151,0	55,2	-197,4	-526,6	-192,5
Crane load/ground side rail (LC7-1)	Combi-wall	402,6	1365,3	366,0	72,4	245,7	65,9
	Vibro-pile	364,0	828,0	363,2	104,4	237,5	104,2
	Anchor	33,5	70,0	25,6	-116,8	-242,9	-88,8
Crane load/ waterside rail (LC7-4)	Combi-wall	400,5	1347,9	361,4	72,1	242,5	65,0
	Vibro-pile	366,0	834,4	366,0	104,9	239,3	105,0
	Anchor	33,6	74,7	27,3	-117,0	-260,3	-95,2
Substructural loads (LC8)	Combi-wall	-141,1	-533,3	-143,0	-25,4	-96	-25,7
	Vibro-pile	171	392,7	172,2	49,1	109,7	48,1
	Anchor	-126,7	-350,3	-128,0	441,9	1221,6	446,7

TUDelft

In the table below, the bending moment for the ULS of the relief floor between the 2D and 2.5D-models are compared.

Table 65. Bending moment comparison 2D vs 2.5D (ULS)

Structural element	Location [m]	My (2D) [kNm]	Myd+ (2.5D) [kNm/m]	Error	My (2D) [kNm]	Myd- (2.5D) [kNm/m]	Error
Relief floor	Wall A	-161,2	-170	5,5%	236,5	232,4	1,7%
	Wall B	-3203	-3300	3,0%	0	0	0,0%
	Between wall B and C	-327	-323,8	1,0%	1633,9	1660,3	1,6%
	Vibro-pile	-1498,3	-1566,4	4,5%	0	0	0,0%
	Wall C	-710	-740,3	4,3%	655,2	700	6,8%

The conclusions drawn from the tables above indicate that the result of the 2D and 2.5D model are comparable. This means that the conventional 2.5D design of the relieving platform has been modeled correctly based on the reaction forces and bending moments.

Modeling in three-dimensional space gives a more accurate solution for determining the reinforcement. This is because the loads are spread automatically, and also because the effect of torsion is considered in the formula of the design bending moment and design normal force.

1.3. Concrete cover and crack width calculation

Between the reinforcement's area and the outside edge of the concrete is a space known as the concrete cover. For the durability of the structure, the thickness of the concrete cover is very important. When cracking occurs, the environment, such as corrosion, may have an impact on the reinforcement if the cover is too small. The minimum requirement for the concrete cover and crack width depends on the environmental conditions and exposure classes. In the picture below, the concrete cover and the maximal crack width is determined using NEN 1992-1-1 with the use of Mathcad Prime.

Concrete cover calculation according to NEN 1992-1-1- C2 (Eurocode 2)

Environmental exposure class:
XC4,XD3,XS3,XF4,XA2

Tabel 4.4N — Waarden van de minimale dekkingseisen, $c_{min,dur}$, met betrekking tot duurzaamheid voor betonstaal volgens EN 10080

Constructie-klasse	Omgevingseisen voor $c_{min,dur}$ (mm)						
	Milieuklasse volgens tabel 4.1						
	X0	XC1	XC2 / XC3	XC4	XD1 / XS1	XD2 / XS2	XD3 / XS3
S1	10	10	10	15	20	25	30
S2	10	10	15	20	25	30	35
S3	10	10	20	25	30	35	40
S4	10	15	25	30	35	40	45
S5	15	20	30	35	40	45	50
S6	20	25	35	40	45	50	55

$cmin\_b := 32 \; \boldsymbol{mm}$ (Diameter of the rebar)
$cmin\_dur := 40 \; \boldsymbol{mm}$ (According to table 4.1 of NEN 1992-1-1)
$\Delta c\_dur := 0 \; \boldsymbol{mm}$
$\Delta c\_dur\_\gamma := 0 \; \boldsymbol{mm}$
$\Delta c\_dur\_st := 0 \; \boldsymbol{mm}$
$\Delta c\_dur\_add := 0 \; \boldsymbol{mm}$

$cmin := \max\left(cmin\_b, cmin\_dur, \Delta c\_dur\_\gamma, \Delta c\_dur\_st, \Delta c\_dur\_add\right) = 0.04 \; \boldsymbol{m}$

$\Delta c\_dev := 5 \; \boldsymbol{mm}$

$cnom := \Delta c\_dev + cmin = 0.045 \; \boldsymbol{m}$

$ctoegepast := 50 \; \boldsymbol{mm}$

$$kx := \frac{ctoegepast}{cnom} = 1.111 \qquad \text{(multiplication factor)}$$

Tabel 7.1N — Aanbevolen waarden van w_{max} en daarvan afgeleide grootheden

Milieuklasse	Elementen met betonstaal en/of voorspanstaal zonder aanhechting	Elementen met een combinatie van betonstaal en voorspanstaal met aanhechting	Elementen met uitsluitend voorspanstaal met aanhechting
	Frequente belastingscombinatie	Frequente belastingscombinatie	Frequente belastingscombinatie
X0, XC1	$w_{max} \le 0{,}40$ mm [a]	$w_{max} \le 0{,}30$ mm	$\Delta\sigma_p \le \xi\, 275$ MPa
XC2, XC3, XC4	$w_{max} \le 0{,}30$ mm	$w_{max} \le 0{,}20$ mm	$\Delta\sigma_p \le \xi\, 175$ MPa
XD1, XD2, XD3, XS1, XS2, XS3	$w_{max} \le 0{,}20$ mm	$w_{max} \le 0{,}10$ mm	$\Delta\sigma_p \le \xi\, 75$ MPa

[a] Voor milieuklasse X0 en XC1 heeft de scheurwijdte geen invloed op de duurzaamheid; deze grens is gesteld om een in het algemeen aanvaardbaar uiterlijk te verkrijgen. Bij afwezigheid van voorwaarden ten aanzien van het uiterlijk mag deze beperking zijn afgezwakt.

$$wmax := 0.2\ mm \qquad \text{(max crack width according to Tabel 7.1N of the national annex to NEN-EN-1992-1-1)}$$

$$wnorm := wmax \cdot kx = 0.222\ mm \qquad \text{(crack width norm)}$$

Crack width calculation according to NEN-EN-1992-1-1

The crack width is determined with the use of the software package Idea Statica which is based on the guidelines of the Eurocode 2. The crack width is calculated according to chapter 7.3.4 of Eurocode 2 using the following equation:

$$w_k = S_{r,max}(\varepsilon_{sm} - \varepsilon_{cm}) \qquad (I.1)$$

Where:

w_k : The design crack width

ε_{sm} : The mean reinforcement strain

ε_{cm} : The mean concrete strain between the cracks

$S_{r,max}$: The maximal crack spacing

The following expression is used to compute the strain differential ($\varepsilon_{sm} - \varepsilon_{cm}$):

$$(\varepsilon_{sm} - \varepsilon_{cm}) = \frac{\sigma_s - k_t \frac{f_{ct.eff}}{\rho_{p,eff}}(1 + \alpha_e \rho_{s,eff})}{E_s} \ge \frac{0{,}6\,\sigma_s}{E_s} \qquad (I.2)$$

Where:

σ_s : The stress in the reinforcement

$f_{ct.eff}$: The mean value of the concrete tensile strength

α_e : Ratio modulus of elasticity: $\frac{E_s}{E_{cm}}$

$\rho_{s,eff}$: Effective reinforcement ratio: $\frac{A_s}{A_{c,eff}}$

$A_{c,eff}$: Effective concrete area: $h_{c,eff} b$

$h_{c,eff}$: Effective height: $\min\{(\frac{(h-c)}{3}; 2{,}5(h-d)\}$
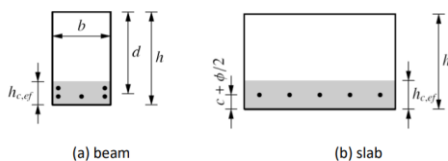
Figure 58. Effective concrete area

The maximal crack spacing for stabilized cracking is calculated based on the guidelines given in Eurocode 2.

$$S_{r,max} = k_3 c + k_1 k_2 k_4 \frac{\phi_{s,eq}}{\rho_{s,ef}}$$

(I.3)

With,

$$\phi_{s,eq} = \frac{(n_1 \phi_1^2 + n_2 \phi_2^2)}{(n_1 \phi_1 + n_2 \phi_2)}$$

(I.4)

Where,

c = cover of the main reinforcement.

$\phi_{s,eq}$ = the equivalent diameter of the reinforcing bars

n = Amount of rebars

The parameters for k_1 to k_4 are given in the table below.

k_1	0.8 for high-bond bars
	1.6 for plain bars
k_2	0.5 for pure bending
	1.0 for pure tension
k_3	3.4 (recommended)
k_4	0.425 (recommended)

1.4. Governing limit state calculation

In this chapter, the governing limit state is determined using the software package Idea Statica which is based on the NEN-EN-1992-1-1.

Using the conventional approach to determine the reinforcement the following general assumptions are made:

- It is considered that strain in concrete and reinforcement is linearly proportional to the distance from the neutral axis (plane sections remain plane).
- Concrete and reinforcement compactness ensures that reinforcement and concrete interact (strain of the reinforcement is the same as the concrete).

For the calculation based on the Ultimate Limit State (ULS), the following assumptions are made:

- Tensile strength of concrete is neglected (all tensile stresses are transmitted by reinforcement).
- Concrete compression stresses in compression zone are calculated in relation to strain calculated from stress-strain diagrams.
- Reinforcement stresses are calculated in relation to strain from stress-strain diagrams.

For the calculation based on the Service Ability Limit (SLS), the following assumptions:

- Uncracked cross-section:
  - o The tensile strength of the concrete is not ignored.
  - o Concrete stress is directly proportional to the distance to neutral axis (linear stress distribution).
  - o Reinforcement stress is directly proportional to the distance to neutral axis (linear stress distribution).
  - o Concrete tensile stress is limited by value fct,eff according to art. 7.1 (2) of the Eurocode 2 .
- Full cracked cross-section:
  - o The tensile strength of the concrete is ignored.
  - o Concrete stress is directly proportional to the distance to neutral axis (linear stress distribution).

TUDelft

o Reinforcement stress is directly proportional to the distance to neutral axis (linear stress distribution) [21].

The difference between the uncracked-and cracked stage lies in the tensile strength of concrete.

To determine the reinforcement, the internal forces (bending moment, normal force, and shear force) of the relief floor at location 1 (sagging bending moments) are used and applied in idea-statica. In the table below, the ULS and SLS results are shown.

Table 66. Idea-statica results (w_{norm}= 0,22 mm) (SLS & ULS)

Myd- (ULS)	Myd- (SLS)	Reinforcement (bottom relief floor)	Area total [mm²]	Strength capacity (ULS)	Crack width (SLS)
1630	1030	Ø20 – 125 + Ø25 – 125	6485	58.5%	95 %

The minimum reinforcement needed to satisfy the ULS-condition is: $\frac{58.5}{100} \times 6485 = 3794$ mm^2. The minimum reinforcement needed to satisfy the SLS-condition is: $\frac{95}{100} \times 6485 = 6161$ mm^2.

From the results above it can be concluded that the SLS-condition is governing. More reinforcement is needed to satisfy this condition.

Difference between the crack width of the norm and TNO

Due to the extremely low probability and potential consequences of corrosion, it is acceptable to depart from this standard. A maximum crack width of 0.4 mm as an upper limit is considered permissible [13].

Table 67.Idea statica result (w_{TNO}= 0,4 mm) (SLS & ULS)

Myd- (ULS)	Myd- (SLS)	Reinforcement (bottom relief floor)	Area total [mm²]	Strength capacity (ULS)	Crack width (SLS)
1630	1030	Ø20 – 125 + Ø25 – 125	6485	58.5%	52.1%

Table 68. Minimum reinforcement (norm vs TNO)

	Crack width (limit)	Minimum reinforcement (ULS) [mm]	Minimum reinforcement (SLS) [mm]
Norm	0.22	3794	6161
TNO	0.4	3794	3379

In Table 68, the difference between the amount of reinforcement needed to satisfy that crack-width condition is shown. From these results, it can be concluded that considering a crack width of 0.4 mm the ULS condition is governing.

1.5. Governing load combinations (2D model)

The load combinations for the governing bending moments around the longitudinal axis, shear forces, and normal forces of the relief floor in the ultimate and- serviceability limit state is shown in the tables below. These results are derived from the 2D - Scia report given in appendix III and will be applied to the smarter model.

For the relief floor, the "positive" side of the moments creates tension at the bottom side of the floor, while the "negative" side creates tension at the top side.

Table 69. Governing load combination for the bending moment of relief floor A-B (ULS)

Structural element	Relief floor A-B			
Bending moment (Mz)	Mz-	Mz-	Mz-	Mz+
Location [m]	x=0,75 (at surface wall A)	x=2,1 (Between wall A and B)	x=4,025 (between wall B and C)	x=0,75 (at surface wall A)

TUDelft

Load combination	ULS 1-2/4	ULS 1-1/1	ULS 1-1/1	ULS 2-2/5
LC1	1,20	1,20	1,20	1,20
LC2-1	1,00	1,00	1,00	1,00
LC2-2				
LC3	1,00	1,00	1,00	1,00
LC4-1	1,05	1,50	1,50	
LC4-2	1,05	1,50	1,50	
LC4-3				
LC5	1,50	1,05	1,05	
LC6				1,50
LC7-1				0,90
LC7-4	0,90	0,90	0,90	
LC8	1,20	1,20	1,20	1,20

Table 70. Governing load combination for the bending moment of relief floor A-B (SLS)

Structural element	Relief floor A-B			
Bending moment (Mz)	Mz-	Mz-	Mz-	Mz+
Location [m]	x=0,75 (at surface wall A)	x=2,1 (Between wall A and B)	x=4,025 (at surface wall B)	x=0,75 (at surface wall A)
Load combination	SLS 1-1/3	SLS 1-1/3	SLS 1-1/3	SLS 1-2/4
LC1	1	1	1	1
LC2-1	1	1	1	1
LC2-2				
LC3	1	1	1	1
LC4-1	0,5	0,5	0,5	
LC4-2	0,5	0,5	0,5	
LC4-3				
LC5	0,3	0,3	0,3	
LC6				0,3
LC7-1				0,6
LC7-4	0,6	0,6	0,6	
LC8	1	1	1	1

Table 71. Governing load combination for the bending moment of relief floor B-C (ULS)

Structural element	Relief floor B-C					
Bending moment (Mz)	Mz-	Mz-	Mz-	Mz-	Mz-	Mz+
Location [m]	x=4,775 (at surface wall B)	x=6,025 (Between wall B and C)	x=10,1 (between wall B and C)	x=14,184 (at vibro pile)	x=16,1 (at surface wall C)	x=10,1 (between wall B and C)
Load combination	ULS 1-2/4	ULS 1-2/12	ULS 1-2/12	ULS 1-2/3	ULS 1-1/23	ULS 2-1/16
LC1	1,20	1,20	1,20	1,20	1,20	1,20
LC2-1	1,00	1,00	1,00	1,00	1,00	1,00
LC2-2						
LC3	1,00	1,00	1,00	1,00	1,00	1,00
LC4-1	1,05	1,05	1,05			

LC4-2	1,05			1,05	1,50	1,50
LC4-3						1,50
LC5	1,50	1,50	1,50	1,50	1,05	
LC6						1,05
LC7-1						0,90
LC7-4	0,90	0,90	0,90	0,90		
LC8	1,20	1,20	1,20	1,20	1,20	1,20

Table 72. Governing load combination for the bending moment of relief floor B-C (SLS)

Structural element	Relief floor B-C				
Bending moment (Mz)	Mz-	Mz-	Mz-	Mz-	Mz+
Location [m]	x=4,775 (at surface wall B)	x=6,025 (Between wall B and C)	x=14,184 (at vibro pile)	x=16,1 (at surface wall C)	x=10,1 (between wall B and C)
Load combination	SLS 1-1/3	SLS 1-1/10	SLS 1-1/2	SLS 1-1/7	SLS 1-2/11
LC1	1	1	1	1	1
LC2-1	1	1	1	1	1
LC2-2					
LC3	1	1	1	1	1
LC4-1	0,5	0,5			
LC4-2	0,5		0,5	0,5	0,5
LC4-3					0,5
LC5	0,3	0,3	0,3	0,3	
LC6					0,3
LC7-1					0,6
LC7-4	0,6	0,6	0,6		
LC8	1	1	1	1	1

Table 73. Governing load combinations for the normal forces of relief floor A-B and B-C (ULS)

	Relief floor A-B	Relief floor B-C
Normal force (Nx)	Nx-	Nx+
Load combination	ULS 2-2/6	ULS 1-2/9
LC1	1,2	1,2
LC2-1	1	1
LC2-2		
LC3	1	1
LC4-1	1,05	
LC4-2		1,05
LC4-3		
LC5		1,5
LC6	1,5	
LC7-1		
LC7-4		

LC8	1,2	1,2

Table 74. Governing load combinations for the normal forces of relief floor A-B and B-C (SLS)

Structural element	Relief floor A-B	Relief floor B-C
Normal force (Nx)	Nx-	Nx+
Load combination	SLS 1-2/5	SLS 1-1/7
LC1	1	1
LC2-1	1	1
LC2-2		
LC3	1	1
LC4-1	0,5	
LC4-2		0,5
LC4-3		
LC5		0,3
LC6	0,3	
LC7-1		
LC7-4		
LC8	1	1

Table 75. Governing load combination for the shear forces of relief floor A-B and B-C (ULS)

Structural element	Relief floor A-B	Relief floor B-C
Shear force (Vz)	Vz-	Vz+
Location [m]	x=4,025 (at surface wall B)	x=4,775 (at surface wall B)
Load combination	ULS 1-1/1	ULS 1-1/8
LC1	1,2	1,2
LC2-1	1	1
LC2-2		
LC3	1	1
LC4-1	1,5	1,5
LC4-2	1,5	1,5
LC4-3		1,5
LC5	1,05	1,05
LC6		
LC7-1		0,9
LC7-4	0,9	
LC8	1,2	1,2

LC1- Dead load

LC2-1 - Earth pressure - Fundamental combination GWS: NAP -0,5m / OWL: NAP -1,0m

LC2-2 - Earth pressure- Incidental extreme low water GWS: NAP -1.00m / OWL: NAP - 2.35m

LC3- Water pressure - Fundamental combination GWS: NAP -0,5m / OWL: NAP -1,0m

LC4-1 - Terrain load -Top of quay (top duct)

LC4-2 - Terrain load -Top of quay (top relief floor)

LC4-3 - Terrain load -Back of the quay

LC5 - Bolder load

LC5 - Fender load

LC7-1 - Crane load on ground side rail towards water

LC7-4- Crane load on water side rail towards water

LC8 - Loads substructure

Appendix II. Advanced part

In Appendix II addition information about the advanced part is added that has been used in this thesis.

2.1. Comparison 2D vs 3D model (linear elastic analysis)

2.1.1. Based on Dummy load

In order to check whether the 3D-model has been successfully modeled. a dummy load of 10 kN has been applied to the top of wall C of the 2D conventional and 3D advanced model.
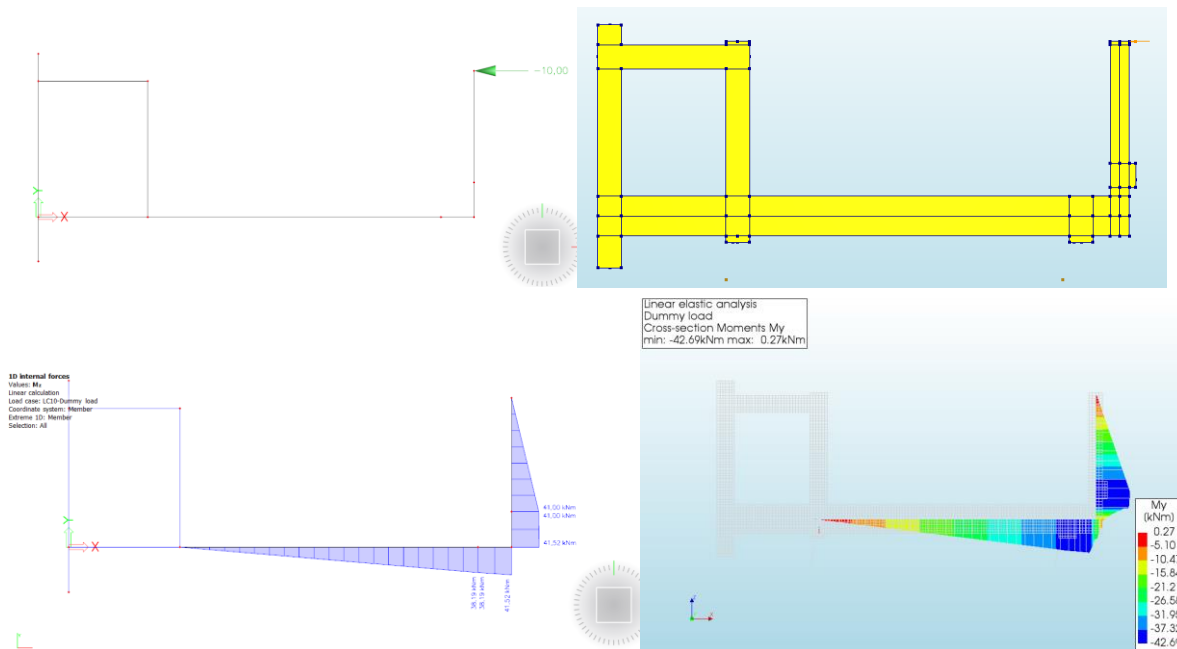
Figure 59. Comparison bending moment between conventional and advance model based on dummy load

Table 76. Comparison dummy load (2D vs 3D model)

	unit	Element	2D-model	3D-model	Accuracy
Horizontal reaction force (Rx)	kN	Combi-wall	0,64	0,65	1,6%
		Vibro-pile	-0,23	-0,24	4,3%
		Anchor	9,59	9,6	0,1%
Vertical reaction force (Rz)	kN	Combi-wall	3,54	3,51	0,8%
		Vibro-pile	-0,79	-0,8	1,3%
		Anchor	-2,75	-2,78	1,1%
Horizontal displacement (Ux)	m	Wall C	-0,002	-0,002	0,0%
Vertical displacement (Uz)	m	General	0	0	0,0%
Bending moments (My)	kNm	Wall C	41,25	-42,39	2,8%
		Relief floor B-C	41,25	-41,69	0,9%

In the table above, the reaction forces, bending moments, and displacement of the 2D and 3D-model are shown. Since the result's accuracy is below 5%, it can be concluded that the 3D model has been modeled correctly based on the dummy load.

2.1.2. Based on the load cases

In the table below the results of horizontal and vertical equilibrium of the external loading for the 2D-conventional model and 3D-smarter model are shown for each load case. Here it is noticed that the forces are

near to being in equilibrium, indicating that the smart model has been modeled correctly based on the load cases. Notice that for some load cases the accuracy is higher. This is because the use of volume elements gives a better distribution of the loading on the area.

Table 77. Equilibrium of forces (2D vs 3D model)

Load case	Vertical resultant (2D)	Vertical resultant (3D)	Error	Horizontal resultant (2D)	Horizontal resultant (3D)	Error
	[kN]	[kN]		[kN]	[kN]	
Self-weight (LC1)	858,350	835,300	2,7%	0	0	0,0%
Ground pressure (LC2-1)	1023,700	1036,000	1,2%	161,800	162,000	0,1%
Water pressure (LC3-1)	-60,000	-61,500	2,5%	1,250	1,250	0,0%
Terrain load above duct profile (LC-4-1)	191,000	191,000	0,0%	0	0	0,0%
Terrain load above relief floor (LC-4-2)	450,630	453,000	0,5%	0	0	0,0%
Terrain back of the quay (LC-4-3)	43,640	43,680	0,1%	120,000	120,000	0,0%
Bollard load (LC-5)	0	0	0,0%	102,300	102,300	0,0%
Fender load (LC-6)	0	0	0,0%	-212,800	-212,800	0,0%
Crane load (LC-7-1)	800,000	800,000	0,0%	60,000	60,000	0,0%
Crane load (LC-7-4)	800,000	800,000	0,0%	60,000	60,000	0,0%
Substructural loads (LC-8)	-96,710	-96,470	0,2%	465,600	465,600	0,0%

Hereafter, a comparison is made between the linear elastic results of the 2D-conventional and 3D- advanced model to determine the accuracy of the models. In the tables below the reaction forces, the bending moments, the normal forces, and the shear forces for the 2D-and 3D model that occur from the governing load combinations given in appendix I are shown.

Table 78. Reaction forces (2D vs 3D)

Load case	Structural element	Vertical reaction force (2D)	Vertical reaction force (3D)	Error	Horizontal reaction force (2D)	Horizontal reaction force (3D)	Error
		[kN]	[kN]		[kN]	[kN]	
Self-weight	Combi-wall	672,3	644,5	4,1%	121,0	116	4,1%
	Vibro-pile	129,9	145,6	12,1%	40,1	41,7	4,0%
	Anchor	46,2	45,2	2,2%	-161,1	-157,7	2,1%
Ground pressure (LC2-1)	Combi-wall	448,0	450,0	0,4%	80,1	81,0	1,1%
	Vibro-pile	554,5	563,2	1,6%	158,7	161,3	1,6%
	Anchor	22,2	23,0	3,6%	-77,5	-80,3	3,6%
Water pressure (LC3-1)	Combi-wall	-28,8	-28,7	0,2%	-5,2	-5,2	0,0%
	Vibro-pile	-27,2	-28,6	5,3%	-7,8	-8,2	5,1%
	Anchor	-4,1	-4,2	2,9%	14,2	14,7	3,5%
Terrain load above duct profile (LC-4-1)	Combi-wall	230,8	230,8	0,0%	41,6	41,6	0,0%
	Vibro-pile	-47,8	-47,8	0,0%	-13,7	-13,7	0,0%
	Anchor	8,0	8,0	0,0%	-27,8	-27,9	0,4%
Terrain load above relief floor (LC-4-2)	Combi-wall	212,2	214,4	1,0%	38,2	38,6	1,0%

	Vibro-pile	209,8	210,3	0,2%	60,2	60,2	0,0%
	Anchor	28,8	28,3	1,7%	-100,3	-98,8	1,5%
Terrain back of the quay (LC-4-3)	Combi-wall	5,7	5,3	6,2%	1,0	1,0	2%
	Vibro-pile	66,6	67,0	0,6%	19,1	19,2	0,5%
	Anchor	-28,6	-28,6	0,1%	100	99,9	0,1%
Bollard load (LC-5)	Combi-wall	42,1	42,1	0,1%	7,6	7,6	0,0%
	Vibro-pile	-13,8	-13,7	0,7%	-4,0	-3,9	2,5%
	Anchor	-28,3	-28,3	0,0%	98,7	98,7	0,0%
Fender load (LC-6)	Combi-wall	-7,31	-7,3	0,1%	-1,3	-1,3	0,0%
	Vibro-pile	-49,3	-49,3	0,0%	-14,3	-14,1	1,4%
	Anchor	56,6	56,6	0,0%	-197,4	-197,4	0,0%
Crane load (LC-7-1)	Combi-wall	402,6	403,1	0,1%	72,4	72,4	0,0%
	Vibro-pile	364,0	363,5	0,1%	104,4	104,1	0,3%
	Anchor	33,5	33,5	0,0%	-116,8	-116,7	0,1%
Crane load (LC-7-4)	Combi-wall	400,5	402,2	0,4%	72,1	73,4	1,8%
	Vibro-pile	366,0	364,3	0,5%	104,9	104,4	0,5%
	Anchor	33,6	33,5	0,3%	-117,0	-116,8	0,2%
Substructural loads (LC-8)	Combi-wall	-141,1	-141,1	0,0%	-25,4	-25,4	0,0%
	Vibro-pile	171	171,1	0,1%	49,1	48,9	0,4%
	Anchor	-126,7	-126,8	0,1%	441,9	442,1	0,0%

Table 79. Bending moments 2D vs 3D-model (ULS)

Structural element	Bending moment	Location [m]	Load combination [ULS]	2D – model [Knm]	3D – model [Knm]	Error
Relief floor A-B	Mz-	x=0,75 (At surface of wall A)	ULS 1-2/4	-309,5	235,1	24,1%
	Mz-	x=2,1 m (Bernoulli zone between wall A and B)	ULS 1-1/1	-982,8	909,4	7,5%
	Mz -	x=4,025 (At surface wall B)	ULS 1-1/1	-2084,7	1985,7	5,7%
	Mz+	x=0,75 (At surface of wall A)	ULS 2-2/5	152,5	-180,1	18,1%
Relief floor B-C	Mz-	x=4,775 (At surface wall B)	ULS 1-2/4	-2818	2737	2,9%
	Mz-	x=6,025 (Bernoulli zone between wall B and C)	ULS 1-2/12	-1781	1764,2	0,9%
	Mz-	x=10,1(Bernoulli zone between wall B and C)	ULS 1-2/12	-327	326,3	0,2%
	Mz-	x=14,814 (At vibro-pile)	ULS 1-2/3	-1499	1582,9	5,6%
	Mz-	x= 16,1 (At surface of wall C)	ULS 1-1/23	-778,2	815,9	4,8%
	Mz+	x=10,1 (Bernoulli zone between wall B and C)	ULS 2-1/16	1633,9	-1635,2	0,1%

TUDelft

Table 80. Bending moment 2D vs 3D (SLS)

Structural element	Bending moment	Location [m]	Load combination [SLS]	2D – model [Knm]	3D – model [Knm]	Error
Relief floor A-B	Mz -	x= 0,75 (At surface wall A)	SLS 1-1/3	-129,7	122,9	5,2%
		x= 2,1 (Bernoulli zone between wall A and B)	SLS 1-1/3	-529,2	485	8,4%
	Mz -	x=4,025 (At surface wall B)	SLS 1-1/3	-1195,5	1119	6,4%
Relief floor B-C	Mz-	x=4,775 (At surface wall B)	SLS 1-1/3	-1531,4	1508,2	1,5%
	Mz-	x=6,025 (Bernoulli zone between wall B and C)	SLS 1-1/10	-733,6	716,1	2,4%
	Mz-	x=14,814 (At vibro-pile)	SLS 1-1/2	-998,2	1060,6	6,3%
	Mz-	x= 16,1 (At surface of wall C)	SLS 1-1/7	-445,4	481,9	8,2%
	Mz+	x=10,1(Bernoulli zone between wall B and C)	SLS 1-2/8	1029,3	-1028,9	0,0%

Table 81. Normal forces 2D vs 3D-model (ULS)

Structural element	Normal force	Load combination [ULS]	2D – model [Knm]	3D – model [Knm]	Error
Relief floor A-B	Nx -	ULS 2-2/4	-253,7	-260,1	2,5%
Relief floor B-C	Nx +	ULS 1-2/3	525,1	531,8	1,3%

Table 82. Normal forces 2D vs 3D-model (SLS)

Structural element	Normal force	Load combination [ULS]	2D – model [Knm]	3D – model [Knm]	Error
Relief floor A-B	Nx -	SLS 1-2/4	-54,4	-62	14,0%
Relief floor B-C	Nx +	SLS 1-1/3	330,5	336,3	1,8%

Table 83. Shear forces 2D vs 3D - model

Structural element	Shear force	Location [m]	Load combination [ULS]	2D – model [Knm]	3D – model [Knm]	Error
Relief floor A-B	Ved-	x=4,025 (At surface wall B)	ULS 1-1/1	-608	590,5	2,9%
Relief floor B-C	Ved+	x=4,775 (At surface wall B)	ULS 1-1/8	1060,9	-1047,4	1,3%

Table 78 shows that the inaccuracy of the reaction forces between the models is less than 5%. This suggests that the reaction forces are equivalent between the models.

Looking at Table 79 and Table 80, it can be observed that the inaccuracy of the bending moments of the relief floor between walls B and C is below 2% (B-region). At the surface of the walls, the inaccuracy is higher (D-region).

TUDelft

Also, notice that the inaccuracy of the bending moment of the relief floor between wall A and B in the Bernoulli zone is below 10%. In the table below, the governing ULS result for the bending moment for relief floor A-B at a distance of 2,1 meters is shown. From this table, it can be concluded that the inaccuracy is caused by small differences per load case.

Table 84. Inaccuracy between wall A and B (ULS 1-1/1)

ULS 1-1/1	Partial loading factor	Diana (SLS)	Scia (SLS)	ULS (DIANA)	ULS (SCIA)	Difference
LC1	1,2	208,9	238	250,68	285,6	34,92
LC2	1	42	55,7	42	55,7	13,7
LC3	1	0	0	0	0	0
LC4-1	1,5	129,5	135	194,25	202,5	8,25
LC4-2	1,5	72	84,2	108	126,3	18,3
LC5	1,05	187,4	206,5	196,77	216,825	20,055
LC7-4	0,9	110,7	106,7	99,63	96,03	3,6
LC8	1,2	0	0	0	0	0
				891,33	982,955	91,625

In the figures below a comparison is made between the governing internal forces of the relief floor between the 2D-conventional and 3D-advanced model. The relief floor is split into two sections by walls A and B (relief floor A-B) and B and C (relief floor B-C).
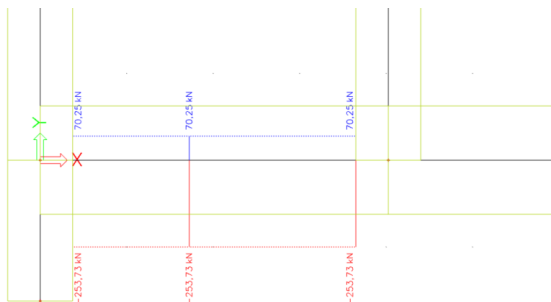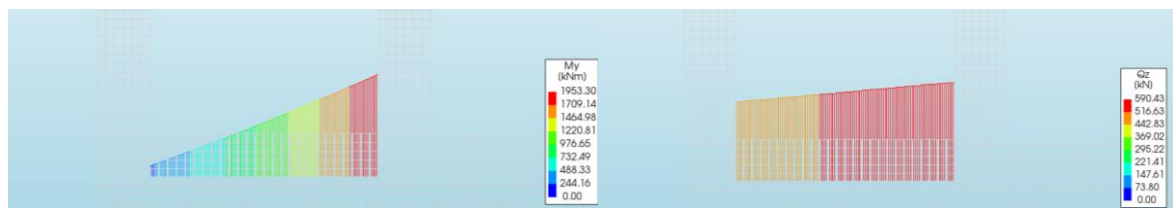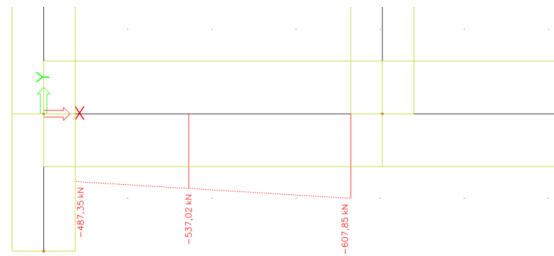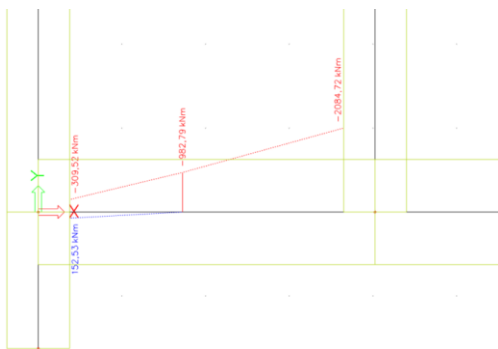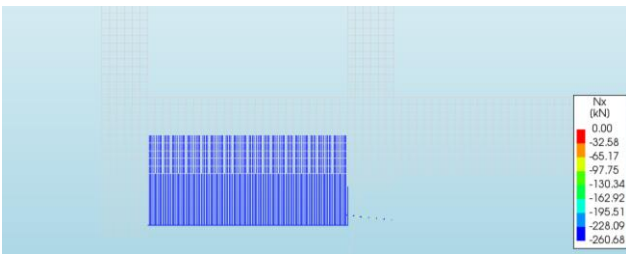
Figure 60. Comparison internal forces at relief floor A-B between conventional and advanced model

Figure 61. Comparison internal forces at relief floor B-C between conventional and advanced model

2.3. Assumptions nonlinear analysis

The material parameters of concrete and steel are determined according to the safety format given in RTD 1016-1:2017.

Table 85. Correct input values for safety format of concrete[19]

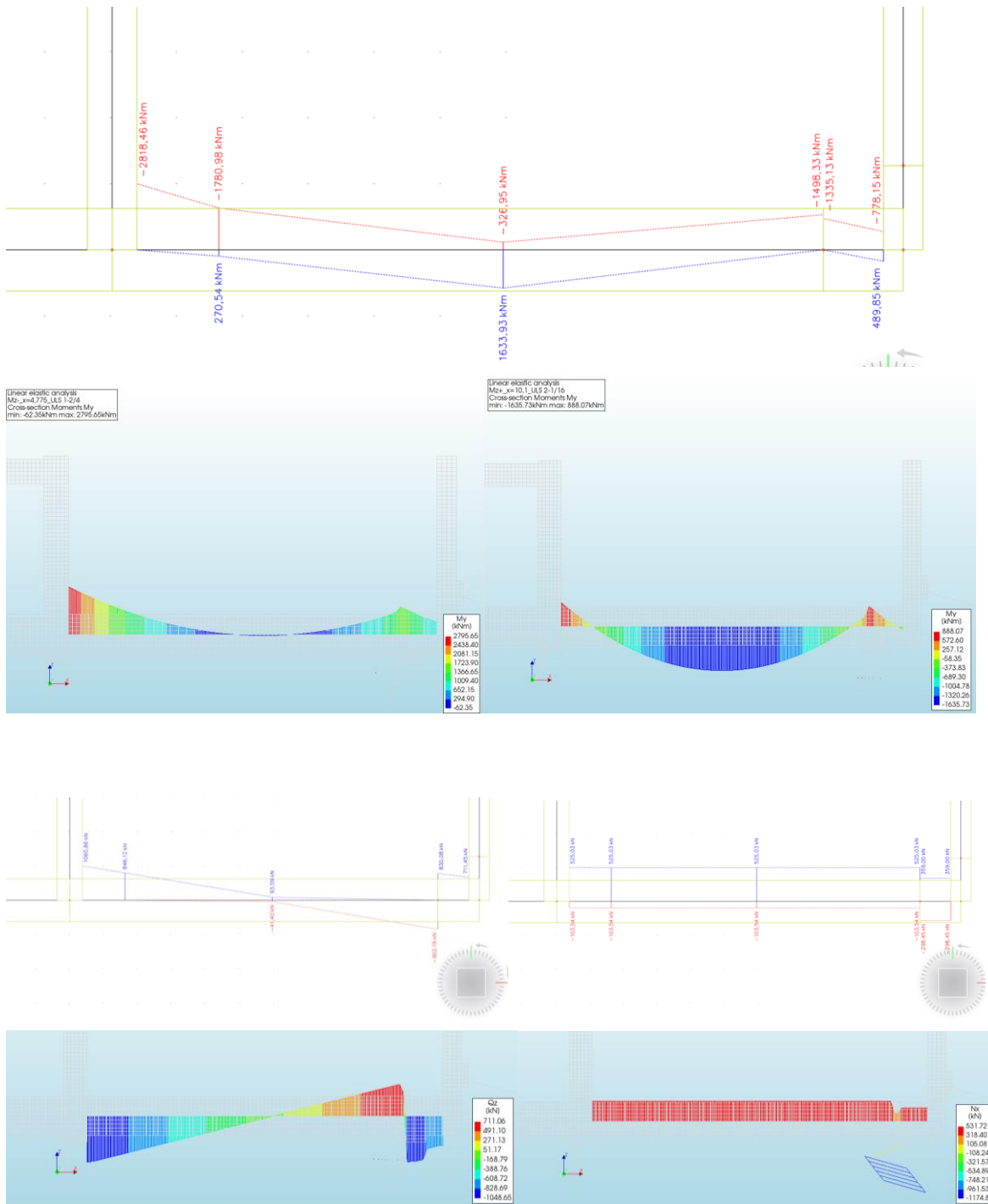|	f_c [MPa]	f_{ct} [Mpa]	E_c [Mpa]	G_F [Nmm/ mm²]	G_c [Nmm/ mm²]
Mean measured	$f_{cm} = f_{ck} + \Delta f$	$f_{ctm} = 0.3(f_{cm})^{\frac{2}{3}}$ for concrete grades $\leq C50$ $f_{ctm} = 2.12 \ln(1 + 0.1(f_{cm})$ for concrete grades $>C50$	$E_{ci} = E_{c0}\left(\frac{f_{cm}}{10}\right)^{\frac{1}{3}}$ $E_{c0} = 21500\ MPa$	$G_f = 0.73\ f_{cm}^{0.18}$	$G_c = 250\ G_F$
Characteristic	$f_{ck} = f_{cm} - \Delta f$	$f_{ctk} = 0.7 f_{ctm}$	$E_{ci} = E_{c0}\left(\frac{f_{ck}}{10}\right)^{\frac{1}{3}}$	$G_f = 0.73\ f_{ck}^{0.18}$	
Mean GRF	$f_{cm,GRF} = 0.85 f_{ck}$	$f_{ctm,GRF} = 0.3(f_{cm,GRF})^{\frac{2}{3}}$ for concrete grades $\leq C50$ $f_{ctm} = 2.12 \ln(1 + 0.1(f_{cm,GRF})$ for concrete grades $>C50$	$E_{ci} = E_{c0}\left(\frac{f_{cm,GRF}}{10}\right)^{\frac{1}{3}}$	$G_f = 0.73\ f_{cm,GRF}^{0.18}$	
Design	$f_{cd} = \frac{f_{ck}}{\gamma_c}$	$f_{ctd} = \frac{f_{ck,min}}{\gamma_c}$	$E_{ci} = E_{c0}\left(\frac{f_{cd}}{10}\right)^{\frac{1}{3}}$	$G_f = 0.73\ f_{cd}^{0.18}$	

Table 86. Correct input values for safety format of steel[20]

	f_y [MPa]	f_t [Mpa]	E_c [Mpa]
Mean measured	f_{ym}	f_{tm}	$\varepsilon_{sy} = \frac{f_{ym}}{E_s}$
Characteristic	$f_{yk} = \exp(-1.65\ v)\ f_{ym}$ $v = 0.6$	$f_{tk} = \frac{f_{tm}}{f_{ym}} f_{yk}$	$\varepsilon_{sk} = \frac{f_{yk}}{E_s}$
Mean GRF	$f_{ym,GRF} = 1.1 f_{yk}$	$f_{tm,GRF} = \frac{f_{tm}}{f_{ym}} f_{ym,GRF}$	$\varepsilon_{ym_{GRF}} = \frac{f_{ym,GRF}}{E_s}$
Design	$f_{yd} = \frac{f_{yk}}{\gamma_s}$	$f_{td} = \frac{f_{tm}}{f_{ym}} f_{yd}$	$\varepsilon_{yd} = \frac{f_{yd}}{E_s}$

For reinforcement C30/37 has been used and for the reinforcement steel B500. The parameters according to the tables above are determined below.

Steel B500 parameters according to characteristic safety format

> $Es := 200000; fyk := 500 : fy := fyk, ftk := 1.08 \cdot 500 : ft := ftk, epsilon[s] := \frac{fyk}{Es}; epsilon[t] := 0.05$

$$Es := 200000$$
$$fy := 500$$
$$ft := 540.00$$
$$\epsilon_s := \frac{1}{400}$$
$$\epsilon_t := 0.05$$

Steel B500 parameters according to the mean GRF safety format

> $A := \frac{ftk}{fyk}$

> $f[ym, GRF] := 1.1 fyk, fy := f[ym, GRF] :$

> $f[tk, GRF] := A \cdot f[ym, GRF]; ft := f[tk, GRF] :$

> $epsilon[ym \cdot GFR] := \frac{f[ym, GRF]}{Es} ;$

$$A := 1.080000000$$
$$f_{ym, GRF} := 550.0$$
$$f_{tk, GRF} := 594.0000000$$
$$\epsilon_{ym \cdot GFR} := 0.002750000000$$

---

[19] Table 1 of Annex A from the RTD 1016-1:2017 guidelines
[20] Table 2 of Annex A from the RTD 1016-1:2017 guidelines

Properties Concrete C30/37 according to the safety format (characterisic):
Characteristic cylinder compressive strength (fck)
> $fck := 30 : fc := fck$

$$fc := 30$$

Mean tensile strength (fctm)
> $fctm := 0.3 \cdot fck^{\left(\frac{2}{3}\right)} : evalf(fctm);$

$$2.896468154$$

Lower-bound characteristic tensile strength (fctk,min)
> $fctk\_min := 0.7 \cdot fctm : evalf(fctk\_min); fct := fctk\_min :$

$$2.027527708$$

Fracture energy (Gf)
> $Gf := \dfrac{73 \cdot fck^{0.18}}{1000}$

$$Gf := 0.1346494817$$

Compressive fracture energy (Gc)
> $Gc := 250 \cdot Gf$

$$Gc := 33.66237042$$

E-modulus after 28 days (Eci)
> $Ec\_0 := 2.15e4 : Ec\_i := Ec\_0 \cdot \left(\dfrac{fck}{10}\right)^{\frac{1}{3}} : Ec := evalf(Ec\_i)$

$$Ec := 31008.36576$$

Properties Concrete C30/37 according to the safety format (GRF):
GRF = global resistance factor
> $fcm\_GRF := 0.85 \cdot fck : fc := fcm\_GRF;$

$$fc := 25.50$$

Concrete grades <=C50
> $fctm\_GRF := 0.3 \cdot fcm\_GRF^{\left(\frac{2}{3}\right)} : fct := fctm\_GRF;$

$$fct := 2.599050442$$

> $Ec\_i := Ec\_0 \cdot \left(\dfrac{fcm\_GRF}{10}\right)^{\frac{1}{3}} : Ec := Ec\_i;$

$$Ec := 29373.23997$$

> $Gf := \dfrac{73 \cdot fcm\_GRF^{0.18}}{1000}$

$$Gf := 0.1307675818$$

> $Gc := 250 \cdot Gf$

$$Gc := 32.69189545$$

2.4.1. Strength advanced verification
In this chapter the behavior of the stirrups when the maximum load is reached is shown.
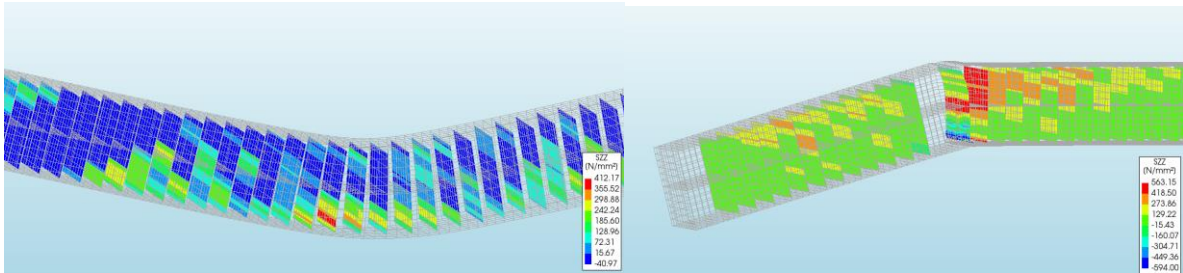
Figure 62. Behavior of the stirrups when the maximum load is reached using the conventionally designed reinforcement (left is location 1 and right is location 2)
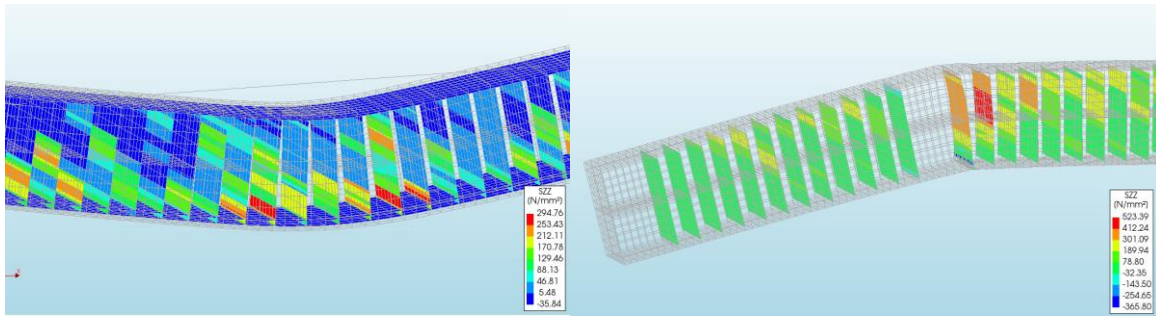
Figure 63. Behavior of the stirrups when the maximum load is reached using the optimized designed reinforcement (left is location 1 and right is location 2)
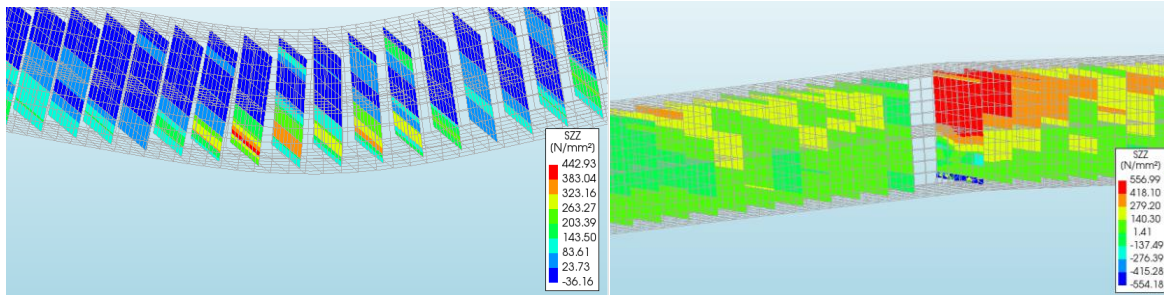
Figure 64, Behavior of the stirrups when the maximum load is reached using the optimized geometry (left is location 1 and right is location 2)

2.4.2. Crack width advanced verification

In this chapter the crack width development at location 1 using a reinforcement set of Ø20-125 + Ø32-200 is determined. The conventional calculated reinforcement where the SLS condition is governing is modeled in Diana FEA. Hereafter, a physical non-linear analysis is performed, and a plot is made of the development of the crack width
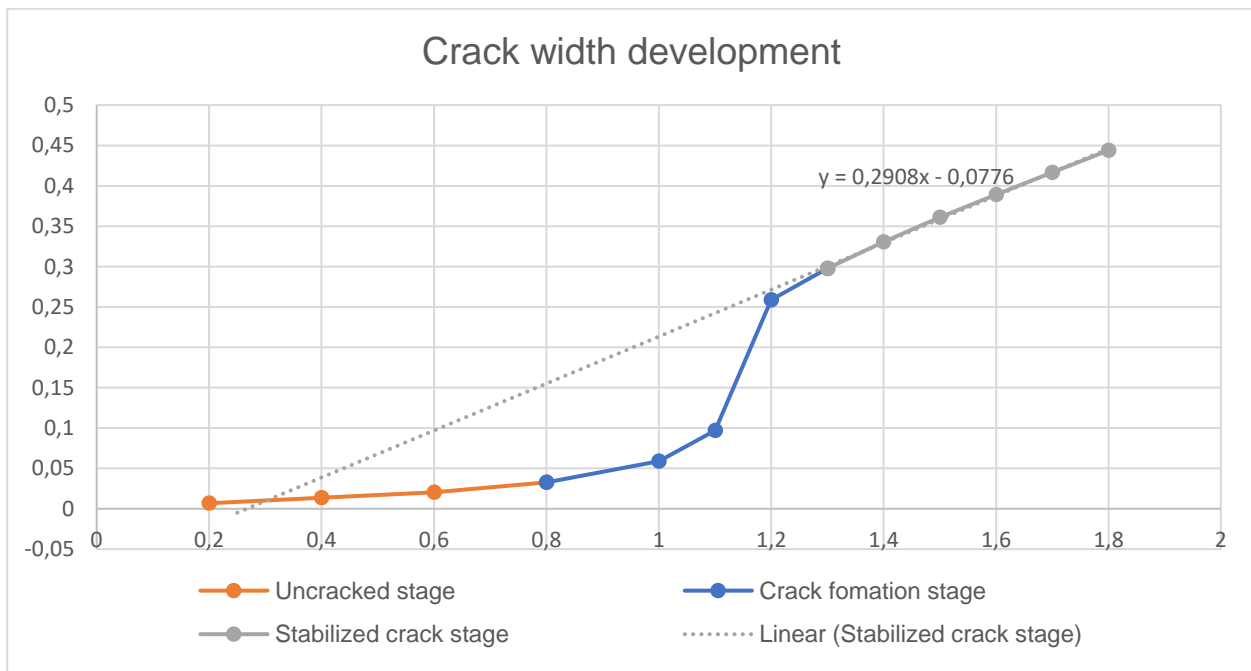
Figure 65. Crack width development reinforcement set Ø20-125 + Ø32-200

Table 87. Crack width comparison IDEA and DIANA reinforcement set Ø20-125 + Ø32-200

Calculation method	Reinforcement	Reinforcement area [mm2]	wk [diana]	wk [norm]	SLS condition
IDEA	Ø20-125 + Ø32-200	6534	0.219	0.22	100%
DIANA	Ø20-125 + Ø32-200	6534	0.2132	0.22	97%

In the table above it can be noticed that the crack width using the advanced method is 3% less than the conventional. Because the difference is slight, it can be concluded that the crack width between the conventional and advanced approaches is comparable.

2.4.3. Bond-slip model

The bond-slip parameters are determined according to table 6.1.1. of the fib Model Code 2010 as seen in the table below.

Table 88. Parameters defining the mean bond stress–slip relationship of ribbed bars according to table 6.1.1. of the fib Model Code 2010

Unfortunately, for an exponent less than one, the stiffness in the function's origin is undefined and so cannot be employed in numerical simulation. To address this issue, a linear stiffness from 0 to an initial slip s0 is considered.

For monotonic loading the reference value τ_b of the bond stresses between concrete and reinforcing bar for pull-out and splitting failure can be calculated as a function of the relative displacement s parallel to the bar axis as follows (**Error! Reference source not found.** according to figure 6.1.1 of the fib Model Code 2010) [11]:

$$\tau_b = \tau_{bmax}\left(\frac{s}{s1}\right)^{\alpha} \qquad\qquad \text{for } 0 \leq s \leq s1$$

$$\tau_b = \tau_{bmax} \qquad\qquad \text{for } s1 \leq s \leq s2$$

$$\tau_b = \tau_{bmax} - \left(\tau_{bmax} - \tau_{bf}\right)(s - s2)(S3 - s2) \qquad\qquad \text{for } s2 \leq s \leq s3$$

$$\tau_b = \tau_{bf} \qquad\qquad \text{for } s3 < s$$

, where the parameters are given in Table 88.

For the main reinforcement good bond conditions and a splitting-stirrups bond-slip model is assumed. The parameters are determined below with the use of maple.

$$tau\_bu\_split\_2 := 8 \cdot \left(\frac{fcm}{25}\right)^{0.25};$$

$$tau\_f\_2 := 0.4 \cdot tau\_bu\_split\_2;$$

$$eq2 := tau\_max \cdot \left(\frac{s}{s1}\right)^{alpha} = tau\_bu\_split\_2 : s1 := 1$$

$$sol := solve(eq2, s)$$

$$s2 := s1; s3 := 0.5 \cdot 10;$$

$$tau\_bu\_split\_2 := 8.882820456$$

$$tau\_f\_2 := 3.553128182$$

$$s1 := 1$$

$$sol := 1.426831477$$

$$s2 := 1$$
$$s3 := 5.0$$

2.5. Comparison conventional and advanced approach in terms of the CO_2 footprint

The amount of reinforcement expressed in cubic meters and kilograms for the ULS and SLS are shown in the table below for the conventional and advanced approach. This is calculated based on the reinforcement distribution.

Table 89. Amount of reinforcement based on the ULS (conventional model)

Conventional model	Reinforcement area per meter [mm2]	Weight of reinforcement per meter [kg/m]	Reinforcement volume over the entire spreading region [m3]	Reinforcement volume a length of 40 meters[m3]	Weight of reinforcement over a length of 40 meters [kg]	Reinforcement volume a length of 220 meters[m3]	Weight of reinforcement over a length of 220 meters [kg]
Location 1	3699	29,0	0,0439	1,757	13792,2	9,7	75857,1
Location 2	7626	59,9	0,0336	1,342	10536,4	7,4	57950,3
Remaining reinforcement top of the relief floor	3927	30,8	0,0479	1,916	15043,6	10,5	82739,5
Remaining reinforcement bottom of the relief floor	2513	19,7	0,0119	0,475	3728,4	2,6	20506,3
				5,491	43100,6	30,198	237053,2

Table 90. Amount of reinforcement based on the ULS (advanced model)

Advanced model	Reinforcement area per meter [mm2]	Weight of reinforcement per meter [kg/m]	Reinforcement volume over the entire spreading region [m3]	Reinforcement volume a length of 40 meters[m3]	Weight of reinforcement over a length of 40 meters [kg]	Reinforcement volume a length of 220 meters[m3]	Weight of reinforcement over a length of 220 meters [kg]
Location 1	3121	24,5	0,0371	1,482	11637,2	8,2	64004,4
Location 2	7150	56,1	0,0315	1,258	9877,9	6,9	54328,4
Remaining reinforcement top of the relief floor	3927	30,8	0,0479	1,916	15043,6	10,5	82739,5
Remaining reinforcement bottom of the relief floor	2513	19,7	0,0119	0,475	3728,4	2,6	20506,3
				5,132	40287,0	28,227	221578,6

TUDelft

Table 91. Amount of reinforcement based on the SLS (conventional model)

Conventional model	Reinforcement area per meter [mm2]	Weight of reinforcement per meter [kg/m]	Reinforcement volume over the entire spreading region [m3]	Reinforcement volume a length of 40 meters[m3]	Weight of reinforcement over a length of 40 meters [kg]	Reinforcement volume a length of 220 meters[m3]	Weight of reinforcement over a length of 220 meters [kg]
Location 1	6161	48,4	0,0732	2,926	22971,9	16,1	126345,4
Location 2	10674	83,8	0,0470	1,879	14747,2	10,3	81109,6
Remaining reinforcement top of the relief floor	3927	30,8	0,0479	1,916	15043,6	10,5	82739,5
Remaining reinforcement bottom of the relief floor	2513	19,7	0,0119	0,475	3728,4	2,6	20506,3
				7,196	56491,1	39,580	310700,8

Table 92. Amount of reinforcement based on the SLS (Advanced model)

Advanced model	Reinforcement area per meter [mm2]	Weight of reinforcement per meter [kg/m]	Reinforcement volume over the entire spreading region [m3]	Reinforcement volume a length of 40 meters[m3]	Weight of reinforcement over a length of 40 meters [kg]	Reinforcement volume a length of 220 meters[m3]	Weight of reinforcement over a length of 220 meters [kg]
Location 1	3881	30,5	0,0461	1,844	14472,9	10,1	79600,9
Location 2	7472	58,7	0,0329	1,315	10323,0	7,2	56776,7
Remaining reinforcement top of the relief floor	3927	30,8	0,0479	1,916	15043,6	10,5	82739,5
Remaining reinforcement bottom of the relief floor	2513	19,7	0,0119	0,475	3728,4	2,6	20506,3
				5,550	43567,9	30,525	239623,3677

In the table below the environmental-data set is shown for different impact categories. These values are derived from a case study of the Tu Delft course "CIE4100 – Material and Ecological Engineering".

Table 93. Environmental- data set for the different impact categories [22].

Shadow prize (Euro) per kg equiva		0,16	0,05	30	0,09	0,03	0,0001	0,06	2	4	9
t category	Unit	Abiotic depletion	Global warming (GWP100)	Ozone layer depletion (ODP)	Human toxicity	Fresh water aquatic ecotox.	Marine aquatic ecotoxicity	Terrestrial ecotoxicity	Photochemical oxidation	Acidification	Eutrophication
Unit		kg Sb eq	kg CO2 eq	kg CFC-11 eq	kg 1,4-DB eq	kg 1,4-DB eq	kg 1,4-DB eq	kg 1,4-DB eq	kg C2H4	kg SO2 eq	kg PO4--- eq
Concrete mix:											
Concrete C20/25 (CEM III)	kg	2,71E-04	9,33E-02	4,42E-09	1,03E-02	2,17E-03	3,57E+00	1,81E-04	7,40E-06	2,22E-04	3,94E-05
Concrete C35/45 (CEM III)	kg	2,79E-04	9,55E-02	4,58E-09	1,05E-02	2,19E-03	3,64E+00	1,85E-04	7,62E-06	2,29E-04	4,06E-05
Concrete C45/55 (CEM I-CEM	kg	3,05E-04	1,07E-01	4,88E-09	1,12E-02	2,28E-03	3,80E+00	2,01E-04	8,24E-06	2,44E-04	4,29E-05
Concrete C55/67 (CEM I-CEM	kg	3,31E-04	1,18E-01	5,19E-09	1,19E-02	2,37E-03	3,96E+00	2,17E-04	8,86E-06	2,60E-04	4,53E-05
Concrete C30/37 (CEM III)	kg	2,76E-04	9,45E-02	4,50E-09	1,04E-02	2,20E-03	3,63E+00	1,83E-04	7,53E-06	2,26E-04	4,02E-05
Steel types:											
Steel S460 heavy duty	kg	1,56E-02	1,82E+00	5,66E-08	6,02E-01	4,57E-01	4,27E+02	1,08E-02	1,08E-03	6,16E-03	1,32E-03
IPE 450 steel profile	kg	1,27E-02	1,49E+00	6,59E-08	5,65E-01	5,90E-01	5,90E+02	2,75E-02	8,47E-04	5,16E-03	1,05E-03
Steel sheet	kg	1,57E-02	1,83E+00	7,84E-08	3,79E+00	1,48E+00	1,30E+03	3,16E-02	9,31E-04	7,61E-03	1,37E-03
Steel reinforcement for concre	kg	1,54E-02	1,79E+00	7,17E-08	3,81E+00	1,49E+00	1,32E+03	3,18E-02	9,27E-04	7,38E-03	1,34E-03
Timber type:											
GL28h	kg	3,86E-03	6,08E-01	6,68E-08	2,62E-01	2,73E-02	6,32E+01	1,45E-03	2,36E-04	6,77E-03	7,69E-04

In the tables below, the CO_2 footprint of the optimized reinforcement based on the SLS is given. These results are derived by multiplying the amount of steel and concrete with the environmental data set given in Table 93

Table 94. Shadow cost concrete and steel (conventional approach (SLS))

Shadow prize (Euro) per kg equivalents		€ 0,05	
Impact category	**Unit**	Global warming (GWP100)	Total Shadow costs
Unit		kg CO2 eq	Euro (€)
Concrete C30/37 (CEM III)	kg	1075553,951	€ 53.777,70
Steel reinforcement for concrete	kg	556579,3159	€ 27.828,97
			€ 81.606,66

Table 95. Shadow cost concrete and steel (advanced approach (SLS)- reinforcement optimized)

Shadow prize (Euro) per kg equivalents		€ 0,05	
Impact category	**Unit**	Global warming (GWP100)	Total Shadow costs
Unit		kg CO2 eq	Euro (€)
Concrete C30/37 (CEM III)	kg	1077692,919	€ 53.884,65
Steel reinforcement for concrete	kg	429253,4797	€ 21.462,67
			€ 75.347,32

Table 96. Shadow cost concrete and steel (advanced approach (SLS)- concrete optimized)

Shadow prize (Euro) per kg equivalents		€ 0,05	
Impact category	**Unit**	Global warming (GWP100)	Total Shadow costs
Unit		kg CO2 eq	Euro (€)
Concrete C30/37 (CEM III)	kg	836875,0658	€ 41.843,75
Steel reinforcement for concrete	kg	556579,3159	€ 27.828,97
			€ 69.672,72

Appendix III

3.1. 2D Scia report

3.1.1. Load cases 2D model

In this paragraph, the load cases applied to the 2D model are shown.

<u>LC2-1 – Earth pressure (fundamental)</u>

Figure 66. 2D model: LC2-1-Earth pressure(fundamental)

<u>LC2-1- Earth pressure (extreme low water levels)</u>

Figure 67. 2D model: LC2-1-Earth pressure (extreme low water)

LC3- Water pressure

Figure 68. 2D model: LC3-water pressure

LC4-1- Terrain load above the deck

Figure 69. 2D model: LC4-1- Terrain load above the deck

TUDelft

LC4-2- Terrain load above the relief floor

Figure 70. 2D model: LC4-2- Terrain load above the relief floor

LC4-3- Terrain load back of wall C
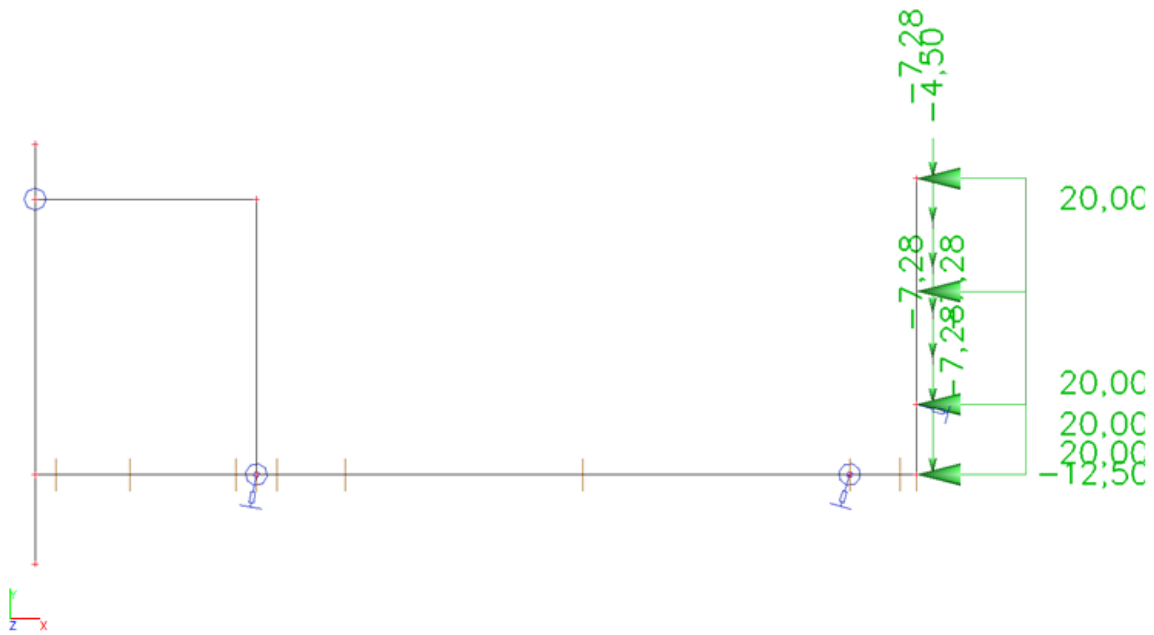
Figure 71. 2D model: LC4-3- Terrain load back of wall C

LC5- Bollard load

Figure 72. 2D model: LC5-Bollard load

LC6- Fender load

Figure 73. 2D model: LC6- Fender loads

LC7-1- Crane load (groundside rail towards water)
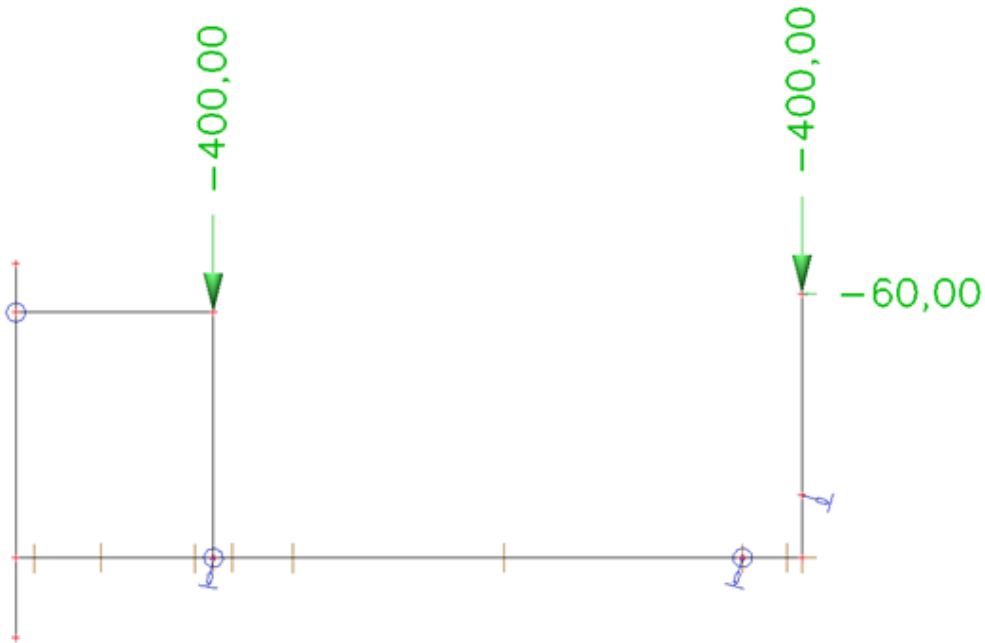
Figure 74. 2D model: LC7-1- Crane load (ground side rail towards water)

LC7-4- Crane load (waterside rail towards water)
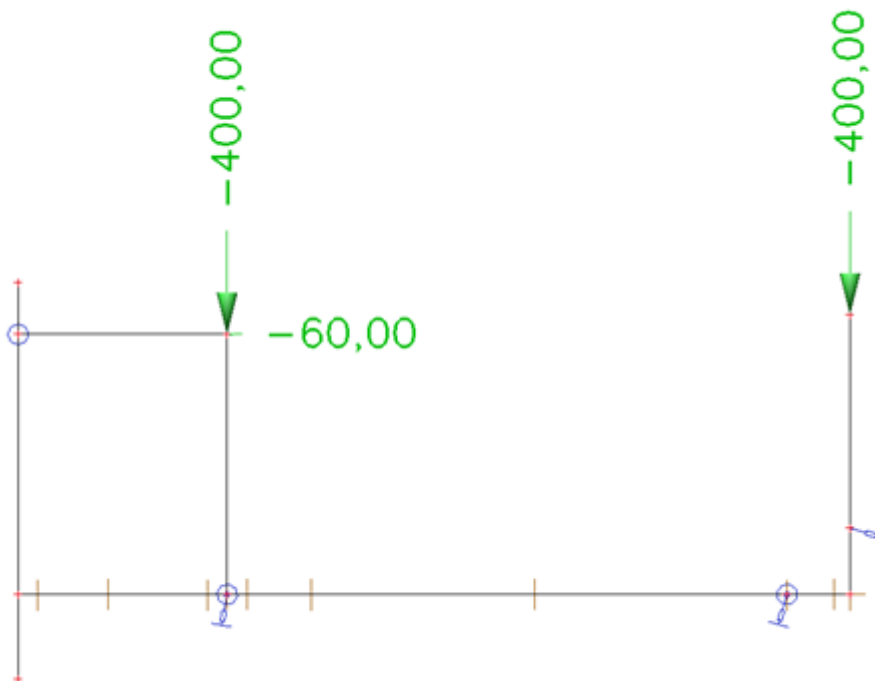
Figure 75. 2D model: LC7-4- Crane load (waterside rail towards water)

LC8- loads from the substructure
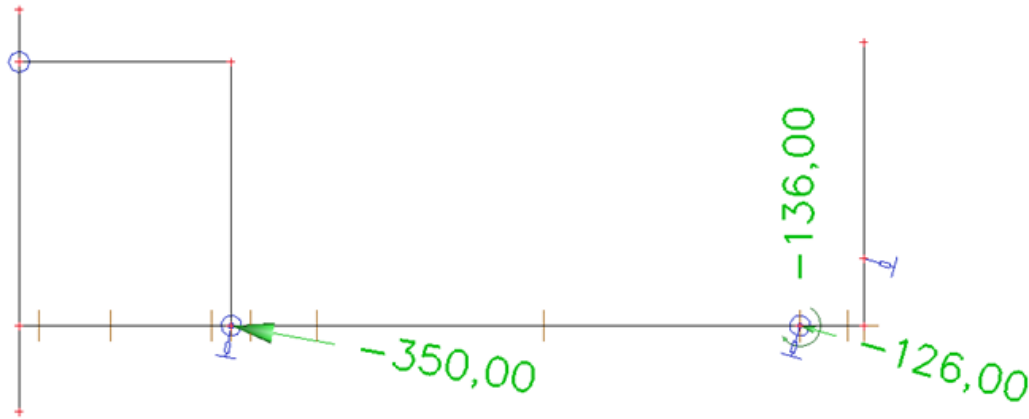
Figure 76. 2D model: LC8- Substructural loads

3.1.2. Internal forces 2D model

In this paragraph, the distribution of the internal forces of the relief floor based on the ULS and SLS of the 2D model are shown.
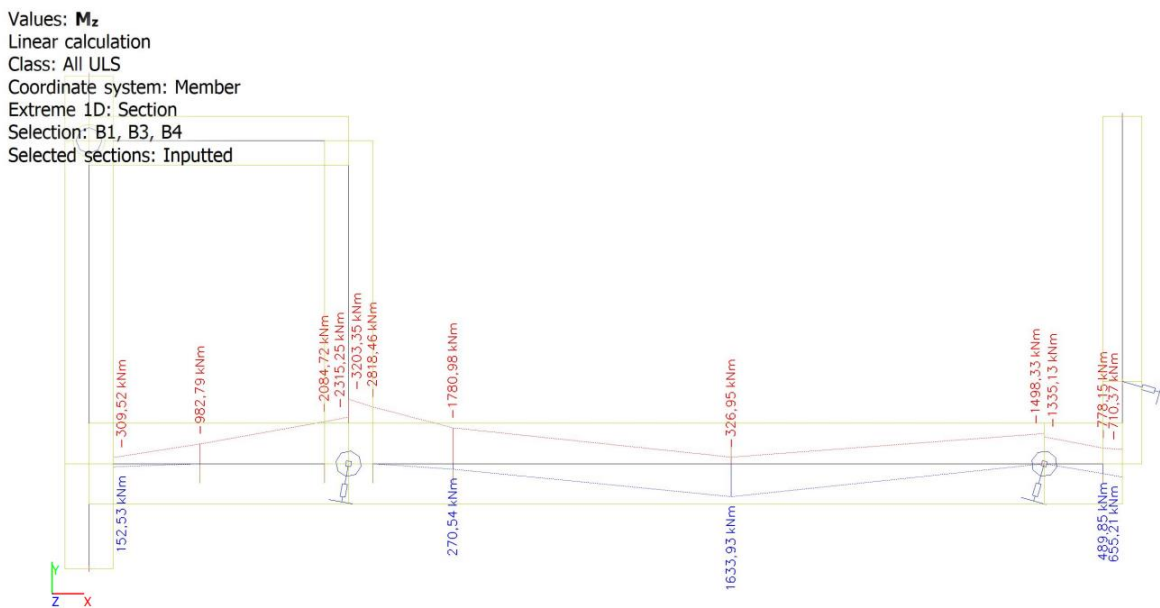
Figure 77. Bending moment relief floor based on the ULS (2D model)

Values: **N**
Linear calculation
Class: All ULS
Coordinate system: Member
Extreme 1D: Global
Selection: B1, B3
Selected sections: Inputted

525,03 kN

−253,73 kN
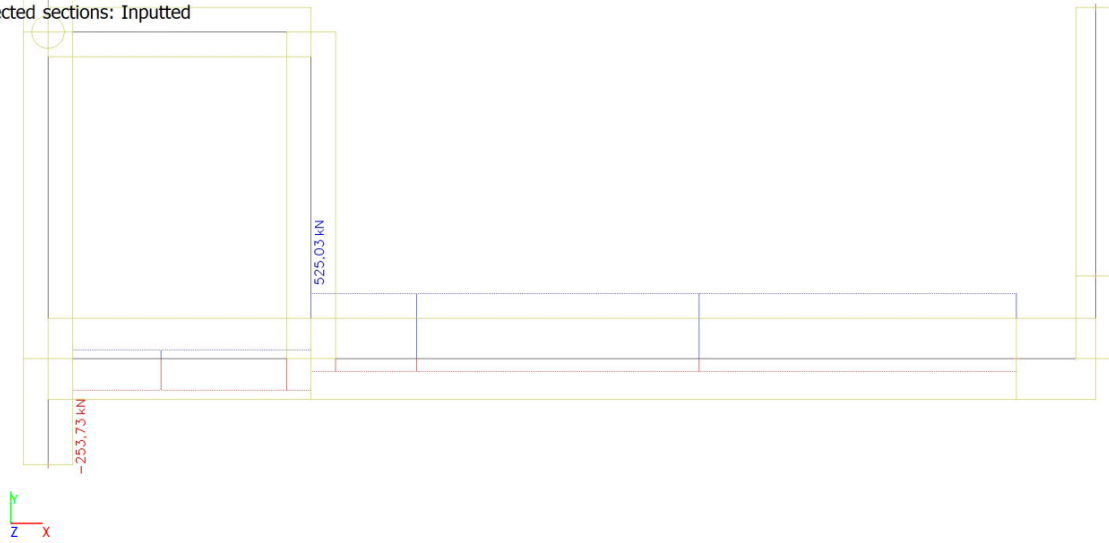
Figure 78, Normal force relief floor based on the ULS (2D model)

Values: **V_y**
Linear calculation
Class: All ULS
Coordinate system: Member
Extreme 1D: Section
Selection: B1, B3, B4
Selected sections: Inputted

1072,78 kN
1060,86 kN

846,12 kN

830,08 kN

711,45 kN
701,91 kN

93,09 kN

−41,40 kN

−487,35 kN

−537,02 kN

−607,85 kN
−621,64 kN

−902,16 kN
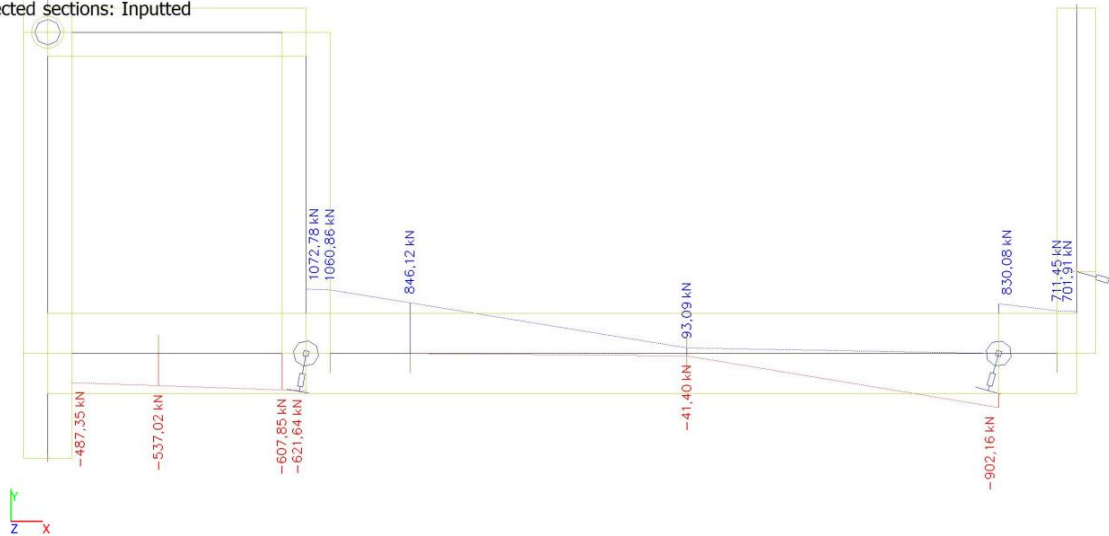
Figure 79. Shear force relief floor based on the ULS (2D model)

Values: **Mz**
Linear calculation
Class: All SLS
Coordinate system: Member
Extreme 1D: Section
Selection: B1, B3, B4
Selected sections: Inputted
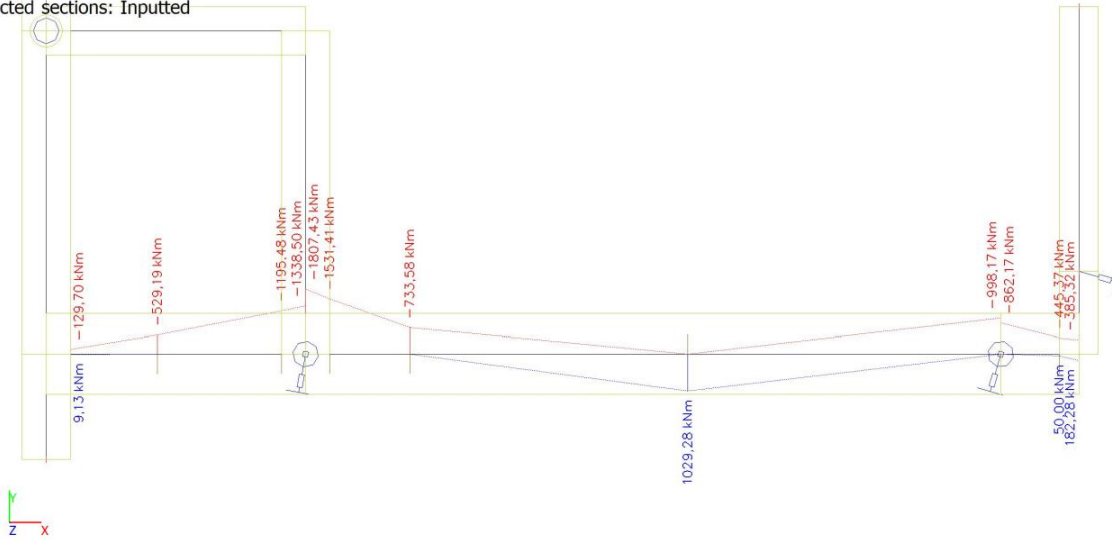
Figure 80. Bending moment relief floor based on the ULS (2D model)

Values: **N**
Linear calculation
Class: All SLS
Coordinate system: Member
Extreme 1D: Global
Selection: B1, B3
Selected sections: Inputted
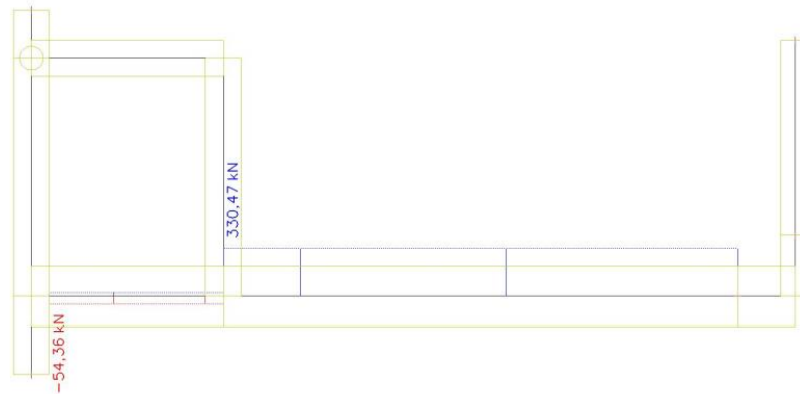
Figure 81. Normal force relief floor based on the SLS (2D model)

TUDelft

3.2. 2.5D Scia report
3.2.1. Load cases 2.5D model
In this paragraph, the load cases applied to the 2.5D model are shown.
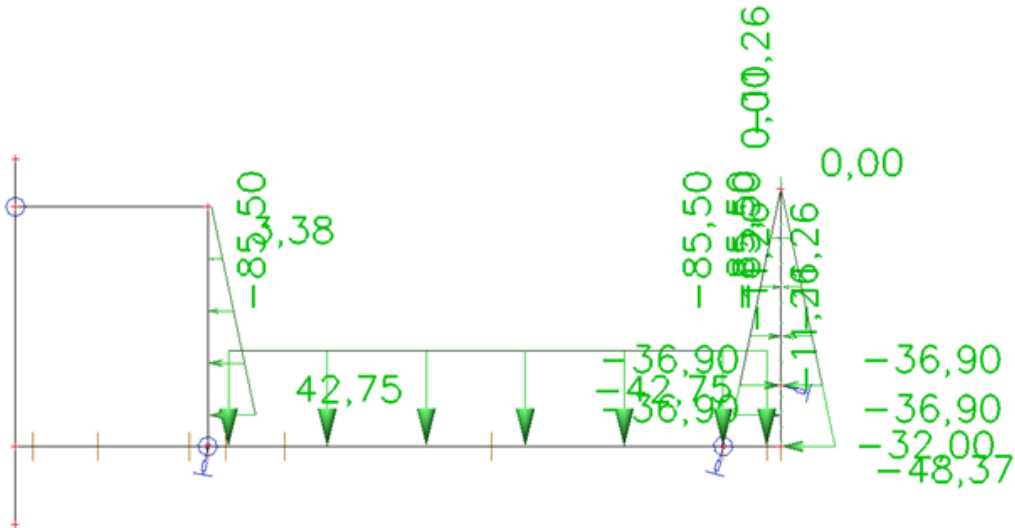
<u>LC2-1 – Earth pressure (fundamental)</u>
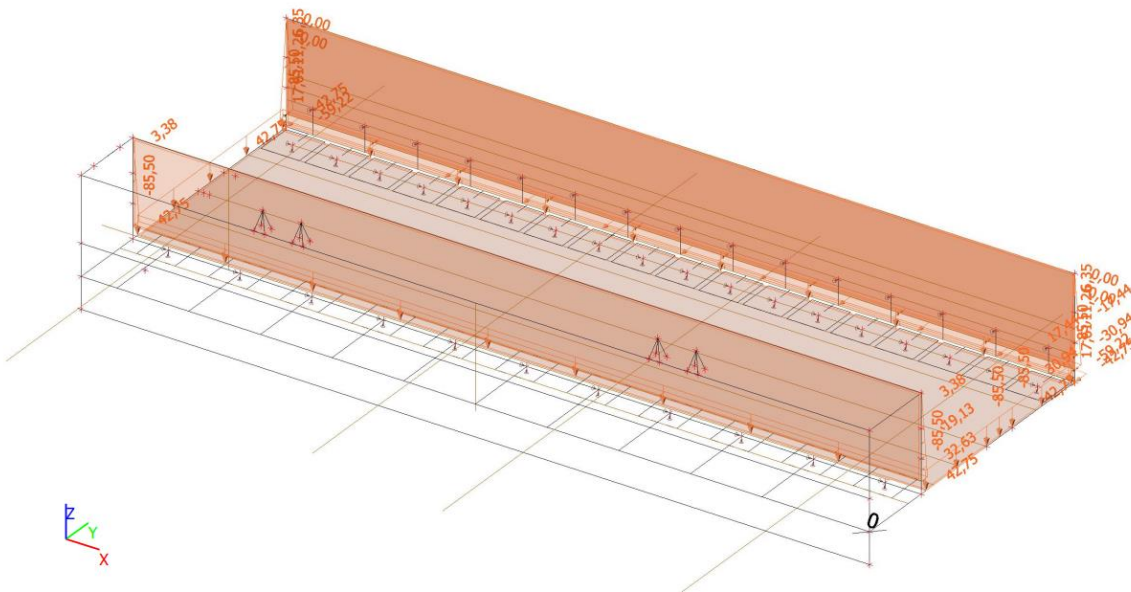
Figure 82. 2.5D model: LC2-1- Earth pressure (fundamental)
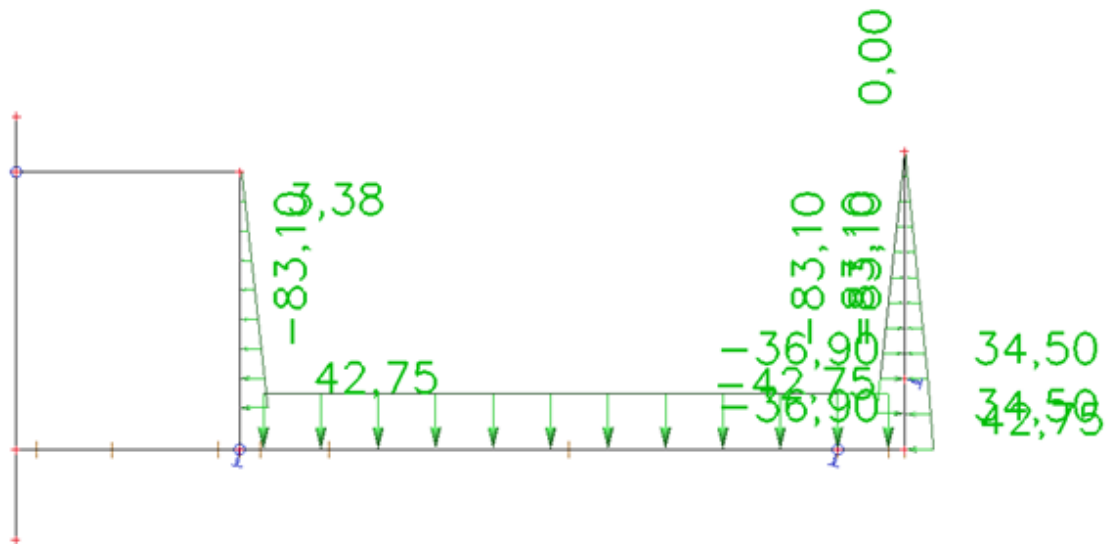
<u>LC2-2- Earth pressure (extreme low water levels)</u>
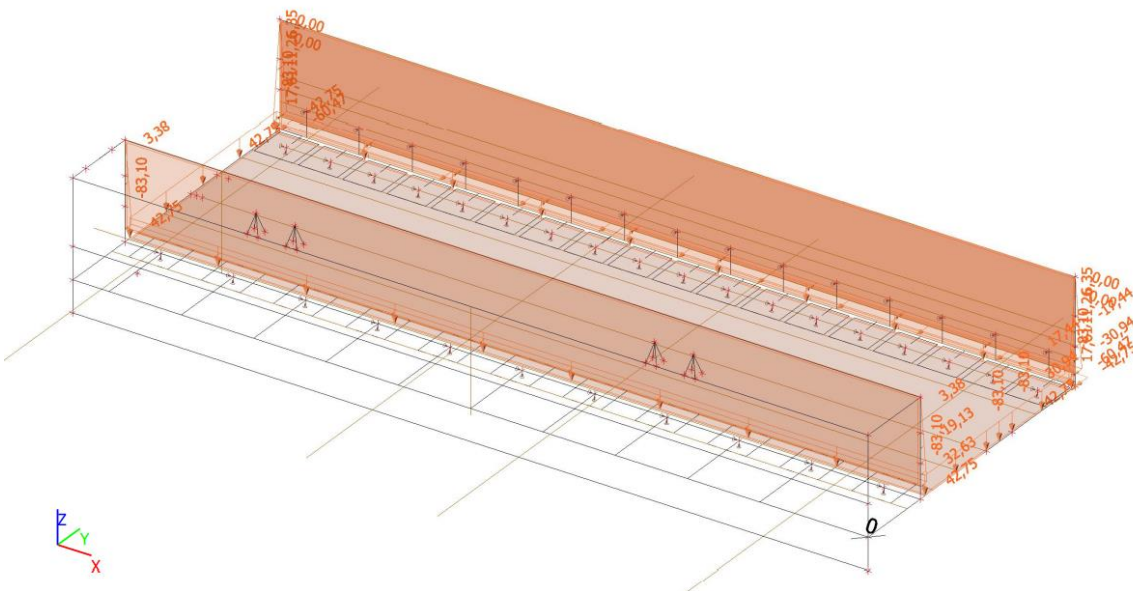
Figure 83. 2.5D model: LC2-2- Earth pressure (extreme low water levels)
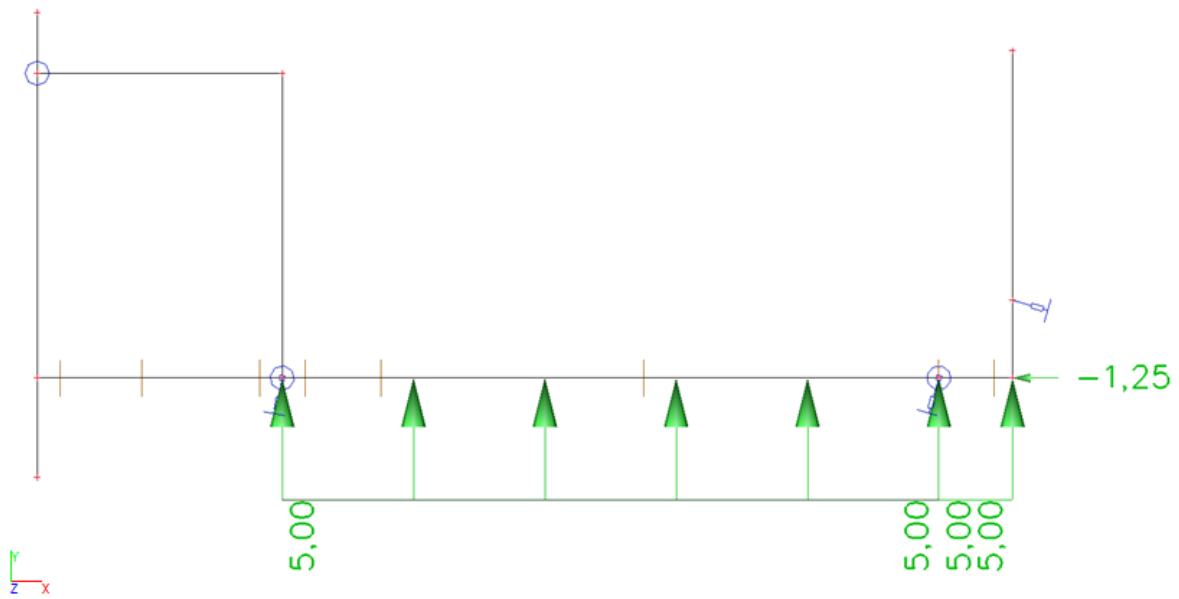
TUDelft
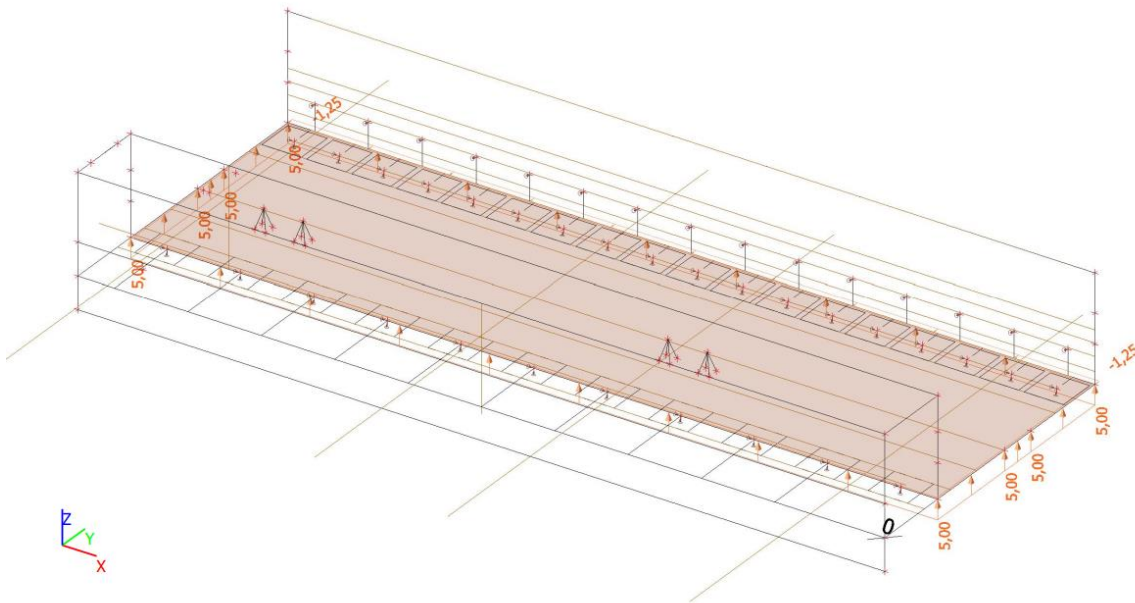
LC3- Water pressure

Figure 84. 2.5D model: LC3- Water pressure
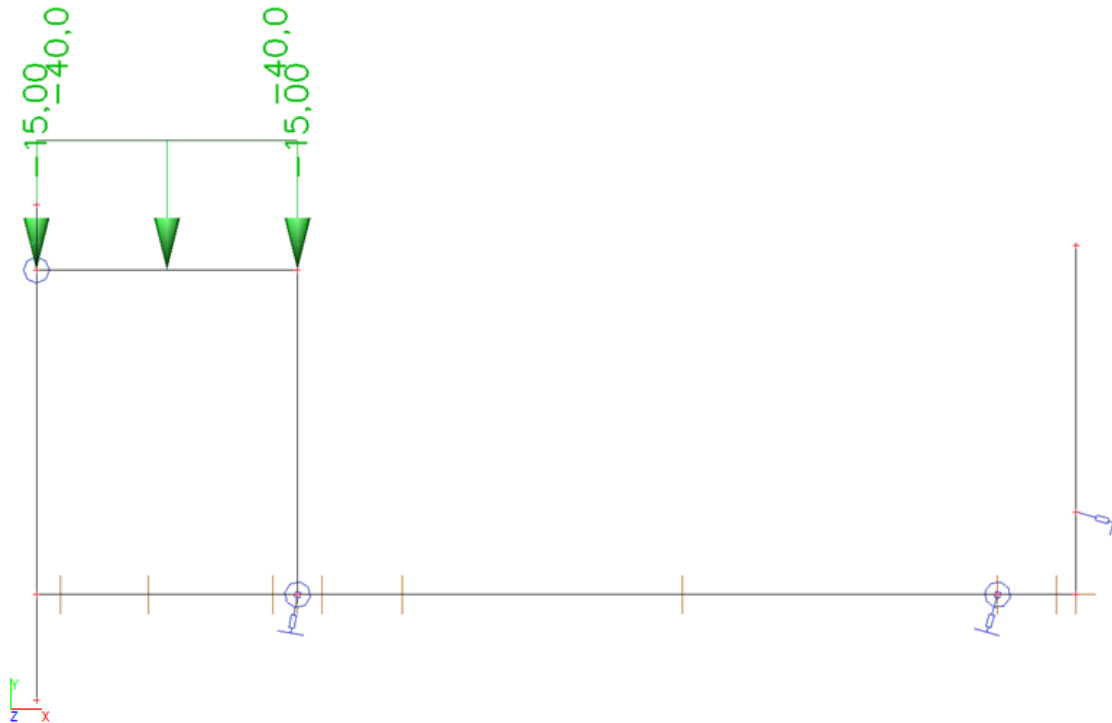
LC4-1- Terrain load above the deck
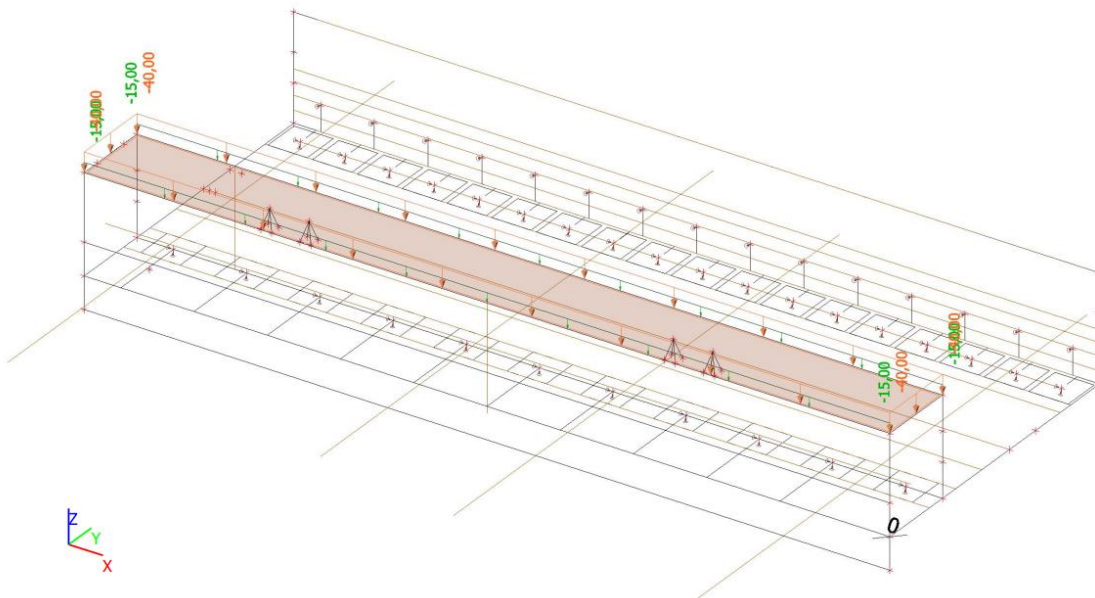
Figure 85. 2.5D model: LC4-1- Terrain load above the deck

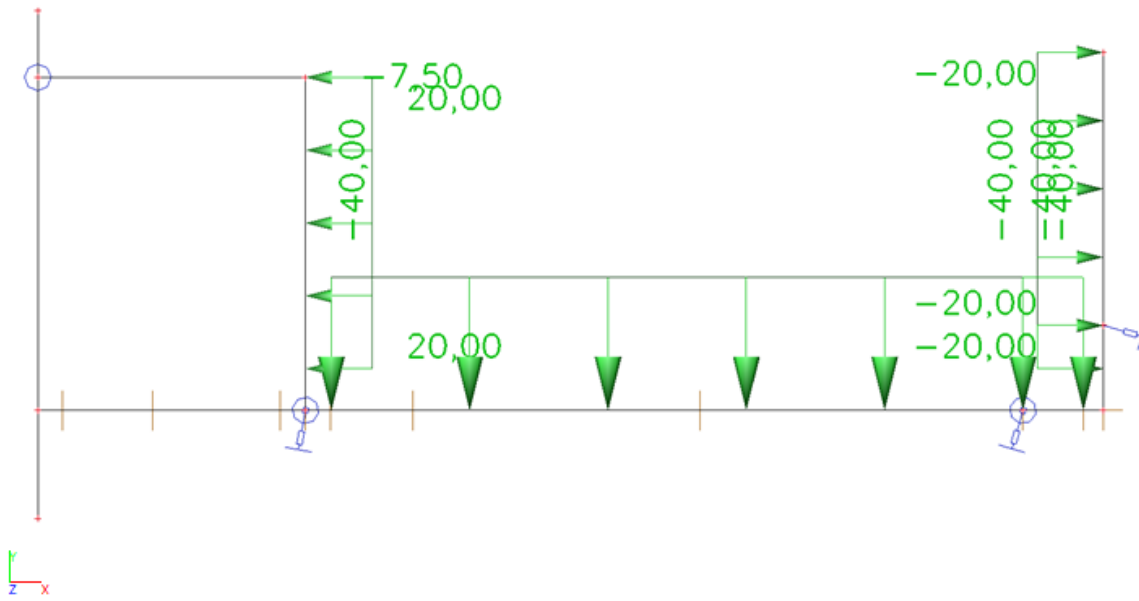LC4-2- Terrain load above the relief floor
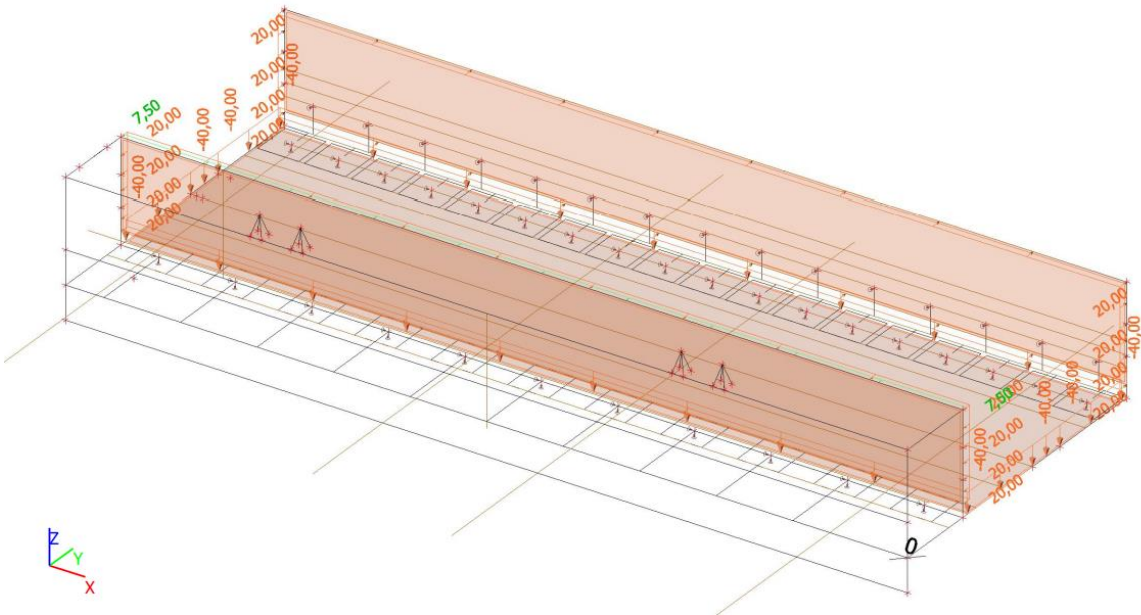
Figure 86. 2.5D model: LC4-2- Terrain load above the relief floor

LC4-3- Terrain load back of the wall C
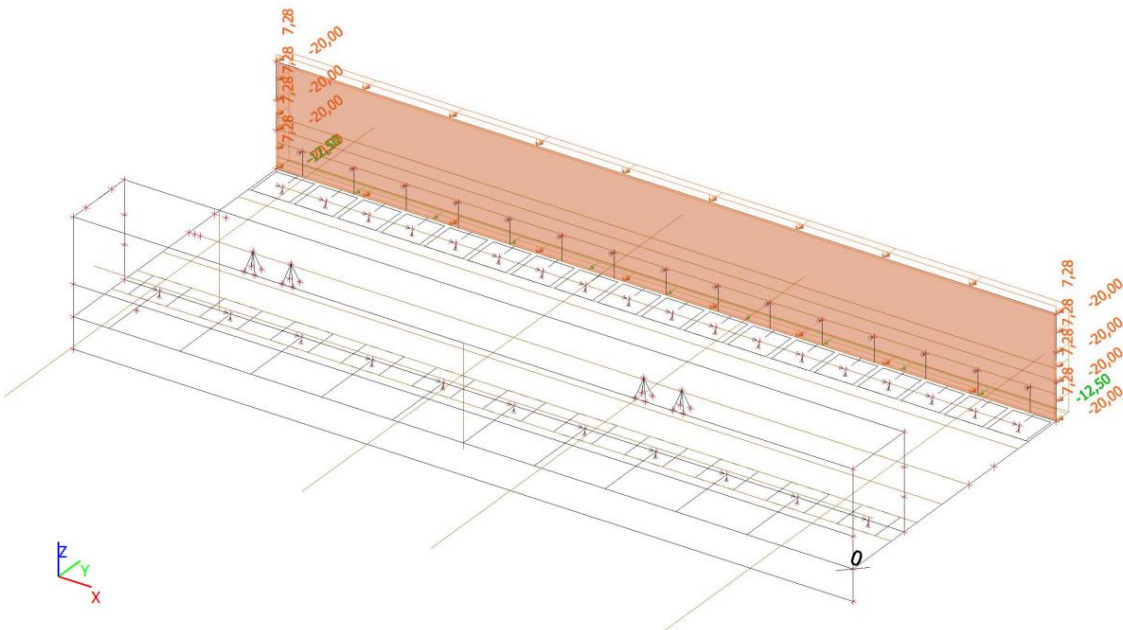
Figure 87. 2.5D model: LC4-3- Terrain load back of the wall C

LC5- Bollard load

TUDelft
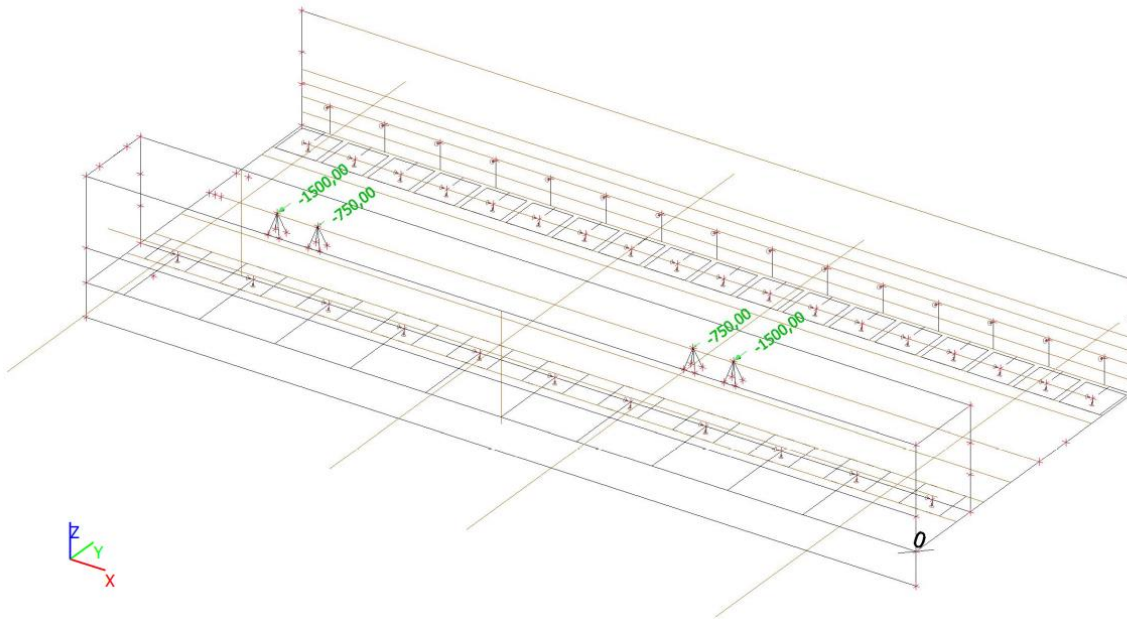
Figure 88. 2.5D model: LC5-Bollard load
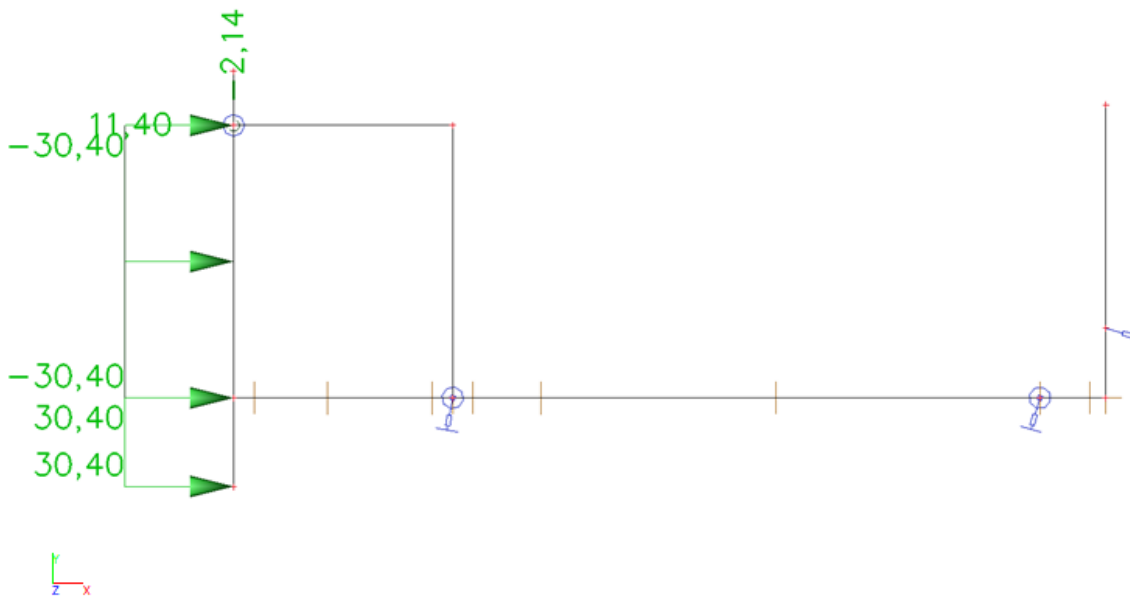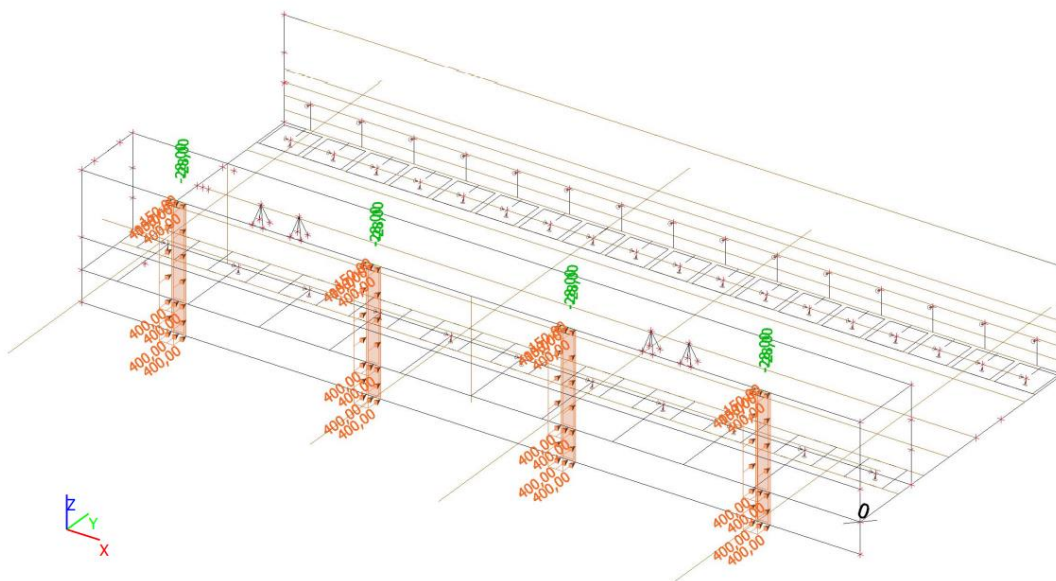
LC6- Fender load

Figure 89. 2.5D model: LC5-Fender load

LC7-1- Crane load (groundside rail towards water)
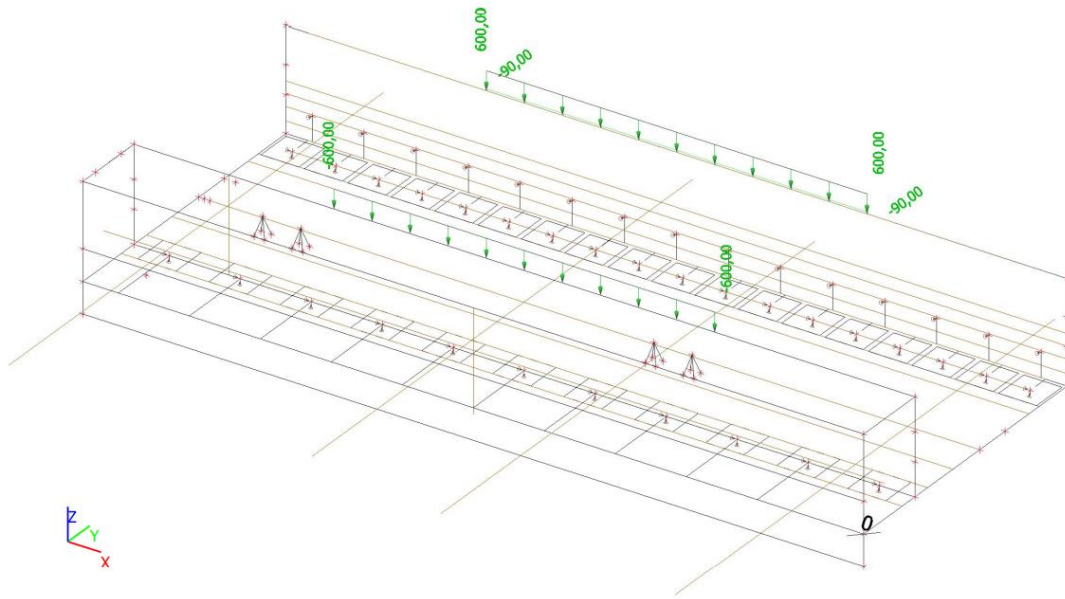
Figure 90. 2.5D model: LC7-1- Crane load (ground side rail towards water)

LC7-4- Crane load (waterside rail towards water)
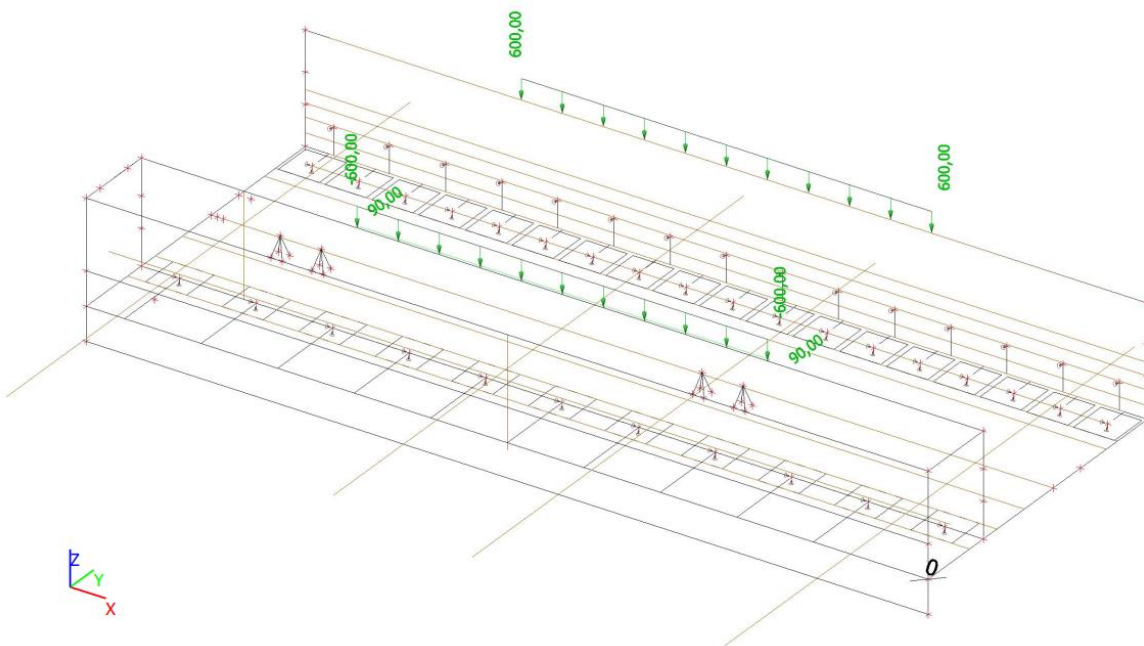
Figure 91. 2.5D model: LC7-4- Crane load (waterside rail towards water)

LC8- loads from the substructure
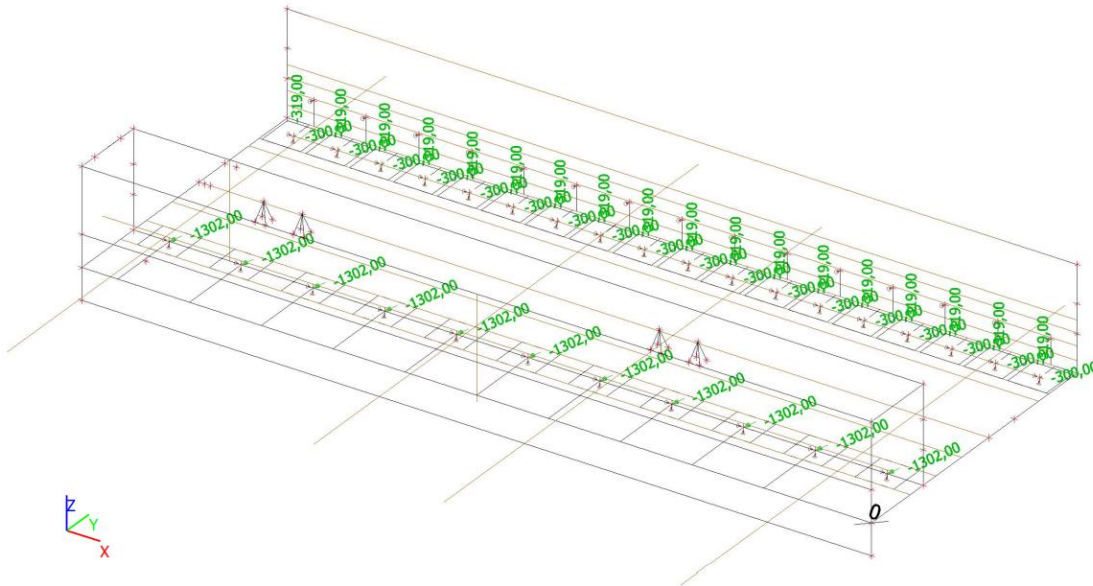
Figure 92. 2.5D model: LC8- loads from the substructure

3.2.2. Internal forces 2.5D model

In this paragraph, the distribution of the internal forces of the relief floor based on the ULS and SLS for the 2.5D model are shown.
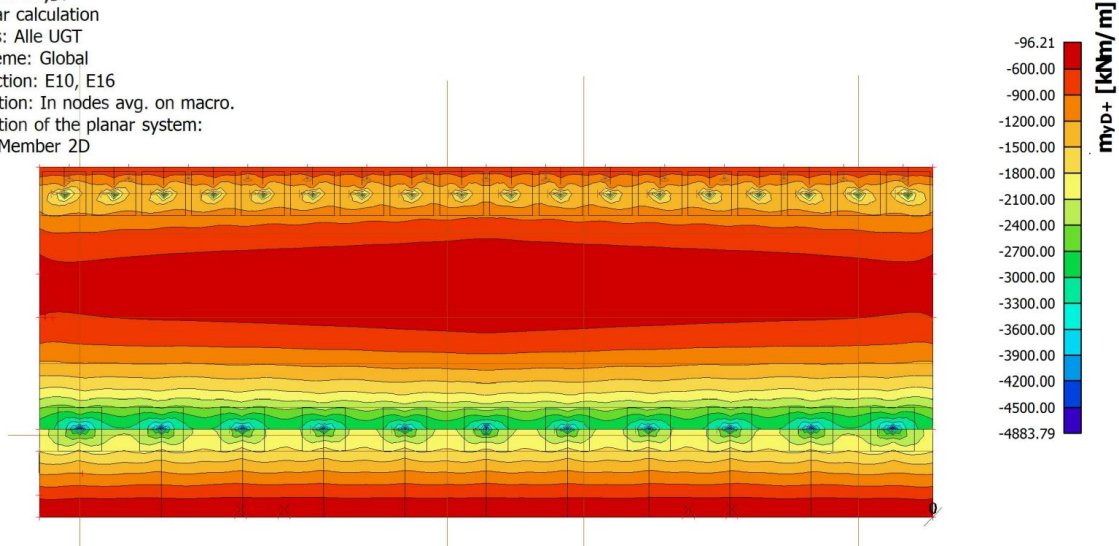
Figure 93. Design bending moment on the positive surface based on the ULS (3D model)

Values: m_{yD+}
Linear calculation
Class: Alle UGT
Course: Average
Extreme: Mesh
Selection: Snede2
Location: In nodes avg. on macro.
Rotation of the planar system:
LCS-Member 2D
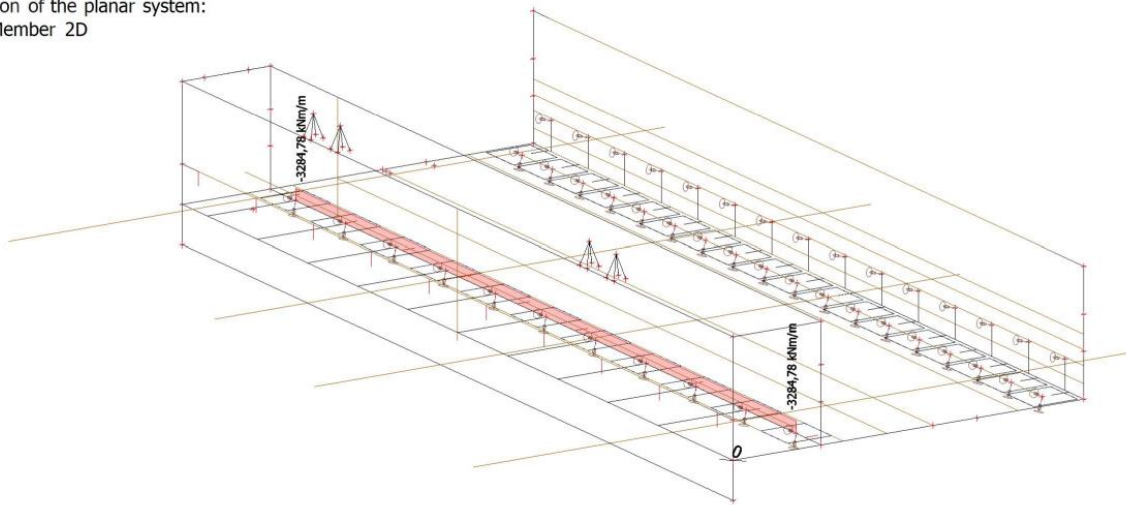
Figure 94. Average design bending moment on the positive surface of the combi-wall based on the ULS (3D model)

Values: m_{yD+}
Linear calculation
Class: Alle UGT
Course: Average
Extreme: Mesh
Selection: Snede4
Location: In nodes avg. on macro.
Rotation of the planar system:
LCS-Member 2D
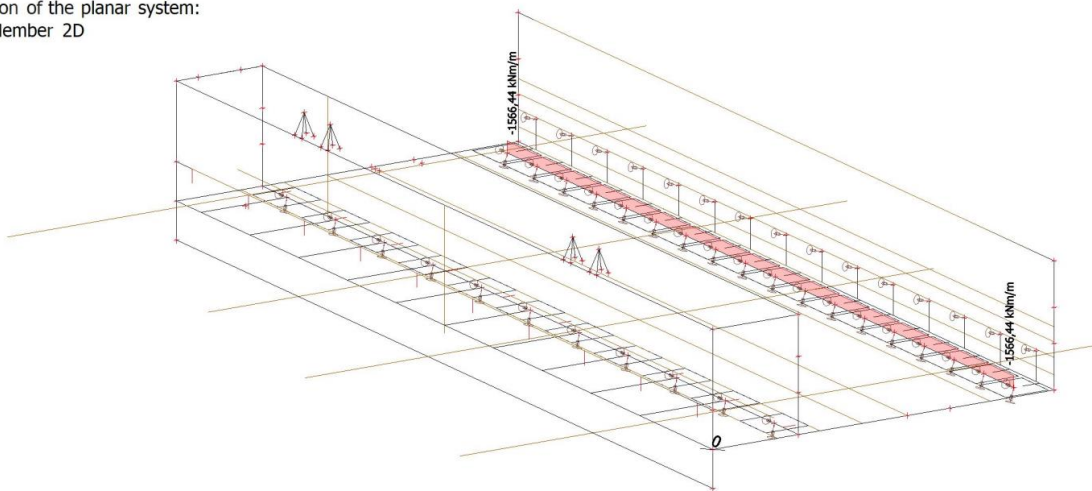
Figure 95. Average design bending moment on the positive surface of the Vibro-piles based on the ULS (3D model)

Values: m_{yD-}
Linear calculation
Class: Alle UGT
Course: Average
Extreme: Mesh
Selection: E10, E16, Snede22, Snede24
Location: In nodes avg. on macro.
Rotation of the planar system:
LCS-Member 2D

m_{yD-} [kNm/m]

1758.70
1400.00
1200.00
1000.00
800.00
600.00
400.00
200.00
0.00

1660,29 kNm/m

795,92 kNm/m
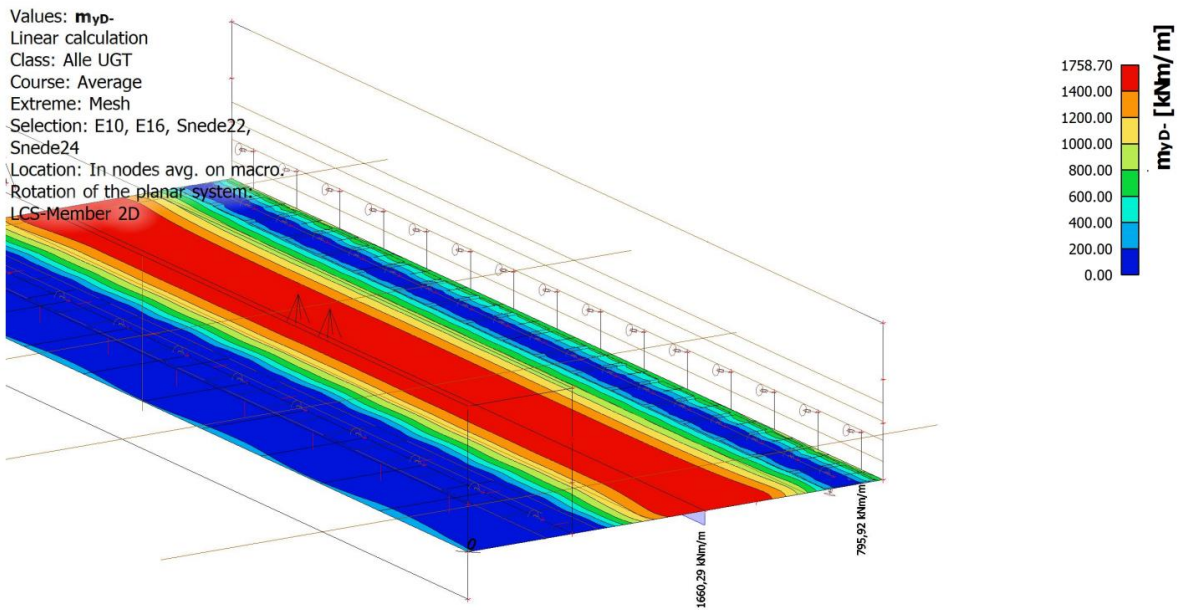
Figure 96. Design bending moment on the negative surface based on the ULS (3D model)

Values: n_{yD}
Linear calculation
Class: Alle UGT
Extreme: Mesh
Selection: E10, E16
Location: In nodes avg. on macro.
Rotation of the planar system:
LCS-Member 2D

n_{yD} [kN/m]

3465.66
3000.00
2700.00
2400.00
2100.00
1800.00
1500.00
1200.00
900.00
600.00
300.00
-0.00
-300.00
-758.82
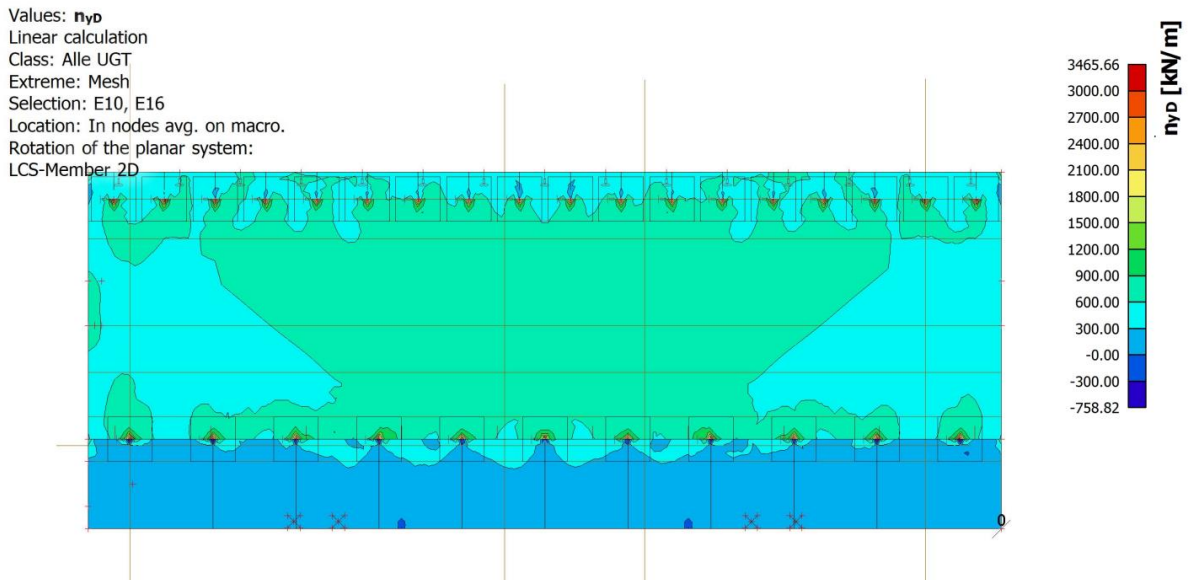
Figure 97. Design normal force based on the ULS (3D model)

Values: n_yD
Linear calculation
Class: Alle UGT
Extreme: Mesh
Selection: E10, E16, Snede3
Location: In nodes avg. on macro.
Rotation of the planar system:
LCS-Member 2D

n_yD [kN/m]

3465.66
3000.00
2700.00
2400.00
2100.00
1800.00
1500.00
1200.00
900.00
600.00
300.00
-0.00
-300.00
-758.82
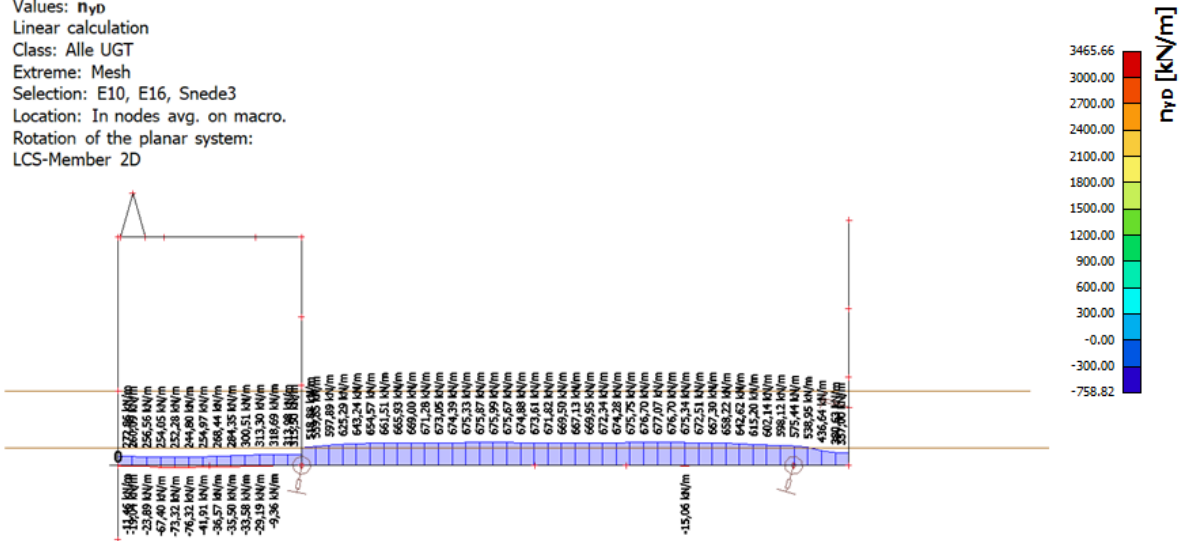
Figure 98. Design normal force distribution based on the ULS (3D model)

Values: q_maxb
Linear calculation
Class: Alle UGT
Extreme: Mesh
Selection: E10, E16
Location: In nodes avg. on macro.
Rotation of the planar system:
LCS-Member 2D

q_maxb [kN/m]

15174.65
1000.00
800.00
700.00
600.00
500.00
400.00
300.00
200.00
100.00
0.00
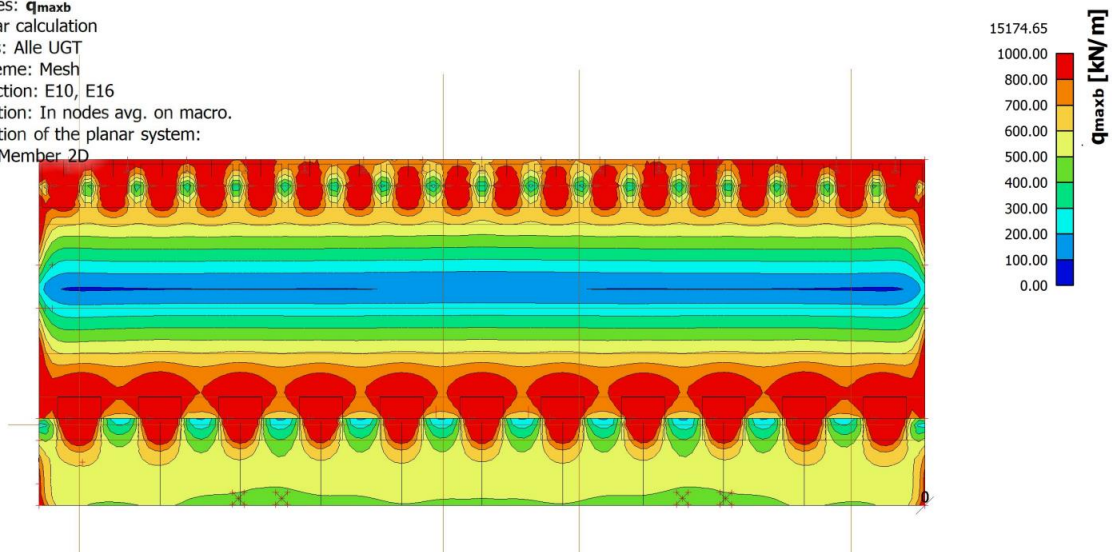
Figure 99. Shear force based on the ULS (3D model)

TUDelft

Values: q_{maxb}
Linear calculation
Class: Alle UGT
Extreme: Mesh
Selection: E10, E16, Snede3
Location: In nodes avg. on macro.
Rotation of the planar system:
LCS-Member 2D

q_{maxb} [kN/m]

15174.65
14000.00
13000.00
12000.00
11000.00
10000.00
9000.00
8000.00
7000.00
6000.00
5000.00
4000.00
3000.00
2000.00
88.94
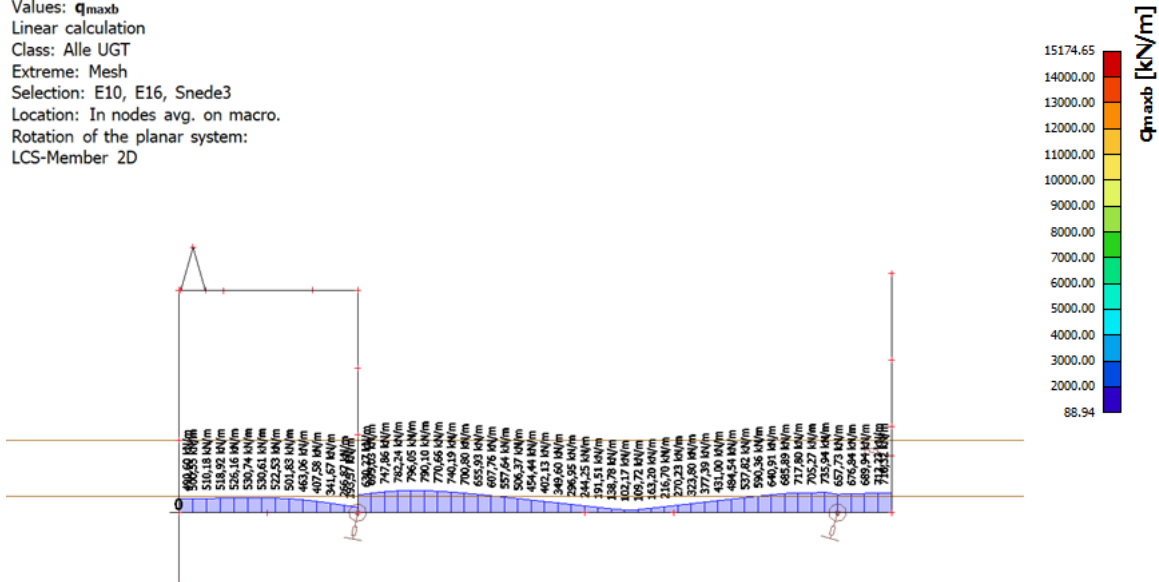
Figure 100. Shear force distribution based on the ULS (3D model)

Values: m_{yD+}
Linear calculation
Class: Alle FREQ
Extreme: Mesh
Selection: E10, E16
Location: In nodes avg. on macro.
Rotation of the planar system:
LCS-Member 2D

m_{yD+} [kNm/m]

0.00
-200.00
-400.00
-600.00
-800.00
-1000.00
-1200.00
-1400.00
-1600.00
-1800.00
-2000.00
-2200.00
-2400.00
-2600.00
-2915.36
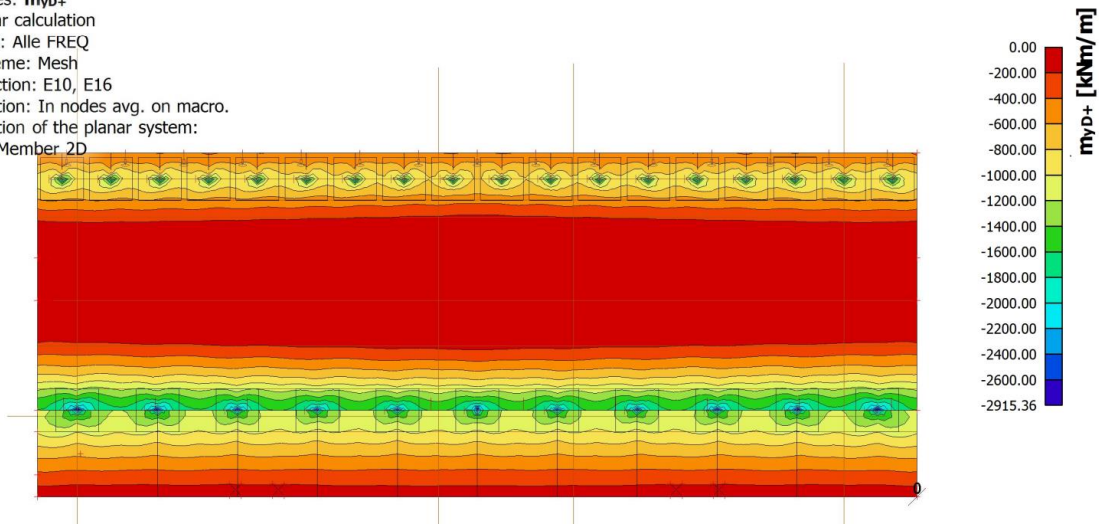
Figure 101. Design bending moment on the positive surface based on the SLS (3D model)

TUDelft

Values: **m_yD+**
Linear calculation
Class: Alle FREQ
Course: Average
Extreme: Mesh
Selection: Snede2
Location: In nodes avg. on macro.
Rotation of the planar system:
LCS-Member 2D

-1849,08 kNm/m

0
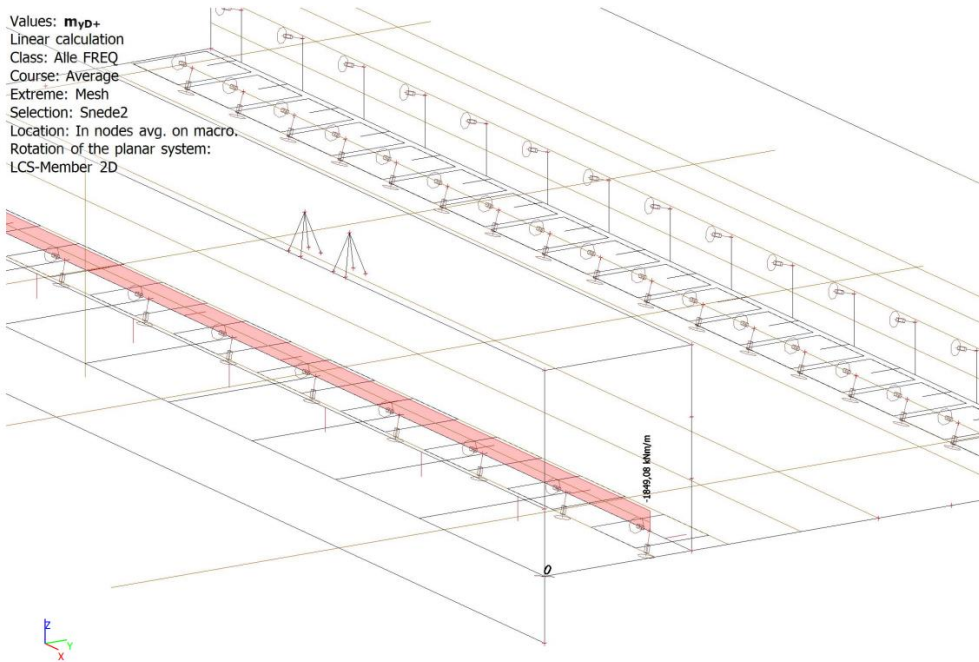
Figure 102. Average design bending moment on the positive surface of the combi-wall based on the SLS (3D model)

Values: **m_yD+**
Linear calculation
Class: Alle FREQ
Course: Average
Extreme: Mesh
Selection: Snede4
Location: In nodes avg. on macro.
Rotation of the planar system:
LCS-Member 2D

-1162,53 kNm/m

-1162,53 kNm/m

0
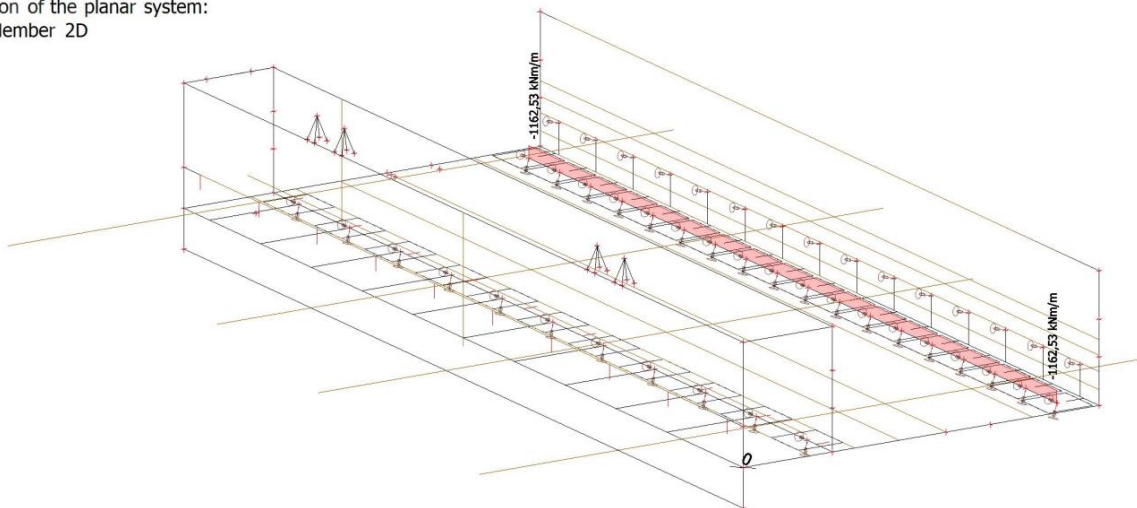
Figure 103. Average design bending moment on the positive surface of the Vibro-piles based on the SLS (3D model)

64.12. 2D internal forces; m_yD-

Values: **m_yD-**
Linear calculation
Class: Alle FREQ
Course: Average
Extreme: Mesh
Selection: E10, E16, Snede22,
Snede24
Location: In nodes avg. on macro.
Rotation of the planar system:
LCS-Member 2D
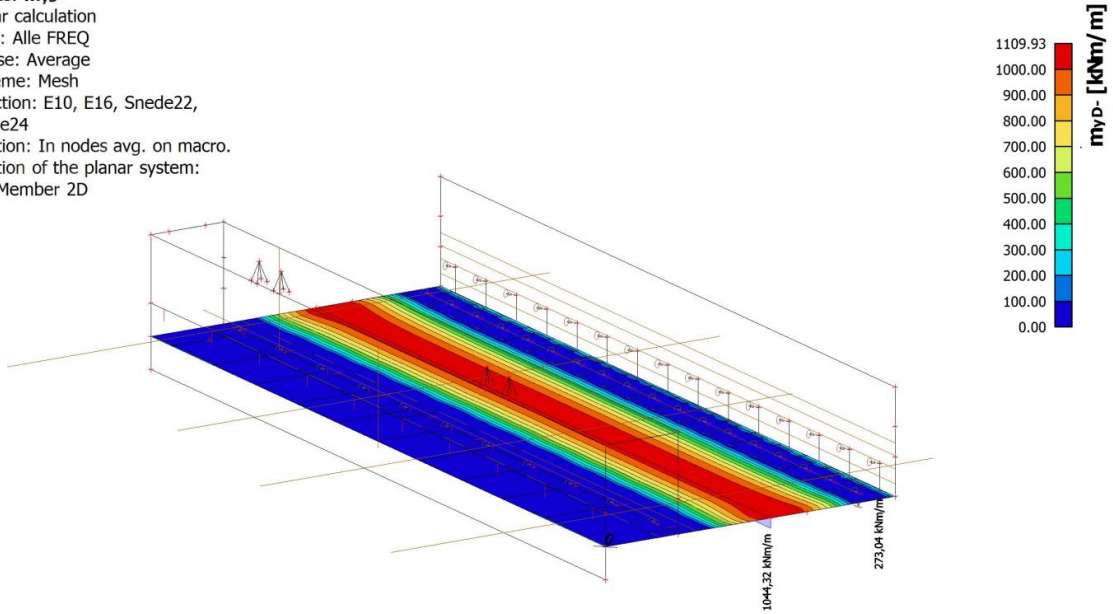
Figure 104. Design bending moment on the negative surface based on the SLS (3D model)

Values: **n_yD**
Linear calculation
Class: Alle FREQ
Extreme: Mesh
Selection: E10, E16
Location: In nodes avg. on macro.
Rotation of the planar system:
LCS-Member 2D
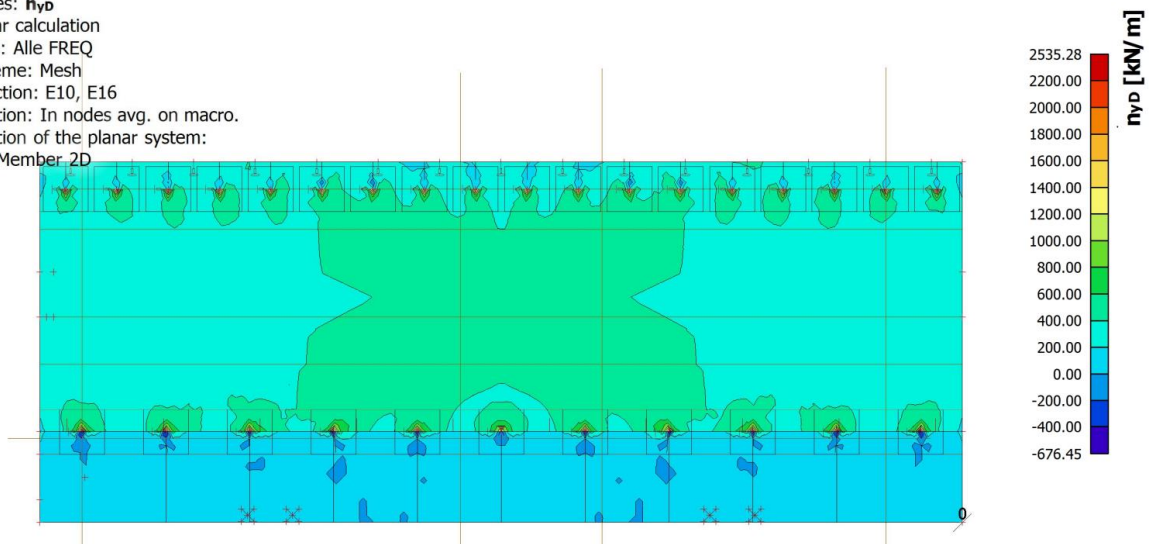
Figure 105. Design normal force based on the SLS (3D model)

Values: n_{yD}
Linear calculation
Class: Alle FREQ
Extreme: Mesh
Selection: E10, E16, Snede3
Location: In nodes avg. on macro.
Rotation of the planar system:
LCS-Member 2D
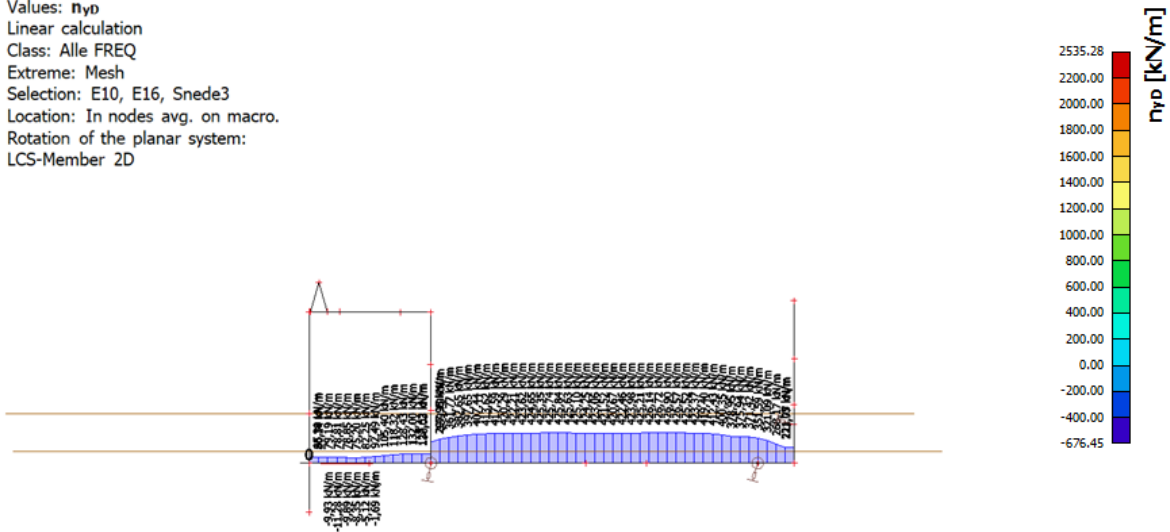
Figure 106. Distribution of the design normal force based on the SLS (3D model)

3.3. Idea Statica Results

In the figures below, the Idea Statica results of the 2D model between walls A and B (location 1), at the combi-walls (location 2), and the vibro-piles (location 3). The reinforcement is calculated based on the conditions where the SLS and ULS are governing. This is carried out because the main objective of the thesis is to optimize the structure based on both conditions.

Reinforced cross-section: R 1

Concrete: C30/37
Age: 28,0 d
Reinforcement: (B 500B)
ø25-125 mm (3927mm²), z = 563 mm
ø20-125 mm (2513mm²), z = -565 mm
ø25-125 mm (3927mm²), z = -513 mm
Links:
3,33ø16 - 200 mm
Cover:
Upper edge: 50 mm
Lower edge: 50 mm

Project Data

Project:

Code:	EN 1992-1-1
National Annex:	Dutch
Design Working Life:	50 years

Current section and extreme

Section:	S 1
Extreme:	S 1 - E 1
Design Member:	M 1
Member Type:	One-way slab
Exposure Class:	XC3, XD1

Current section check

Current section status: ✓
Current extreme status: ✓

Check	Value	Status
Capa	58,5	✓
Shea	73,6	✓
Inter	83,8	✓
Crac	94,7	✓
Flexi	0,0	✓

Current extreme forces

	ULS	Freq
N [kN]	550,0	350,0
My [kNm]	1630,0	1030,0
Mz [kNm]	0,0	0,0
Vy [kN]	0,0	0,0
Vz [kN]	1060,0	0,0
T [kNm]	0,0	0,0

Overall | Capacity N-M-M | Shear | Interaction | Crack Width | Flexural Slenderness | Detailing

Overall

Governing type of check	N_{Ed} [kN]	$M_{Ed,y}$ [kNm]	$M_{Ed,z}$ [kNm]	V_{Ed} [kN]	T_{Ed} [kNm]	Value [%]	Check
Crack Width	350,0	1030,0	0,0			94,7	OK

Type of check	N_{Ed} [kN]	$M_{Ed,y}$ [kNm]	$M_{Ed,z}$ [kNm]	V_{Ed} [kN]	T_{Ed} [kNm]	Value [%]	Check
Capacity N-M-M	550,0	1630,0	0,0			58,5	OK
Shear	550,0			1060,0	0,0	73,6	OK

Figure 107. Idea Statica reinforcement calculation at location 1 based on the SLS

Figure 108 (top)

Reinforced cross-section: R 1

Concrete: C30/37
Age: 28,0 d
Reinforcement: (B 500B)
ø25-125 mm (3927mm²), z = 563 mm
ø20-125 mm (2513mm²), z = -565 mm
ø32-120 mm (6702mm²), z = 509 mm
Links:
3,33ø16 - 200 mm
Cover:
Upper edge: 50 mm
Lower edge: 50 mm

Dimensions: 1250 (height), 1000 (width)

Project Data

Project:

Code: EN 1992-1-1
National Annex: Dutch
Design Working Life: 50 years

Current section and extreme

Section: S 1
Extreme: S 1 - E 1
Design Member: M 1
Member Type: One-way slab
Exposure Class: XC3, XD1

Current section check

Current section status: ✓
Current extreme status: ✓

Check	Value	Status
Capa	68,0	✓
She	76,5	✓
Inter	88,2	✓
Crac	99,7	✓
Flexi	0,0	✓

Current extreme forces

	ULS	Freq
N [kN]	550,0	350,0
My [kNm]	-3200,0	-1800,0
Mz [kNm]	0,0	0,0
Vy [kN]	0,0	0,0
Vz [kN]	1060,0	0,0
T [kNm]	0,0	0,0

Overall

Tabs: Overall | Capacity N-M-M | Shear | Interaction | Crack Width | Flexural Slenderness | Detailing

Governing type of check	N_{Ed} [kN]	$M_{Ed,y}$ [kNm]	$M_{Ed,z}$ [kNm]	V_{Ed} [kN]	T_{Ed} [kNm]	Value [%]	Check
Crack Width	350,0	-1800,0	0,0			99,7	OK

Type of check	N_{Ed} [kN]	$M_{Ed,y}$ [kNm]	$M_{Ed,z}$ [kNm]	V_{Ed} [kN]	T_{Ed} [kNm]	Value [%]	Check
Capacity N-M-M	550,0	-3200,0	0,0			68,0	OK
Shear	550,0			1060,0	0,0	76,5	OK

Figure 108. Idea Statica reinforcement calculation at location 2 based on the SLS

Figure 109 (bottom)

Reinforced cross-section: R 1

Concrete: C30/37
Age: 28,0 d
Reinforcement: (B 500B)
ø25-125 mm (3927mm²), z = 563 mm
ø20-125 mm (2513mm²), z = -565 mm
ø16-110 mm (1828mm²), z = 517 mm
Links:
3,33ø16 - 200 mm
Cover:
Upper edge: 50 mm
Lower edge: 50 mm

Dimensions: 1250 (height), 1000 (width)

Project Data

Project:

Code: EN 1992-1-1
National Annex: Dutch
Design Working Life: 50 years

Current section and extreme

Section: S 1
Extreme: S 1 - E 1
Design Member: M 1
Member Type: One-way slab
Exposure Class: XC3, XD1

Current section check

Current section status: ✓
Current extreme status: ✓

Check	Value	Status
Capa	60,0	✓
She	72,5	✓
Inter	90,0	✓
Crac	97,9	✓
Flexi	0,0	✓

Current extreme forces

	ULS	Freq
N [kN]	550,0	350,0
My [kNm]	-1500,0	-1000,0
Mz [kNm]	0,0	0,0
Vy [kN]	0,0	0,0
Vz [kN]	1060,0	0,0
T [kNm]	0,0	0,0

Overall

Tabs: Overall | Capacity N-M-M | Shear | Interaction | Crack Width | Flexural Slenderness | Detailing

Governing type of check	N_{Ed} [kN]	$M_{Ed,y}$ [kNm]	$M_{Ed,z}$ [kNm]	V_{Ed} [kN]	T_{Ed} [kNm]	Value [%]	Check
Crack Width	350,0	-1000,0	0,0			97,9	OK

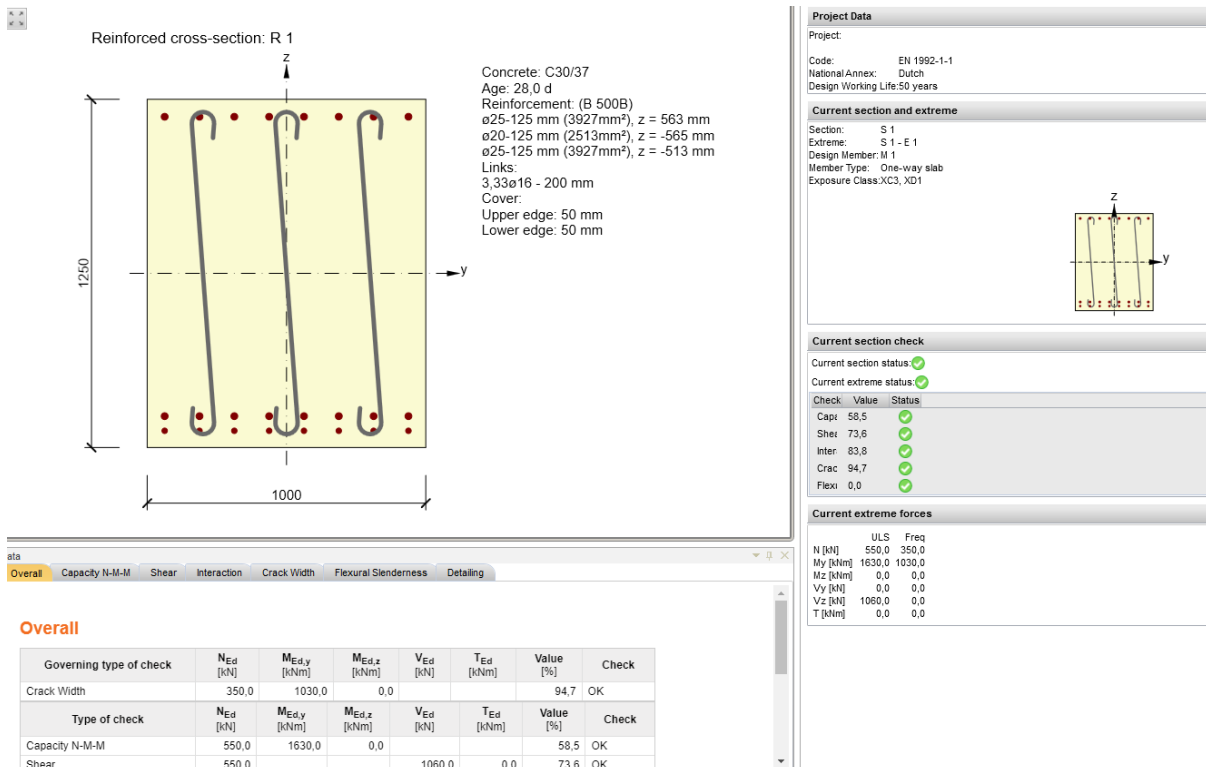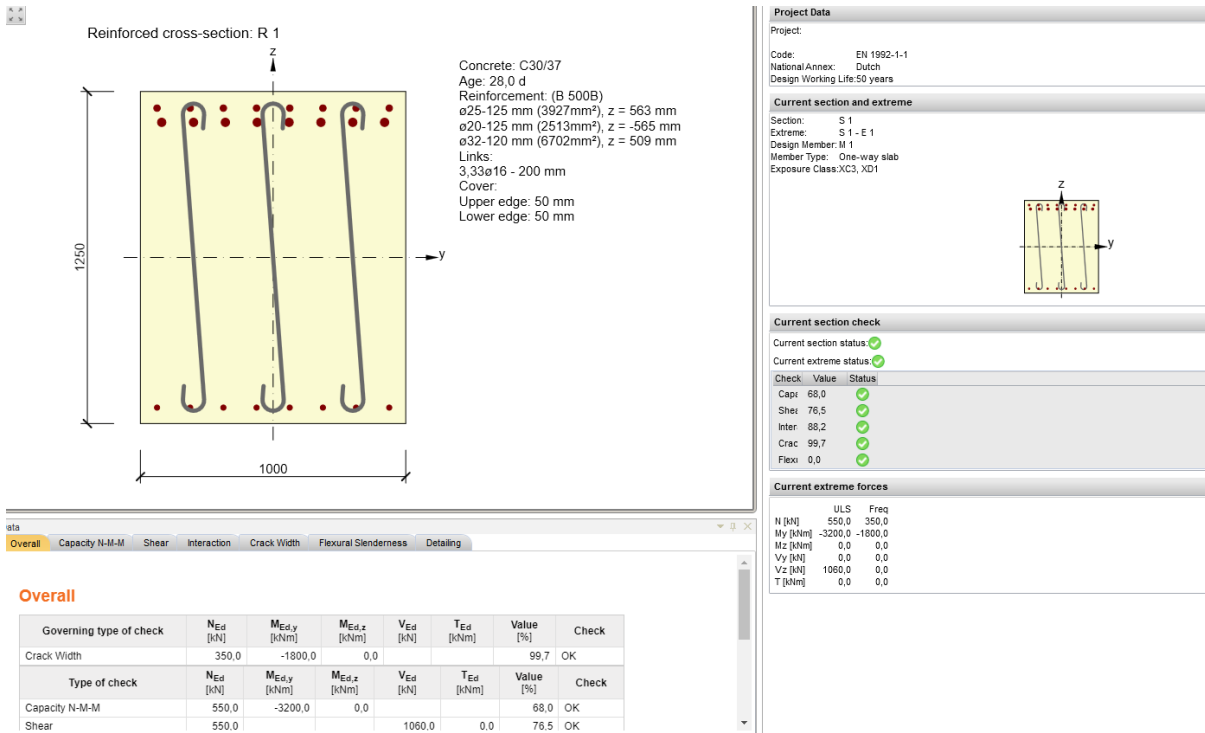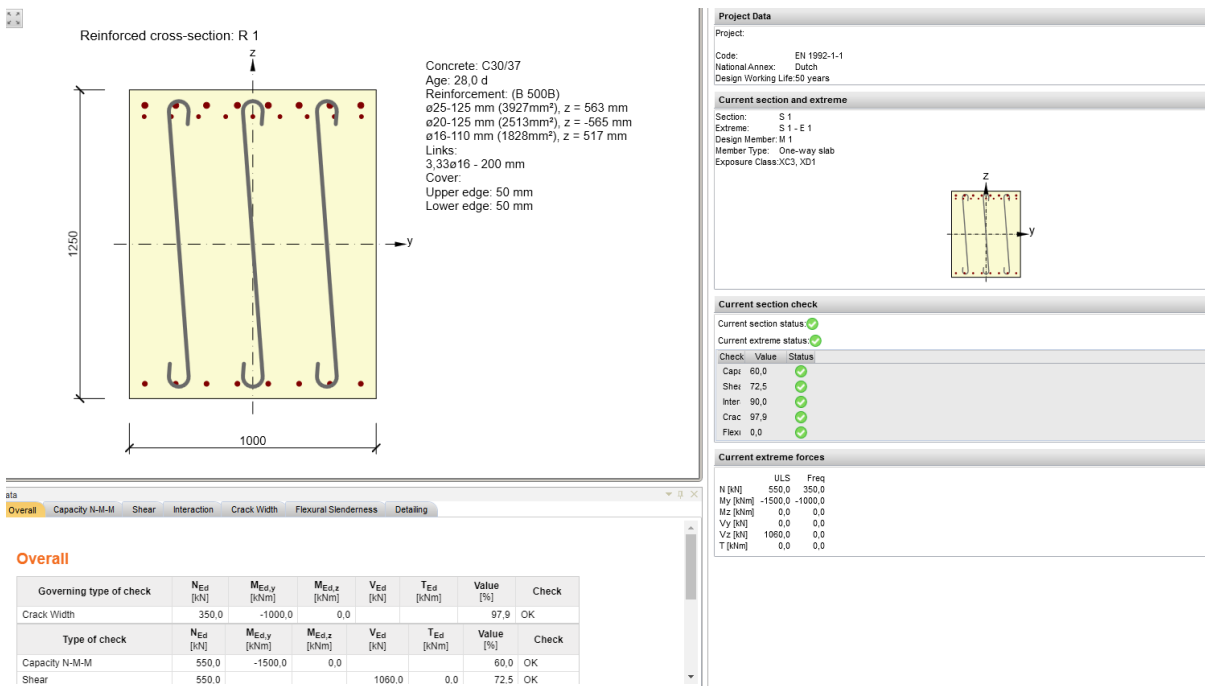| Type of check	N_{Ed} [kN]	$M_{Ed,y}$ [kNm]	$M_{Ed,z}$ [kNm]	V_{Ed} [kN]	T_{Ed} [kNm]	Value [%]	Check
Capacity N-M-M	550,0	-1500,0	0,0			60,0	OK
Shear	550,0			1060,0	0,0	72,5	OK

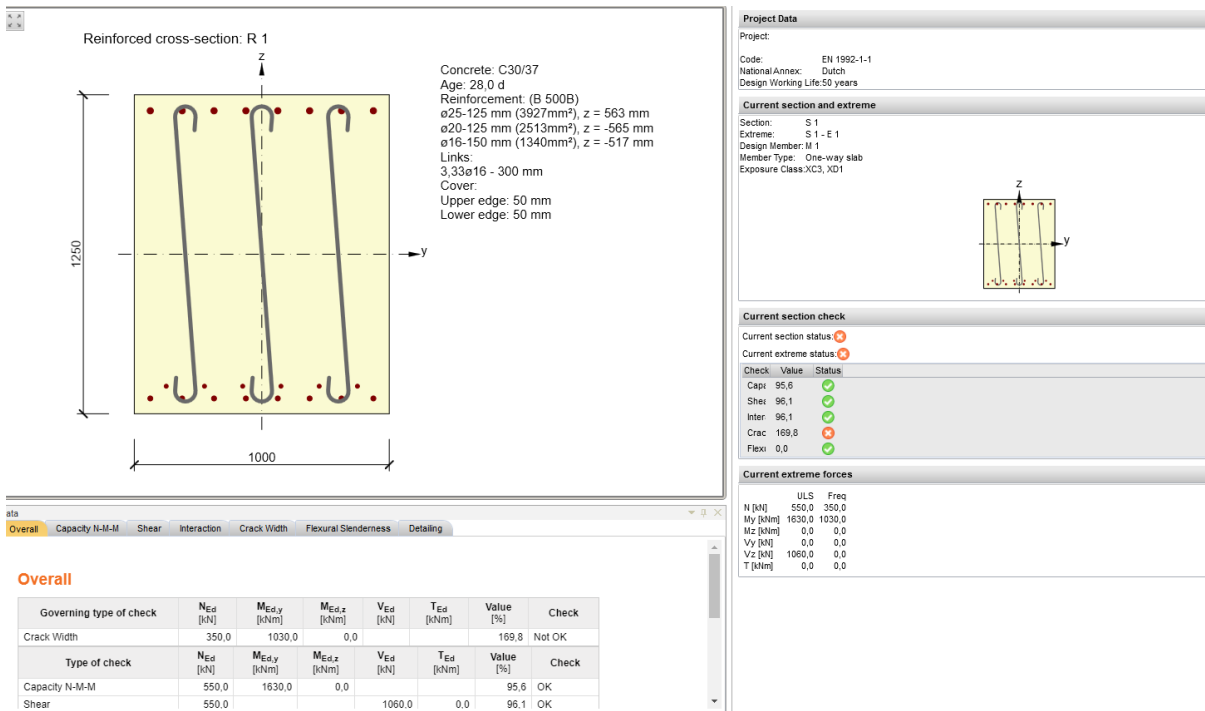*Figure 109. Idea Statica reinforcement calculation at location 3 based on the SLS*

Figure 110. Idea Statica reinforcement calculation at location 1 based on the ULS
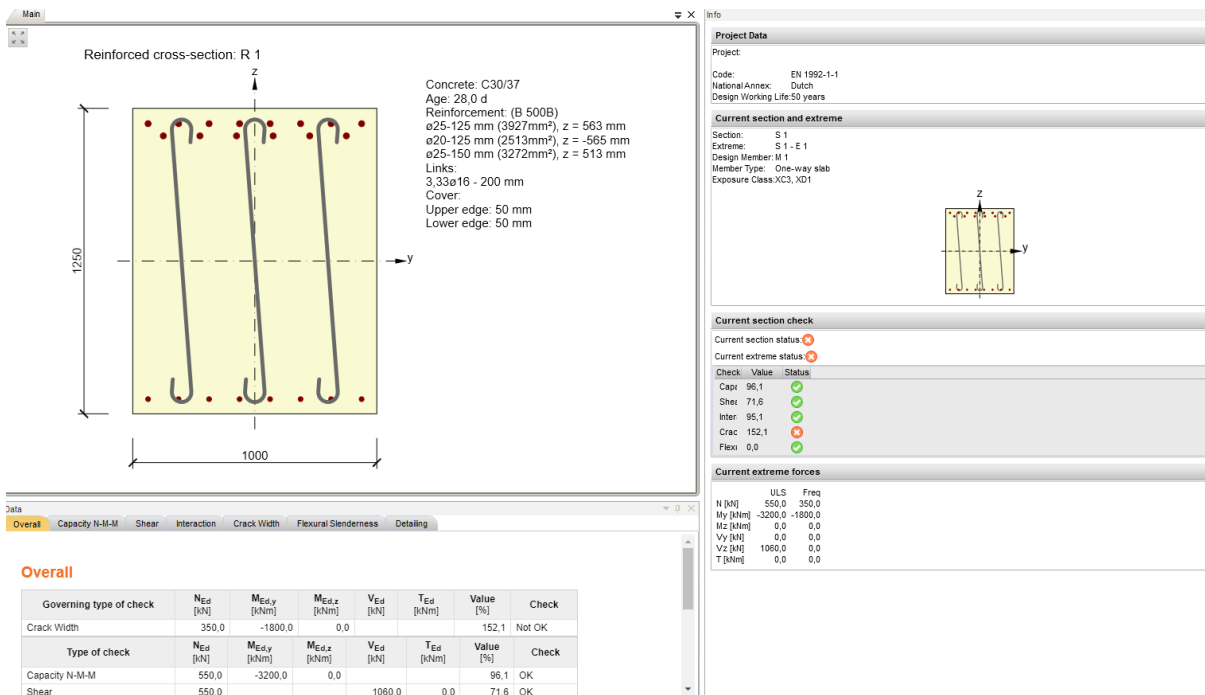

Figure 111. Idea Statica reinforcement calculation at location 2 based on the ULS

Main

Reinforced cross-section: R 1

Concrete: C30/37
Age: 28,0 d
Reinforcement: (B 500B)
ø25-125 mm (3927mm²), z = 563 mm
ø20-125 mm (2513mm²), z = -565 mm
Links:
3,33ø16 - 200 mm
Cover:
Upper edge: 50 mm
Lower edge: 50 mm

1250

1000

Current section check
Current section status: ✖
Current extreme status: ✖

Check	Value	Status
Capa	86,7	✔
Shea	70,8	✔
Inter	93,6	✔
Crac	170,1	✖
Flexi	0,0	✔

Current extreme forces

	ULS	Freq
N [kN]	550,0	350,0
My [kNm]	-1500,0	-1000,0
Mz [kNm]	0,0	0,0
Vy [kN]	0,0	0,0
Vz [kN]	1060,0	0,0
T [kNm]	0,0	0,0

Data

Overall | Capacity N-M-M | Shear | Interaction | Crack Width | Flexural Slenderness | Detailing

Overall

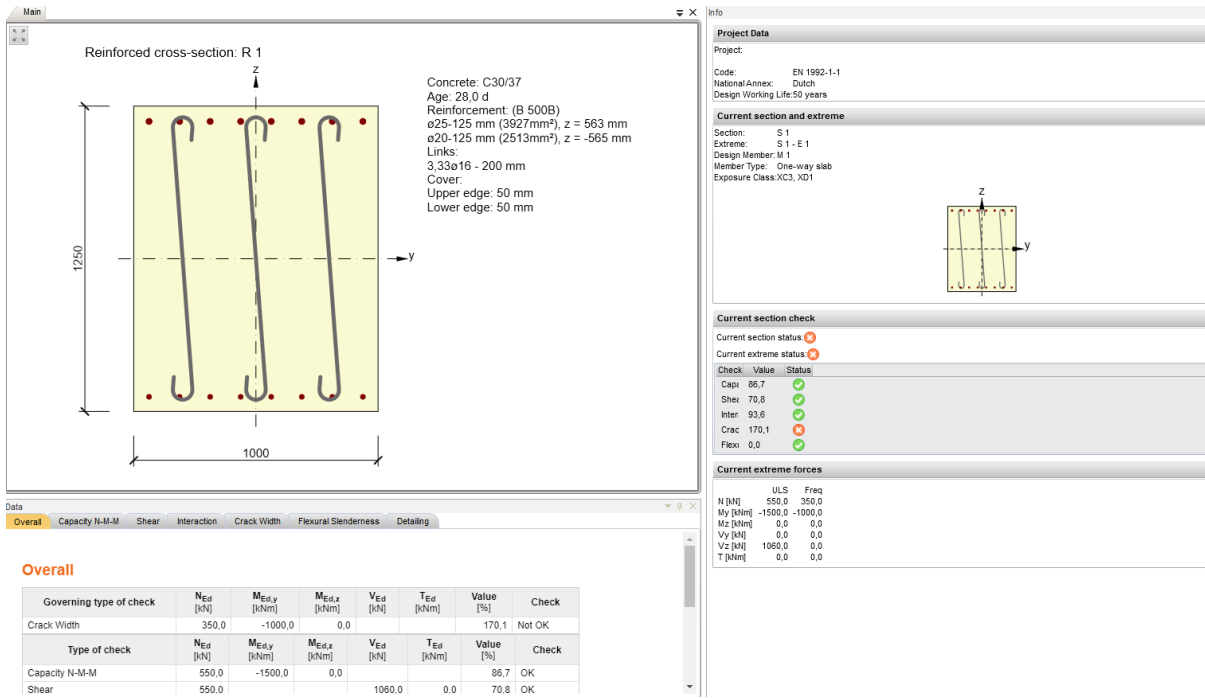| Governing type of check	N_{Ed} [kN]	$M_{Ed,y}$ [kNm]	$M_{Ed,x}$ [kNm]	V_{Ed} [kN]	T_{Ed} [kNm]	Value [%]	Check
Crack Width	350,0	-1000,0	0,0			170,1	Not OK
Type of check	N_{Ed} [kN]	$M_{Ed,y}$ [kNm]	$M_{Ed,x}$ [kNm]	V_{Ed} [kN]	T_{Ed} [kNm]	Value [%]	Check
Capacity N-M-M	550,0	-1500,0	0,0			86,7	OK
Shear	550,0			1060,0	0,0	70,8	OK

Figure 112. Idea Statica reinforcement calculation at location 3 based on the ULS